学位論文

Design principles in the stochastic thermodynamics of molecular motors

（微小熱力学系としての生体分子モーター設計原理）

平成 26 年 12 月 博士（理学）申請

東京大学大学院理学系研究科
物理学専攻　川口 喬吾

Doctorate thesis

Design principles in the stochastic thermodynamics of molecular motors

Kyogo Kawaguchi

Department of Physics, Graduate School of Science,
The University of Tokyo

Abstract

This thesis is dedicated to the theoretical studies on molecular motors, which are fascinating well-designed protein nanomachines that work in various biological systems. Recent progresses in experimental techniques have led to the measurement of precise physical properties of molecular motors, such as the heat dissipation of rotary motors and the cooperative dynamics of linear cytoplasmic motors. In parallel, there has been considerable advance in the understanding of stochastic thermodynamics, where the behavior of thermodynamic machines in the fluctuating world is the main target of study. In light of these developments, both in experiments and theory, we are now in position to elucidate the fundamental design principles hidden behind the molecular motors.

Two phenomenological models are discussed in this thesis. First is the model for F_1-ATPase (or F_1), which is a rotary motor with outstanding properties in its thermodynamic efficiency. We focus on the recent experimental result on the heat dissipative feature of F_1, which showed that the dissipation inside the motor is close to zero, irrespective of the velocity of rotation. We arrive at a model with totally asymmetric rules in the rotational angular dependence on the chemical reaction, and find significant consistency with this model to other experimental data such as the characteristic torque-velocity curve of F_1. Through the model, we give predictions on the physics of the reverse rotation of F_1, where ATP synthetic reactions occur.

Secondly, we consider a model for cytoplasmic molecular motors, which are proteins that transport cargoes along pseudo-one-dimensional rails called cytoskeletons. Experiments have clarified the large dependence of the transport velocity on the number of tied molecular motors such as myosins and dyneins. In our model, we take into account the typical two states of molecular motor heads, the highly diffusive state and the strongly bound state, and consider the stochastic switching between them through a force-sensor controlled rule. The scheme allows diffusive and bidirectional elements to produce unidirectional transport through collective interaction. We analyze how the sensitivity of the force-sensor affects the cooperativity of the motors, defined by the ratio between the value of velocity with two molecules and infinitely many molecules. We discuss on the possibility to classify the various cytoplasmic motors through the phase diagram obtained in our simple model.

Acknowledgements

I offer my sincerest gratitude to Prof. Masaki Sano, who supervised me for the five years of study in his lab. I appreciate the inspiration, support, and especially the generosity he held for my projects. It was not without his broad outlook that I would have been able to explore various research fields during my student years.

I express my warm thanks to Prof. Shin-ichi Sasa and Takahiro Sagawa for their aspiring guidance and invaluably constructive criticism. My theoretical thinking has been greatly enhanced by these two outstanding researchers. I also thank Prof. Shoichi Toyabe and Eiro Muneyuki for sharing their insights and experimental data of F_1-ATPase. My sincere thanks goes to Dr. Takayuki Torisawa, Ken'ya Furuta, and Mr. Kei Saito for engaging me in the research of cytoplasmic motors by presenting wonderful experimental works on cytoplasmic dyneins. I am thankful to Prof. Hideo Higuchi, Hiroyuki Noji, Dr. Rikiya Watanabe, and Takayuki Ariga for teaching me so many aspects of single molecule biology.

I am also extremely grateful to the past and present lab members of Sano lab for their kind support and interesting discussions on numerous topics. Dr. Kazumasa Takeuchi greatly inspired me through his attitude toward research and critical reading of my papers. Dr. Ken Nagai and Yuki Izumida encouraged me in the startup of my projects. Mr. Yohei Nakayama and Sosuke Ito allowed me to discuss so many issues related to stochastic thermodynamics throughout the five years of graduate school life. I acknowledge Mr. Takahiro Nemoto, Kiyoshi Kanazawa, Sho Sugiura, and Masato Itami, and the all the young generation of Japanese statistical physicists for the continuous influence through their interesting works.

I take this opportunity to thank Prof. Ryoichiro Kageyama for letting me stay in his lab in Kyoto through 2013-2014 to learn and conduct experiments on cell differentiation. Discussing and working with him was a wonderful opportunity for me to rethink on how theoretical works can possibly contribute to fundamental understandings of biology. I express my appreciation to the kind and invigorating group of people in Kageyama lab. I was greatly motivated by discussions with Prof. Hiroshi Kori, Dr. Akihiro Isomura, and Prof. Itaru Imayoshi through the project on cultured cell experiments.

Finally, I thank my family for supporting me throughout the various stages of my life.

List of publications

In reverse chronological order of publication[1]:

1. Kyogo Kawaguchi, “Collective motion by force-sensor switching: unified model for cooperative molecular motors”, *Manuscript in preparation* (2015).

2. Naoto Shiraishi, Sosuke Ito, Kyogo Kawaguchi, and Takahiro Sagawa, “Role of measurement-feedback separation in autonomous Maxwell’s demons”, *Submitted to New Journal of Physics*, Arxiv:1501.06071.

3. Yohei Nakayama and Kyogo Kawaguchi, “Invariance of steady state thermodynamics between different scales of description”, Physical Review E, 91, 012115 (2014). Arxiv:1211.3805.

4. Kyogo Kawaguchi, Shin-ichi Sasa and Takahiro Sagawa, “Nonequilibrium dissipation-free transport in F_1-ATPase and the thermodynamic role of asymmetric allosterism”, Biophysical Journal 106, 2450 (2014). Arxiv:1307.3998.

5. Itaru Imayoshi, Akihiro Isomura, Yukiko Harima, Kyogo Kawaguchi, Hiroshi Kori, Hitoshi Miyachi, Takahiro Fujiwara, Fumiyoshi Ishidate, and Ryoichiro Kageyama, “Oscillatory control of factors determining multipotency and fate in mouse neural progenitors”, Science, 342, 1203 (2013).

6. Kyogo Kawaguchi and Yohei Nakayama, “Fluctuation theorem for hidden entropy production”, Physical Review E, 88, 022147 (2013). Arxiv:1209.6333.

7. Kyogo Kawaguchi and Masaki Sano, “Efficiency of free energy transduction in autonomous systems”, Journal of the Physical Society of Japan, 80 083003 (2011). Arxiv:1103.1961.

[1]Papers 1 and 4 include the content of the main part of this thesis described in Chapters 4 and 3, respectively. Some motivations behind the works presented in 2, 3, 4 and 7 are mentioned in Chapter 2. The author contributed in the numerical modeling and simulation of the transcription factor dynamics in neural stem cells in 5, which is not described in this thesis.

Table of contents

Chapter 1

General introduction

1.1 Molecular motors and thermodynamics

No matter how special we feel about ourselves as living beings, or fascinating other creatures make us aware of the depth of mother nature, we cannot deny, at this stage of science, that living systems are composed of purely physical matter. It is therefore so natural to study the physical property of biological systems, just like how we investigated the night sky so well to know the age of the universe, or dug deep into the microscopic high-energy region so much to fulfill the dream of atomism.

Among many of the interesting progresses in the quantitative understanding of biophysics, studies on molecular motors have a special position characterized by the highly quantitative results provided by the fascinating and truly innovative experiments. The relatively simple goal in the field of single molecule biology was to take the spatio-temporal resolution of the microscopes to its limits: to the level where nanometer steps are distinguishable in the timescale of sub-milliseconds.

What is truly fascinating about researches on molecular motors is not only that profound new techniques were required in these experiments, but also the fact that such pure engines that are so small can actually exist, and can function as thermodynamic machines to some extent in our understanding. Thus the conceptual interest arises: comparing such small stochastic systems with macroscopic thermodynamic systems will inevitably reveal the the basic features of bio-molecules.

The experimental studies on bio-molecular motors have thus brought new questions to the field of statistical physics [1, 2, 3]. Since the leading actors that drive transport in the scale of bio-molecules are thermal diffusion and stochastic chemical reactions, it is expected that the thermodynamical properties underlying in such systems differ from that in macroscopic motors.

For example, how the second law of thermodynamics is obeyed in such fluctuating world has caught much attention over the past twenty years. It has been discussed [4, 5] that the irreversible entropy production is itself a stochastic quantity which may turn negative in single outcomes, although in the ensemble average the macroscopic law of inequality recovers. Further studies have shown that appropriate feedback protocols indeed allow small systems to utilize the

thermal fluctuation [6], while paying the cost in a macroscopic external system [7] or through other small systems dynamics [8]. Historically, one of the most important literature in the context of Maxwell's demon [9] was in fact written with a large motivation toward understanding the specialty of living systems; can we define intelligence through thermodynamic inequalities? The field of stochastic thermodynamics has thus reached the point where abstract theories are answering practical and long standing questions in statistical physics.

Given the progress in the theoretical understanding of stochastic thermodynamics, we now desire to come back to the study on molecular motors; interest is on how real bio-molecules are actually benefiting or suffering from the large stochasticity [10]. Modern experimental and theoretical studies have so far unveiled the interesting features of bio-micromachines, for example the ratchet mechanism [11] including the potential switching scheme [12], large collective behavior [13, 14], and seemingly high efficiency in terms of thermodynamic properties [15, 16]. These phenomenological studies are aimed at elucidating the fundamental and possibly universal properties of molecular motors; seemingly different and complicated structures of motor protein families may well be understood through simple models that focus on specific aspects of the motors.

In this thesis, we present the current understanding on molecular motors, with focus on the thermodynamic and cooperative features. Through the phenomenological models inspired by specific experimental data, we aim to describe the possible design principles hidden in molecular motors in a quantitative manner. The aim of this thesis is to demonstrate how our understanding of molecular motors have reached to the stage where the quantitative understandings are now allowing us to imagine and discuss the fundamental physics governing in the world of nanomachines.

1.2 Organization of the thesis

In the following, we shall start by describing the basis of stochastic thermodynamics. Most part of Chapter 2 is meant to play the role as a theoretical minimum required to understand the modeling of molecular motors and their interpretations. The principle aim here is to introduce heat in terms of the stochastic Markov dynamics, and to describe in what ways it can be indirectly measured and how those measured quantities are related to the thermodynamic laws. The other parts are aimed at describing the fundamental questions in statistical physics that are related to the experimental measurements of thermodynamic quantities in small thermodynamic systems.

Based on these introductory parts, we consider the theoretical model for the rotary motor F_1-ATPase (or F_1) in Chapter 3, as the first main topic in this thesis. F_1 is one of the most well studied molecular machines due to its obviously important role in the thermodynamics of cellular processes; it is responsible for generating over 90% of the ATP consumed in the eukaryotic cells. F_1 has the remarkable feature that the rotary angle of the γ shaft is a single variable that almost dominates the full chemical reaction of of ATP synthesis and hydrolysis. Recent *in vitro* experiments for F_1 in the ATP hydrolytic regime (i.e., the F_1 motor) have found that the dissipation inside the motor is close to zero, irrespective of the velocity of rotation. Using the framework of

stochastic thermodynamics, we arrive at the conclusion that these experimental results should be explained by an asymmetric design principle in the angular dependent chemical reaction rates. We present and discuss the significant consistency of our model to other experimental data including the torque response of F_1 .

In Chapter 4, we move our focus to linear motors, which are molecular motors that function typically in cytoplasms in order to transport the cargos on rails such as cytoskeletons. Motivated by the recent systematic experiments that quantified the extent of cooperativity in molecular motors, we consider a simple model which allows bidirectional elements to produce unidirectional motion though collective interactions. The attempt here is to unite the previously proposed different perspectives in independent motor protein experiments, and to give a conceptual understanding on the origin of cooperativity in linear motors.

Introduction to the specific molecular motors of interest are given in detail in the corresponding chapters; in both presented models, we aim to clarify the relation of our phenomenology to past and future experiments. In the final concluding remarks chapter, we aim to position our thesis in the general prospective of biological physics.

Chapter 2

Stochastic thermodynamics
-Phenomenological description of molecular motors-

Here we review on the basic concepts of stochastic thermodynamics, which is a theoretical framework that links general stochastic phenomena to thermodynamics. We first explain the physical background of Markov processes, including the overdamped Langevin equation and jump processes concerning chemical reactions. We then introduce the energetics of Brownian motion, and note on the general principles of thermodynamics in Markov processes. Based on these setups, we describe the motion of molecular motors by the combination of Brownian motion and chemical reaction-induced switching. We note on various theoretical tools that are useful in quantifying the heat dissipation and elucidating the model parameters in such systems, with special focus on the fluctuation response relation studied in nonequilibrium systems. Remarks on the treatment of stochastic differential equations is also given.

2.1 Mesoscopic description and stochastic dynamics

2.1.1 Brownian motion: overdamped Langevin system

Consider a bead (submicron particle) suspended in water with uniform room temperature. The motion of such particle is known to be well described by the Brownian motion, which is written as a stochastic differential equation:

$$\dot{\vec{x}} = \sqrt{2D}\vec{\xi}(t). \tag{2-1-1}$$

Here, $\vec{x} = (x_1, x_2, x_3)$ is the position of the particle in three dimensions, $\dot{}$ represents the time-derivative, D is the diffusion coefficient, and $\vec{\xi}(t) = (\xi_1(t), \xi_2(t), \xi_3(t))$ is the Gaussian white noise vector with unit variance:

$$\langle \xi_i(t)\xi_j(t')\rangle = \delta_{ij}\delta(t - t'). \tag{2-1-2}$$

We used $\langle\cdot\rangle$ to describe the ensemble average. δ_{ij} $(i, j = 1, 2, 3)$ and $\delta(\cdot)$ are Kronecker's delta and Dirac's delta function, respectively. It is known that the value of D obeys the Stokes-Einstein law:[1]

$$D = \frac{k_{\mathrm{B}}T}{\Gamma} = \frac{k_{\mathrm{B}}T}{6\pi\eta a}. \tag{2-1-3}$$

We introduced the viscous friction coefficient Γ, the Boltzmann constant $k_{\mathrm{B}}(= 1.38\times10^{-23}\mathrm{m^2kg\cdot s^{-2}K^{-1}})$, the temperature T $(\simeq 300\mathrm{K})$ and the viscosity η $(= 0.890\mathrm{mPa{\cdot}sec}$ for 298K water) of the substance. The relation $\Gamma = 6\pi\eta a$ is derived for the case of a spherical particle[2] with the diameter of the suspended particle a.

Equation (2-1-1) is an example of Markov process [18]. Markov process is a special type of stochastic process where the probability in the future does not depend on the past dynamics (see definition in Sect. 2.3). Now, if we interpret Eq. (2-1-1) as the equation of motion, what is nontrivial is that such closed and memory-independent equation of motion well describes the dynamics of the position variable of the bead, $\vec{x}$.

In a closed system which includes all the water molecules and a single bead, it is expected that there is a deterministic equation of motion[3] which takes into account all the degrees of freedom including the position and velocity of water molecules. Therefore, even if we focus on the motion of the single bead, the dynamics should depend on the combination of all the forces that affect the bead, which is the interaction with the huge number of water molecules.

In short, the reason for the closed form of Eq. (2-1-1) is that the other degrees of freedom in the total equation of motion are very fast compared to the observation time-scale of our interest. This assumption allows the detail of the degrees of freedom of the water molecules to be packed

[1] Since η, a, T, and D can be obtained independently in experiments, Eq. (2-1-3) can be used to measure k_{B} [17].

[2] A useful formula to remember is D =0.25/(diameter of particle in μm) [μm^2/sec].

[3] We only consider classical systems in this thesis. Therefore, the origin of fluctuation is all assumed as thermal, and not quantum.

into a system we call the thermal reservoir, and its interaction with the bead to be effectively included in the equation of motion through the thermal force. Such elimination of variables from the original equation of motion to obtain phenomenological descriptions, is referred to as the reduction of dynamics [19].

Although there is no mathematically rigorous way to derive Eq. (2-1-1) from the full classical equation of motion[4], there are several cases where the singular perturbation method allows explicit understanding of the phenomenological descriptions, with the separation of time-scale playing a role as the small parameter. In fact, there exists an intermediate layer of description in the case of Brownian motion:

$$\dot{\vec{x}} = \vec{v}, \qquad M\dot{\vec{v}} = -\Gamma\vec{v} + \sqrt{2\Gamma k_{\mathrm{B}}T}\vec{\xi}(t). \tag{2-1-4}$$

Here we have introduced the velocity of particle $\vec{v}$ an additional variable, and the mass of the particle M. Equation (2-1-4) is called the underdamped Langevin equation, whereas Eq. (2-1-1) is called the overdamped Langevin equation. Equation (2-1-4) has a clear interpretation as an equation of motion; the right hand side of the second equation corresponds to the force that the bead feels. The origin of such force is obviously the interaction with the surrounding molecules, therefore it is called the thermal force. Note that the thermal force already includes the phenomenological description using Γ and the fluctuation term with simple statistical property, $\xi(t)$. The reduction of dynamics from Eq. (2-1-4) to Eq. (2-1-1) is justified when the fastest time-scale in the motion of x (typically the frame rate of camera used to observe the position of the particle), is much larger than M/Γ, which is the time-scale for the velocity of the particle to relax to equilibrium.

In practical regimes of the bio-molecular experiments, we need not to be concerned with the underdamped description, Eq. (2-1-4)[5]. This is because the protein molecules including molecular motors, and even the utilized probe particles that are typically much larger than the bio-molecules, have small mass relative to the accessible time-scale $\times\,\Gamma$.

2.1.2 Chemical reactions

Another key ingredient in the dynamics of bio-molecules is the stochastic chemical reaction. In terms of chemical potential, the cell is in a largely nonequilibrium situation: ions such as Na^+, K^+ and Ca^{2+} are abundant and highly nonuniform among the different compartments made with lipid membranes. Such nonequilibrium situation plays important roles in the macroscopic character of cells such as in the formation of action potentials and determining the direction of motility.

[4]The Mori projection operator scheme [20, 21] gives phenomenological understandings to this problem. The Zwanzig model [22] describes a concrete example of the underdamped Langevin equation obtained from the the Newtonian dynamics of a particle interacting with many small particles. In both cases, however, the Markov approximation plays a key role in deriving the white Gaussian noise. There are other cases like the billiard model [23] which are rigorous in the context of dynamical systems, but do not correspond exactly to the physical situation we have in mind.

[5]It was only recently that experiment first captured the dynamics of the underdamped variable, v [24].

The chemically nonequilibrium situation is cascaded into various forms of nonequilibrium, for instance through active pumping of ions, motions of molecular motors, and cell proliferation. The origin of all such free energy transduction is the metabolic system, where the free energy of the external source is packed into the forms of high energy molecules such as adenosine triphosphates (or ATP).

The high free energy-involving reaction of ATP hydrolysis reads

$$\mathrm{ATP} + \mathrm{H_2O} \rightleftharpoons \mathrm{ADP} + \mathrm{Pi}. \tag{2-1-5}$$

Here we also wrote the reverse reaction, where ADP (adenosine diphosphate) and Pi (phosphoric acid) bonds to form ATP. The reaction from left to right is referred to as the hydrolysis reaction, where as the opposite is called the synthetic reaction. It is known that the reaction (2-1-5) is largely biased to the right; in the usual situation, the ATP is unstable and prefers to be hydrolyzed. The extent of the bias is quantified by the free energy difference accompanying the hydrolysis reaction:

$$\Delta\mu = \Delta\mu_0 + k_\mathrm{B}T \log \frac{[\mathrm{ATP}][\mathrm{H_2O}]}{[\mathrm{ADP}][\mathrm{Pi}]}. \tag{2-1-6}$$

The second term in the right hand side of Eq. (2-1-6) is the concentration dependent term[6], which is derived for the case of low concentration of ATP, ADP, and Pi in the solution of $\mathrm{H_2O}$. The value of the standard free energy $\Delta\mu_0 \sim 11\ k_\mathrm{B}T$, varies in literature, although the error is around $1\ k_\mathrm{B}T$.[7]

It is critical that the large free energy accompanying the hydrolysis reaction (2-1-5) is timely released and coupled to useful motion or pumping in the physiological context. To this end, the natural hydrolysis rate needs to be sufficiently low compared with the time scale of biochemical reactions. Indeed, the nonenzymatic reaction for (2-1-5) has a time scale of $> 10^5$ sec [25]. Therefore, it is safe to assume that the concentrations in Eq. (2-1-6) are kept constant during single molecular-level experiment; the bulk concentration does not change so much over the time scale of experiment.

The remarkable fact in biological systems is that the hydrolysis rate jumps to a much higher value in the presence of catalytic enzymes or motor proteins. Under this situation, it makes sense to ask what statistical laws rule the reaction of (2-1-5). We expect that the hydrolysis reaction rate, which we denote as R^+ and the synthetic reaction rate, denoted as R^-, should satisfy the condition

$$\frac{R^+}{R^-} = \exp\left[\frac{\Delta\mu}{k_\mathrm{B}T}\right]. \tag{2-1-7}$$

In fact, such relation should hold irrespective of the existence of enzyme; if the value of R^+ is very low in a certain pathway of reaction, the value of R^- corresponding to the reverse of this pathway

[6]This term is sometimes written as $k_\mathrm{B}T \log([\mathrm{ATP}]/[\mathrm{ADP}][\mathrm{Pi}])$, which means that [ATP], [ADP], and [Pi] are treated as non-dimensional quantities, $[\mathrm{ATP}] = N_\mathrm{ATP}/N_{\mathrm{H_2O}}$ etc., with N representing the number of molecules of the substance.

[7]The value is obtained for the case of 1 mM excess Mg^{2+}, 25°C, and pH 6.5. See for instance, the supplementary material for [16].

should also be very low. We cannot, however, compare two reactions of different pathways, for instance one escorted by an enzyme and its reverse reaction without the enzyme.

The natural assumption behind Eq. (2-1-7) is that the process of stochastic reactions are written as a Markov jump dynamics, which is again a stochastic and memory-independent process. The reason for this assumption can be understood in the same way as the Brownian motion description; the water surrounding the ATP, ADP, and Pi is so abundant and fast that it acts as a thermal reservoir, and the detailed dynamics of them is effectively included in the statistical properties of R^+ and R^-.

One way to look at Eq. (2-1-7) is that the distribution of the state of the water molecules including ATP, ADP, and Pi, is given by the grand canonical ensemble. In this picture, we assume a subsystem being attached to an external reservoir with fixed temperatur and concentration of ATP, ADP, and Pi (that determines $\Delta\mu$), which is essentially satisfied in our setup of interest since the time scale of natural reaction is so slow compared with the enzymatic reaction. Then, Eq. (2-1-7) corresponds to the detailed balance between two states, where there are M molecules of ATP and $M-1$ molecules of ATP in the subsystem, for instance. Thus, the nonequilibrium large bias characterized by Eq. (2-1-7) when focusing on a single molecule dynamics, is nothing but the equilibrium dynamics from the point of view of the subsystem. Such way of considering the nonequilibrium local dynamics as a part of the larger equilibrium dynamics is the heart of the fluctuation theorem, which we will introduce in Sect. 2.3.

2.2 Stochastic energetics: defining heat in Brownian motion

Let us consider again the overdamped Brownian dynamics. We remark that all the discussions given here can be extended to the case of underdamped dynamics (see for example, [2]).

We consider the one-dimensional dynamics of a molecule that is subjected to a general force:

$$\Gamma\dot{x} = F_{\lambda(t)}(x) + \sqrt{2\Gamma k_{\mathrm{B}}T}\xi(t). \tag{2-2-1}$$

We introduced the position dependent force $F(x)$, which may be decomposed into a position independent driving force and an effective potential force:

$$F_{\lambda(t)}(x) = f_{\lambda(t)} - \frac{\partial U_{\lambda(t)}}{\partial x}. \tag{2-2-2}$$

Here and throughout, the we consider $\xi(t)$ to be the white-Gaussian noise with unit variance, $\langle\xi(t)\xi(s)\rangle = \delta(t-s)$.

A typical situation which corresponds to Eq. (2-2-1) is a Brownian particle being trapped in some effective potential $U_{\lambda(t)}(x)$ made by an applied optical tweezer or the conformation of the probed protein molecule. The driving force $f_{\lambda(t)}$ that brings the motion of the macromolecule into nonequilibrium may be applied externally or through chemical reactions in the phenomenological description. We have introduced $\lambda(t)$, which is a deterministic or stochastic parameter that controls the value of f and the functional form of $U(x)$. Changing of λ corresponds for instance

to moving the center of the optical tweezer or switching the chemical states of the protein that traps the probe bead.

In [26], Sekimoto introduced the following definition of heat (hereafter referred to as Langevin heat):

$$Q := -\int_0^\tau dt\left(-\Gamma\dot{x}(t) + \sqrt{2\Gamma k_{\rm B}T}\xi(t)\right)\circ\dot{x}(t). \tag{2-2-3}$$

We denoted the Stratonovich integral[8] as $\circ$ and set a time interval $t\in[0,\tau]$. The physical meaning of Eq. (2-2-3) is that it is quantifying the energy transferred from the bead to the water: the ( ) part is the thermal force, so the quantity inside the integral is the instantaneous work per time that is done by the thermal force to the bead.[9]

Let us consider the case where $f = 0$. By defining the potential energy difference between the time interval τ as $\Delta U := U_{\lambda(\tau)}(x(\tau)) - U_{\lambda(0)}(x(0))$, we may write

$$\begin{aligned}\Delta U &= \int_0^\tau dt\left(\frac{\partial U_{\lambda(t)}(x(t))}{\partial\lambda}\dot{\lambda}(t) + \frac{\partial U_{\lambda(t)}(x(t))}{\partial x}\circ\dot{x}(t)\right) &(2\text{-}2\text{-}4)\\ &= \int_0^\tau dt\frac{\partial U_{\lambda(t)}(x(t))}{\partial\lambda}\dot{\lambda}(t) + \int_0^\tau dt\left(-\Gamma\dot{x}(t) + \sqrt{2\Gamma k_{\rm B}T}\xi(t)\right)\circ\dot{x}(t) &(2\text{-}2\text{-}5)\\ &= W - Q. &(2\text{-}2\text{-}6)\end{aligned}$$

We here defined W as the first term in Eq. (2-2-5), which is the energy shift caused by the change of the parameter λ. For example, if λ represents the center position and the stiffness of the optical tweezer which is controlled from an external system, W quantifies the work that is put in by this external system. Another example is when λ represents a certain chemical state of the motor protein, and the discrete switching of this parameter is induced by some stochastic chemical reaction such as nucleotide binding. In both cases, Eq. (2-2-6) describes the energy conservation of this Langevin system, which is why it is referred to as the First Law of stochastic thermodynamics. Notice that since ΔU, W, and Q depend on the trajectory of $x(t)$, they are all stochastic quantities even when the time-course of the parameter $\lambda(t)$ is predetermined. The claim of Eq. (2-2-6) is that the First Law is obeyed precisely for each single trajectory.

Let us next consider a dynamics with fixed λ under the periodic boundary condition, $x\in[0,L]$ with $U(x=0) = U(x=L)$ [or simply, $U(x) = U(x-L)$]. We call such case the tilted periodic potential setup:

$$\Gamma\dot{x} = f - \frac{\partial U(x)}{\partial x} + \sqrt{2\Gamma k_{\rm B}T}\xi(t). \tag{2-2-7}$$

Under this setup, we have a steady-state velocity $v_{\rm st}$, which may be analytically obtained as [27]

$$v_{\rm st} = DL\frac{1-\exp[-fL/k_{\rm B}T]}{\int_0^L dx\int_0^L dy\exp\{[U(x+y)-U(x)-fy]/k_{\rm B}T\}}. \tag{2-2-8}$$

[8]Note on the different interpretations of integrals is given in Sect. 2.4. The reason why we take the Stratonovich interpretation in Eq. (2-2-3) is because it satisfies the ordinary chain rules, as utilized in Eq. (2-2-4). Another important point is that only by adopting the definition Eq. (2-2-3) can we arrive at a quantity consistent with the logratio of the transition probability. The latter point will be confirmed in Sect. 2.3.

[9]We have adopted the opposite sign convention for Q from [2].

Noticing that Eq. (2-2-3) is rewritten as

$$Q = \int_0^\tau dt \left(f - \frac{\partial U_{\lambda(t)}(x)}{\partial x} \right) \circ \dot{x}(t) = f \int_0^\tau dt \dot{x}(t) - \Delta U. \tag{2-2-9}$$

The steady heat dissipation rate may be obtained as

$$\langle \dot{Q} \rangle_{\rm st} = \lim_{\tau \to \infty} \frac{\langle Q \rangle}{\tau} = f v_{\rm st}. \tag{2-2-10}$$

Since the steady-state velocity and the driving force have the same sign [Eq. (2-2-8)], we immediately find

$$\langle \dot{Q} \rangle_{\rm st} \geq 0, \tag{2-2-11}$$

which implies that a positive energy flux should be observed from the external driver to the thermal reservoir under this setup. This is related to the Second Law of thermodynamics, which will be discussed under a more general setup in Section 2.3.2. Here we note that, is in contrast to the First Law [Eq. (2-2-6)] which is satisfied for every single trial, there is a small but finite probability that the inequality for the single outcomes of Q can be violated, $Q < 0$.

Some remarks should be made. Firstly, the Langevin heat defined by Eq. (2-2-3) does not necessarily correspond to the actual energy flux between the particle and the surrounding environment. This is because the effective potential described by $U(x)$ does not always have an energetic interpretation. For example, the phenomenological description by Eq. (2-2-1) can be satisfied for the case where a Brownian particle is trapped by an entropic spring. In such case, the force is the entropic force, so there is no energy flow accompanying the motion of the probe in the trap, in contrary to the case where the trap is a real energetic potential. In this sense, the potential $U(x)$ should be considered as the effective potential, that governs the dynamics as Eq. (2-2-1), but may have unknown physical origin.

Secondly, under the typical experimental setup, it is very difficult to determine the form of $U(x)$ from first principles.[10] This is why in most experimental studies, the functional form of $U(x)$ is determined by the motion of the probe itself. In the case of fixed λ and $f = 0$, which is referred to as equilibrium dynamics, the simplest way to estimate $U(x)$ is to measure the equilibrium probability density function of the position of the particle:

$$P_{\rm eq}(x) = \frac{1}{Z} \exp\left[-\frac{U(x)}{k_{\rm B} T} \right]. \tag{2-2-12}$$

Here, Z is the partition function (see Sect. 2.4 for the general discussion on the Fokker-Planck equation, which describes the time evolution of the probability density function). It is typical to estimate the spring constant k of an applied tweezer by fitting a Gaussian [assuming $U(x) = kx^2/2$] to the density function, and use k to estimate the force applied to a bio-molecule by measuring the displacement of the probe from the center of the tweezer.

[10] The non-linear potential force exerted by an optical tweezer has been theoretically studied for instance in [28].

In the case where there is finite f with fixed λ, it is also generally possible to reconstruct the potential $U(x)$ and the value of f by measuring the steady-state probability density function, $P_{\rm st}(x)$, together with the steady-state velocity, $v_{\rm st}$ [29]. If we may for instance estimate the form of $U_\lambda(x)$ and the value of f for various λ, then we may calculate the thermodynamic quantities that appear in Eq. (2-2-6) under the determined protocol or the stochastic switching of λ.

Even using these methods, there are certain cases that the estimate of the form of $U(x)$ is challenging. The typical example is the case of molecular motors, as will be described in Sect. 2.5 and 2.6.

2.3 Markov process and the Second Law

We here remark on the stochastic thermodynamics of Markov processes. We will find that the empirically defined Langevin heat in the previous section can be understood as a special case of heat defined in general Markov processes. The principle behind this relation is the local detailed balance, which is sometimes referred to as the (detailed) fluctuation theorem.

2.3.1 Entropy production in general Markov dynamics

Let us first introduce the Markov process. The stochastic variable x may be discrete or include many variables, nevertheless we treat it as a continuous variable with a single variable notation. The definition of Markov process is that the conditional probabilities satisfy

$$P(x_{t_n}|x_{t_0}, x_{t_1}, ..., x_{t_{n-1}}) = P(x_{t_n}|x_{t_{n-1}}), \tag{2-3-1}$$

for any set of successive times, $t_0 < t_1 ... < t_n$. This means that the probability of the event in the future (t_n) and the past ($t_0, t_1, ..., t_{n-2}$) are independent under the condition of the present (t_{n-1}) state. For simplicity, let us consider a discrete time dynamics with an infinitesimal time increment Δt, and denote the time points $t_n := n\Delta t$ by n in this section (and also in Sect. 2.4). To avoid confusion in the notation, let us also write the right hand side of Eq. (2-3-1), which is the transition probability, as $W(x_n|x_{n-1})$.

The time evolution of the probability density function $P_{n\Delta t}(x)$ follows the Chapman-Kolmogorov equation,

$$P_{n+1}(x) = \int dx' P_n(x') W_{\lambda(n)}(x|x'). \tag{2-3-2}$$

We assume that the transition probability it is controlled by the time-dependent external parameter $\lambda(t)$. The integral by x' in Eq. (2-3-2) is taken over the whole phase space of x. Note that $\int dx W_{\lambda(t)}(x|x') = 1$.

Let $\boldsymbol{x}_N = (x_0, x_1, ..., x_N)$ be the stochastic path taken by x during the N time steps starting from $t = 0$. From the Markov property [Eq. (2-3-1)], the path probability $P_\lambda(\boldsymbol{x}_N)$ is obtained by $P_\lambda(\boldsymbol{x}_N) = P_0(x_0) W_\lambda(\boldsymbol{x}_N|x_0)$, where we defined the path transition probability as

$$W_\lambda(\boldsymbol{x}_N|x_0) := \prod_{n=0}^{N-1} W_{\lambda(n)}(x_{n+1}|x_n). \tag{2-3-3}$$

We also define the reverse trajectory of $\boldsymbol{x}_N$ as $\boldsymbol{x}_N^\dagger$, where $\boldsymbol{x}_N^\dagger = (\bar{x}_N, \bar{x}_{N-1}, ..., \bar{x}_0)$, with $\bar{x}_i$ being the time reversal of x_i (i.e., if x represents velocity or momentum, $\bar{x} = -x$).

Now, we define the heat entropy production (entropy production of the thermal bath) corresponding to the N step trajectory as [30, 31, 32],

$$\sigma(\boldsymbol{x}_N) := \log \frac{W_\lambda(\boldsymbol{x}_N|x_0)}{W_{\lambda^\dagger}(\boldsymbol{x}_N^\dagger|\bar{x}_N)}. \tag{2-3-4}$$

Here, $W_{\lambda^\dagger}$ is the transition probability assigned to the time-reversed protocol,

$$W_{\lambda^\dagger}(\boldsymbol{x}_N^\dagger|\bar{x}_N) := \prod_{n=0}^{N-1} W_{\bar{\lambda}(N-n)}(\bar{x}_n|\bar{x}_{n+1}), \tag{2-3-5}$$

which is defined using $\bar{\lambda}(t)$, the time reversal of $\lambda(t)$ [for example if the control is by the magnetic field, $\bar{\lambda}(t)$ corresponds to $\lambda(t)$ with reversed coordinates]. The relation Eq. (2-3-4) is referred to as the local detailed balance, or the detailed fluctuation theorem [32].

The assumption behind the definition Eq. (2-3-4) is that the stochastic property in the system of interest is a consequence of thermal fluctuation. In other words, our system of interest is open, and therefore the dynamics of x is coupled to a large degree of freedom which act as the thermal reservoir, as in the case of the Brownian motion description discussed in Sect. 2.1.1. The meaning of Eq. (2-3-4) is that each stochastic step in the variable x is accompanied by an energy transfer from the system of interest to the thermal reservoir. The law of the transition probabilities in the system of interest is thus restricted by the equilibrium dynamics in the thermal reservoir, which is the usual detailed balance.

The simplest example which explains Eq. (2-3-4) is the case of chemical reaction. Consider that the state of the chemical substance ATP is of interest. Let us take this opportunity to note that in the case of chemical reactions, the stochastic process should be considered in continuous time and discrete states. Such dynamics is called the Markov jump process. The relation between the transition probabilities, denoted as W, and the jump rates, denoted as R, is simply $W = R\Delta t$ if we take a sufficiently small Δt. Thus, for the single switching event, ATP $\to$ ADP + Pi, the right hand side of Eq. (2-3-4) is simply equal to R^+/R^-. The entropy production of the thermal bath in this reaction is $\Delta\mu/k_{\rm B}T$ [33, 34] which means that Eq. (2-1-7) was an example of Eq. (2-3-4).

Another example is the overdamped Langevin system described by Eq. (2-2-1). Let us take a small time increment and discretize the dynamics to obtain the transition probability:

$$W_{\lambda(n)}(x'|x) \propto \exp\left\{-\frac{1}{4\Gamma k_{\rm B}T\Delta t}\left[\Gamma(x'-x) - F_{\lambda(n)}(x)\Delta t\right]^2\right\}. \tag{2-3-6}$$

The original Langevin dynamics may be considered as the limit $N \to \infty$ ($\Delta t \to 0$) with fixed $N\Delta t = \tau$ for this discretized dynamics. Noticing that $\bar{x} = x$ since we are only considering overdamped dynamics, and

$$\frac{x_{n+1} - x_n}{\Delta t}[F_{\lambda(n)}(x_n) + F_{\lambda(n+1)}(x_{n+1})] \xrightarrow{\Delta t\to 0} \dot{x} \circ F_{\lambda(t)}(x), \tag{2-3-7}$$

we obtain

$$\log \frac{W_\lambda(\boldsymbol{x}_N|x_0)}{W_{\lambda^\dagger}(\boldsymbol{x}_N^\dagger|x_N)} \xrightarrow{\Delta t\to 0} \frac{1}{k_{\rm B}T}\int_0^\tau dt\dot{x}\circ F_{\lambda(t)}(x) = \frac{Q}{k_{\rm B}T}. \tag{2-3-8}$$

The right hand side of Eq. (2-3-8) is the Langevin heat [Eq. (2-2-3)] divided by the temperature of the heat reservoir, which can be interpreted as the entropy production (in the unit of $k_{\rm B}$) of the heat bath during the time interval τ.

2.3.2 Second Law

To further discuss the Second Law of thermodynamics under the setup of Markov process, we need to introduce the entropy increment of the system of interest during the time interval. This is achieved by adopting the Shannon entropy as the entropy of the system:

$$S(t) := -\int dx P_t(x)\log P_t(x). \tag{2-3-9}$$

By defining the stochastic Shannon entropy difference assigned to the path $\boldsymbol{x}_N$ as[11]

$$s(\boldsymbol{x}_N) := \log\frac{P_0(x_0)}{P_N(x_N)}, \tag{2-3-10}$$

we have $\langle s(\boldsymbol{x}_N)\rangle_{\lambda,N} = S(\tau) - S(0)$. Here the bracket $\langle\cdot\rangle_{\lambda,N}$ denotes the average $\int d\boldsymbol{x}_N P_\lambda(\boldsymbol{x}_N)\cdot$, where $d\boldsymbol{x}_N := \prod_{i=0}^N dx_i$. One reason to take the Shannon entropy as the entropy of the system is that it becomes equivalent to the thermodynamic entropy if the density is in equilibrium, $P_t(x) = P_{\rm eq}(x)$. Although the physical meaning of Eq. (2-3-9) is not clear for general nonequilibrium density, it is useful in proving various relations which we discuss as follows.

Considering that the thermal reservoir and the system of interest compose the total closed system, we expect that $\Sigma(\boldsymbol{x}_N)$ defined as

$$\Sigma(\boldsymbol{x}_N) := s(\boldsymbol{x}_N) + \sigma(\boldsymbol{x}_N), \tag{2-3-11}$$

is positive, from the analogy of macroscopic thermodynamics. In fact, we can prove

$$\langle\Sigma(\boldsymbol{x}_N)\rangle_{\lambda,N} = \int d\boldsymbol{x}_N P_\lambda(\boldsymbol{x}_N)\log\frac{P_\lambda(\boldsymbol{x}_N)}{P_{N\Delta t}(x_N)W_{\lambda^\dagger}(\boldsymbol{x}_N^\dagger|\bar{x}_N)} \geq 0, \tag{2-3-12}$$

where the inequality comes from the positivity of the Kullback-Leibler divergence[12]. Although Eq. (2-3-12) holds for the general initial condition $P_0(x)$ and for any time point in the Markov

[11] The denominator inside the log of the right hand side of Eq. (2-3-10) must be taken as $P_{N\Delta t}(x_N)$ instead of $P_{N\Delta t}(\bar{x}_N)$ in order to make $s(\boldsymbol{x}_N)$ an additive quantity in time. In contrast, we must take $W_{\lambda^\dagger}(\boldsymbol{x}_N^\dagger|\bar{x}_N)$ instead of $\prod_{n=0}^{N-1} W_{\lambda(N-n)}(x_n|x_{n+1})$ in the definition Eq. (2-3-4), for the consistency with the Hamiltonian dynamics.

[12] Since $\int d\boldsymbol{x}_N P_{N\Delta t}(x_N)W_{\lambda^\dagger}(\boldsymbol{x}_N^\dagger|\bar{x}_N) = 1$, the denominator inside the log in Eq. (2-3-12) is a probability density. Note that for the general case where $\bar{x}\neq x$, this density has no sensible meaning; it is different to the reverse path probability. This subtle issue plays a critical role in the problem of whether the irreversible entropy production increases or decreases upon the reduction of dynamics [35], since it is related to the condition in the proof of the monotonicity of Kullback-Leibler divergence [36].

process, in the case for a steady-nonequilibrium dynamics after a sufficiently long time ($N \to \infty$ with fixed Δt, thus $\tau \to \infty$), we have

$$\frac{\langle \Sigma(\boldsymbol{x}_N)\rangle_{\lambda,N}}{N\Delta t} \geq 0 \xrightarrow{N\to\infty} \frac{\langle \sigma(\boldsymbol{x}_N)\rangle_{\lambda,N}}{N\Delta t} \geq 0, \tag{2-3-13}$$

since the contribution from the Shannon entropy production does not diverge in time. This inequality (2-3-13) is the generalization of the positivity of the heat flux shown in Eq. (2-2-11).

Let us remark that Eq. (2-3-12) can also be derived by another general relation

$$\left\langle e^{-\Sigma(\boldsymbol{x}_N)} \right\rangle_{\lambda,N} = 1, \tag{2-3-14}$$

which is referred to as the integral fluctuation theorem [5, 37].

2.4 Stochastic differential equations

Here we briefly note on the treatment of stochastic differential equations. Different interpretations of the integral in the Langevin description is linked to the Fokker-Planck equation. We also mention the calculation of the irreversible entropy production.

2.4.1 Fokker-Planck equation

Consider the overdamped Langevin dynamics,

$$\Gamma \dot{x} \quad = \quad F(x) + \sqrt{2\Gamma k_{\mathrm{B}} T}\xi(t). \tag{2-4-1}$$

Let us first assume that Γ and T both do not depend on x. The discretized version of the dynamics can be written as

$$\Gamma(x_{n+1} - x_n) = F(x_n)\Delta t + \sqrt{2\Gamma k_{\mathrm{B}} T \Delta t} B_n, \tag{2-4-2}$$

where t is now replaced by $n\Delta t$. The term B_n is a stochastic variable that takes random values with the probability density

$$P(B_n) = \frac{1}{\sqrt{2\pi}} e^{-{B_n}^2/2}. \tag{2-4-3}$$

From Eq. (2-4-3), we obtain the transition probabilities of the Langevin dynamics, such as in Eqs. (2-3-6, 2-6-8). Assuming that each B_n is chosen independently for each time point n with respect to the density Eq. (2-4-3), we have

$$\langle B_n B_{n'} \rangle = \begin{cases} \int_{-\infty}^{\infty} dB P(B) B^2 = 1 & (n = n') \\ \int_{-\infty}^{\infty} dB P(B) B \times \int_{-\infty}^{\infty} dB' P(B') B' = 0 & (n \neq n') \end{cases} \tag{2-4-4}$$

Here, $\langle\cdot\rangle$ denotes the ensemble average. Now, by setting

$$\xi(t) := \lim_{\Delta t\to 0} B_n/\sqrt{\Delta t}, \tag{2-4-5}$$

we have

$$\langle\xi(t)\xi(s)\rangle = \lim_{\Delta t\to 0}\left\langle\frac{B_n B_{n'}}{\Delta t}\right\rangle = \begin{cases}\lim_{\Delta t\to 0} 1/\Delta t & (t=s)\\ 0 & (t\neq s)\end{cases}, \tag{2-4-6}$$

which can be written as

$$\langle\xi(t)\xi(s)\rangle = \delta(t-s). \tag{2-4-7}$$

Let us introduce a simple derivation of the Fokker-Planck equation using this discretized dynamics. For some function $g(x)$, consider the Taylor expansion

$$g(x_{n+1}) - g(x_n) = (x_{n+1}-x_n)\left.\frac{dg(x)}{dx}\right|_{x=x_n} + \frac{1}{2}(x_{n+1}-x_n)^2\left.\frac{d^2g(x)}{dx^2}\right|_{x=x_n} + \ldots \tag{2-4-8}$$

The ensemble average of the left hand side of Eq. (2-4-8) is, using the density functions $P_n(x)$ and $P_{n+1}(x)$,

$$\langle g(x_{n+1}) - g(x_n)\rangle = \int_{-\infty}^{\infty} dx[P_{n+1}(x)-P_n(x)]g(x) = \Delta t\int_{-\infty}^{\infty} dx g(x)\frac{\partial P_t(x)}{\partial t} + O(\Delta t^2). \tag{2-4-9}$$

The ensemble average of the right hand side

$$\left\langle (x_{t+\Delta t}-x_t)\left.\frac{dg(x)}{dx}\right|_{x=x_t} + \frac{1}{2}(x_{t+\Delta t}-x_t)^2\left.\frac{d^2g(x)}{dx^2}\right|_{x=x_t} + \ldots\right\rangle, \tag{2-4-10}$$

can be rewritten as

$$\left\langle \frac{F(x_n)}{\Gamma}\Delta t\left.\frac{dg(x)}{dx}\right|_{x=x_n} + \frac{k_{\mathrm{B}}T\Delta t}{\Gamma}\left.\frac{d^2g(x)}{dx^2}\right|_{x=x_n} + O(\Delta t^2)\right\rangle, \tag{2-4-11}$$

by using Eq. (2-4-2) and

$$\langle B_n h(x_n)\rangle = 0 \tag{2-4-12}$$

$$\langle {B_n}^2 h(x_n)\rangle = \langle h(x_n)\rangle, \tag{2-4-13}$$

which holds for arbitrary functions $h(x)$. The term (2-4-11) further be rewritten as

$$\Delta t\int_{-\infty}^{\infty} dx P_t(x)\left[\frac{F(x)}{\Gamma}\frac{dg(x)}{dx} + \frac{k_{\mathrm{B}}T}{\Gamma}\frac{d^2g(x)}{dx^2}\right] + O(\Delta t^2) \tag{2-4-14}$$

$$= \Delta t\int_{-\infty}^{\infty} dx g(x)\left\{\frac{1}{\Gamma}\frac{\partial}{\partial x}[-F(x)P_t(x)] + \frac{T}{\Gamma}\frac{\partial^2}{\partial x^2}P_t(x)\right\} + O(\Delta t^2), \tag{2-4-15}$$

Comparing (2-4-9) with (2-4-15), we obtain

$$\frac{\partial P_t(x)}{\partial t} = -\frac{1}{\Gamma}\frac{\partial}{\partial x}[F(x)P_t(x)] + \frac{k_{\rm B}T}{\Gamma}\frac{\partial^2}{\partial x^2}P_t(x). \tag{2-4-16}$$

which is the Fokker-Planck equation.

The time evolution equation (2-4-16) can also be written using the current $J_t(x)$:

$$\frac{\partial P_t(x)}{\partial t} = -\frac{\partial}{\partial x}\left\{\frac{F(x)}{\Gamma}P_t(x) - \frac{k_{\rm B}T}{\Gamma}\frac{\partial}{\partial x}P_t(x)\right\} \tag{2-4-17}$$

$$= -\frac{\partial}{\partial x}J_t(x). \tag{2-4-18}$$

Since $J_t(x) = 0$ is a sufficient condition for the left hand side of Eq. (2-4-18) to be zero, we have the equilibrium density described in Eq. (2-2-12), if $F(x) = -U'(x)$. In general, under the presence of nonequilibrium driving force, $F(x) = f - U'(x)$, it is impossible to obtain a density which satisfies $J_t(x) = 0$. Nevertheless, the steady-state density can be obtained as the solution to $J_t(x) = J_{\rm st}$ =const.

2.4.2 Case of position dependent temperature/friction

Let us next consider the case where the temperature is not uniform in space:

$$\Gamma\dot{x} = F(x) + \sqrt{2\Gamma k_{\rm B}T(x)} \bullet \xi(t). \tag{2-4-19}$$

Such case where the noise term depends on the value of the stochastic variable is called a dynamics with multiplicative noise. Given Eq. (2-4-19), we have multiple ways to define the discrete version of the dynamics corresponding to different interpretations of the multiple denoted as $\bullet$:

$$\Gamma(x_{n+1} - x_n) = F(x_n)\Delta t + \sqrt{2\Gamma k_{\rm B}T(\tilde{x}_n)\Delta t}B(t), \tag{2-4-20}$$

where $\tilde{x}_n$ is defined using a parameter $0 \le p \le 1$:

$$\tilde{x}_n = px_n + (1-p)x_{n+1}. \tag{2-4-21}$$

Interpreting $\bullet$ as $p = 1$ in Eq. (2-4-20) is called the Itô interpretation (typically written as $\cdot$), where as $p = 1/2$ (written as $\circ$) and $p = 0$ are called the Stratonovich and anti-Itô interpretations, respectively [38].

In contrast to the usual differential equation where the dependence of the dynamics on such p becomes negligible for sufficiently small Δt, the stochastic differential equation described by Eq. (2-4-20) has strong dependence on p, irrespective of the smallness of Δt. To see this, we start from

$$\sqrt{T(\tilde{x}_n)} = \sqrt{T(x_n)}\left[1 + \frac{1}{2}(\tilde{x}_n - x_n)\frac{1}{T(x)}\left.\frac{dT(x)}{dx}\right|_{x=x_n} + O(\Delta t^{3/2})\right]. \tag{2-4-22}$$

Noticing that

$$\tilde{x}_n - x_n \;=\; (1-p)(x_{n+1}-x_n) = (1-p)\sqrt{\frac{2k_{\rm B}T(x_n)}{\Gamma}\Delta t}B(t) + O(\Delta t), \tag{2-4-23}$$

we arrive at

$$\Gamma(x_{n+1}-x_n) = F(x_n)\Delta t + \sqrt{2\Gamma k_{\rm B}T(x_n)\Delta t}B_n + (1-p){B_n}^2 k_{\rm B}\left.\frac{dT(x)}{dx}\right|_{x=x_n}\Delta t + O(\Delta t^2). \tag{2-4-24}$$

The third term in Eq. (2-4-24) is the non-negligible contribution from p and the inhomogeneity of the temperature. Recalling Eq. (2-4-13), we substitute ${B_n}^2$ in the third term with 1[13]. Thus, we obtain the Langevin equation for general p with an Itô interpretation in the multiplicative noise:

$$\Gamma\dot{x} = (1-p)k_{\rm B}T'(x) + F(x) + \sqrt{2\Gamma k_{\rm B}T(x)}\cdot\xi(t). \tag{2-4-25}$$

Starting from Eq. (2-4-25), we can follow the path that we obtained Eq. (2-4-16) to show

$$\frac{\partial P_t(x)}{\partial t} = -\frac{1}{\Gamma}\frac{\partial}{\partial x}\left\{\left[F(x) + (1-p)k_{\rm B}T'(x)\right]P_t(x)\right\} + \frac{\partial^2}{\partial x^2}\left[\frac{k_{\rm B}T(x)}{\Gamma}P_t(x)\right]. \tag{2-4-26}$$

For an equilibrium density to exist, it should satisfy

$$\frac{d}{dx}P_{\rm eq}(x) = \frac{F(x) - pk_{\rm B}T'(x)}{k_{\rm B}T(x)}P_{\rm eq}(x), \tag{2-4-27}$$

which means that if x is subjected to some boundary condition like $0 \le x \le L$, we can define

$$V(x) = -\int_0^x dx\frac{F(x')}{k_{\rm B}T(x')}, \tag{2-4-28}$$

and then $P_{\rm eq}(x) \propto \exp[-V(x)]/T(x)^p$ is the solution. Notice that this density different to the usual canonical density for any p, even in the case of $F(x) = -U'(x)$. This means that the inhomogeneous temperature is an intrinsically nonequilibrium setup.

A similar discussion follows for the case where the friction coefficient Γ depends on the position

$$x_{t+\Delta t} - x_t = -\frac{k}{\Gamma(x_t)}x_t\Delta t + \sqrt{\frac{2k_{\rm B}T\Delta t}{\Gamma(\tilde{x}_t)}}B(t), \tag{2-4-29}$$

by using $\tilde{x}$ in Eq. (2-4-21) again. We arrive at

$$\frac{\partial P_t(x)}{\partial t} = -\frac{\partial}{\partial x}\left\{\left[\frac{F(x)}{\Gamma(x)} + (1-p)\left(\frac{1}{\Gamma(x)}\right)' k_{\rm B}T\right]P_t(x)\right\} + \frac{\partial^2}{\partial x^2}\left[\frac{k_{\rm B}T}{\Gamma(x)}P_t(x)\right], \tag{2-4-30}$$

[13]Since ${B_n}^2$ is a stochastic quantity, it fluctuates around its average value, 1. It is reasonable to neglect this fluctuation, since it will only contribute to a term proportional to Δt, which is order $\sqrt{\Delta t}$ smaller than the second term in the right hand side of Eq. (2-4-24).

where we wrote $d\Gamma(x)^{-1}/dx$ as $(1/\Gamma(x))'$. In contrast to the case of inhomogeneous temperature, an equilibrium density can be obtained for $F(x) = -U'(x)$ in this case:

$$P_{\rm eq}(x) \propto [\Gamma(x)]^p \exp\left[-\frac{U(x)}{k_{\rm B}T}\right]. \tag{2-4-31}$$

For the case of $p = 0$, we recover the canonical distribution, Eq. (2-2-12).

2.4.3 Physical interpretation

Although we considered p as a general parameter up to here, the value of p is actually determined in the physical system if we start from the underdamped Langevin equation

$$\dot{x} = v, \qquad M\dot{v} = -\Gamma(x)v + F(x) + \sqrt{2\Gamma(x)k_{\rm B}T(x)}\xi(t), \tag{2-4-32}$$

and consider the elimination of the velocity variable v. The key here is that there is no issue in the interpretation of the multiple in Eq. (2-4-32), since the fluctuation term appears in the differential equation of v and not in that of x. The overdamped Langevin equation is obtained as

$$\dot{x} = F(x) + \frac{\Gamma'(x)}{\Gamma'(x)}k_{\rm B}T + \sqrt{2\Gamma(x)k_{\rm B}T(x)}\cdot\xi(t), \tag{2-4-33}$$

which means that we should take the Itô interpretation in Eq. (2-4-19) and the anti-Itô interpretation in Eq. (2-4-29).

Equation (2-4-33) is obtained for the case where the position dependence of T and Γ are static. In other words, this is the case where the time it takes for Γ and T to change its value according to the motion of x is faster than the time-scale of the velocity variable, M/Γ. It is natural that in such situations, the position dependent friction coefficient alone cannot derive the system out of equilibrium, as proved by substituting $p = 0$ in Eq. (2-4-31). As will be discussed in Chapter 4, the situation changes when the time-scale of the change in Γ is slower than M/Γ, which allows nonequilibrium phenomena to arise.

2.4.4 Positivity of irreversible entropy production

Let us come back to Eq. (2-4-1) and prove the positivity of the irreversible entropy production rate:

$$\left\langle \dot{\Sigma}(t) \right\rangle_t = \dot{S}(t) + \frac{\langle \dot{Q} \rangle_t}{k_{\rm B}T} \geq 0. \tag{2-4-34}$$

where we denoted the ensemble average at a transient time t as $\langle\rangle_t$ Although the inequality (2-4-34) is included in the general scheme, Eq. (2-3-12), we note here for convenience [see Eq. (2-6-21)] and the sake of completeness.

From Eq. (2-4-18), the time derivative of the Shannon entropy is simply obtained as,

$$\dot{S}(t) = -\int dx \frac{\partial P_t(x)}{\partial t}\log P_t(x) = -\int dx \frac{J_t(x)P_t'(x)}{P_t(x)}. \tag{2-4-35}$$

Next, the average of the Langevin heat becomes

$$\langle \dot{Q} \rangle_t = \langle \dot{x} \circ F(x) \rangle_t = \left\langle \frac{F(x)^2}{\Gamma} + \sqrt{\frac{2k_{\rm B}T}{\Gamma}} \xi(t) \circ F(x) \right\rangle_t . \tag{2-4-36}$$

The second term in the bracket in the right hand side has the Stratonovich integral, thus by using Eqs. (2-4-12) and (2-4-13), it should be rewritten as

$$\begin{aligned} \langle \xi(t) \circ F(x) \rangle_t &= \left\langle \frac{B_n}{\sqrt{\Delta t}} F\left(\frac{x_{n+1} + x_n}{2} \right) \right\rangle_t \\ &= \left\langle \frac{B_n}{\sqrt{\Delta t}} \left[F\left(x_n\right) + \frac{x_{n+1} - x_n}{2} F'(x_n) + O(\Delta t) \right] \right\rangle_t \\ &= \left\langle \frac{B_n}{\sqrt{\Delta t}} \left[F\left(x_n\right) + \sqrt{\frac{k_{\rm B}T\Delta t}{2\Gamma}} B_n F'(x_n) + O(\Delta t) \right] \right\rangle_t \\ &= \sqrt{\frac{k_{\rm B}T}{\Gamma}} \langle F'(x_n) \rangle_t, \end{aligned} \tag{2-4-37}$$

where we used = in the sense of equality obtained at $\Delta t \to 0$ in the first and last lines. Hence, we arrive at the simple formula [39]:

$$\begin{aligned} \left\langle \dot{\Sigma}(t) \right\rangle_t &= \int dx \left[P_t(x) \frac{F(x)^2}{\Gamma k_{\rm B}T} + \frac{1}{\Gamma} P_t(x) F'(x) + \frac{J_t(x) P_t'(x)}{P_t(x)} \right] \\ &= \frac{\Gamma}{k_{\rm B}T} \int dx \frac{J_t(x)^2}{P_t(x)} \geq 0. \end{aligned} \tag{2-4-38}$$

2.5 Phenomenological model of molecular motors

Here we consider a specific type of stochastic process, a chemically-induced single-molecule transport. The model we introduce is a mixture of Brownian motion and discrete stochastic switching.

2.5.1 Setup

We are interested in the transport driven by molecular motors. Although the motion of molecular motors was first observed as a sliding and continuous motion [1], we now know that the discrete chemical reaction steps are responsible for the fundamental dynamics, as will be described in the following chapters for various motors. Since the center of mass of the motors are undergoing the usual overdamped Brownian motion, we need to combine this stochastic motion in the continuous space with the discrete space (chemical reaction) in order to discuss the physics. Here we introduce a general framework that includes such dynamics.

We start from the overdamped dynamics, Eq. (2-2-1), but consider that the parameter λ takes discrete values, $\lambda = m = 0, \pm 1, \pm 2, ...$ The dynamics of λ is given by the Markov jump process.

The Markov jump process is described by the switching rates, which generally depend on the position of the particle, x. We further assume that the stochastic switching occurs only between nearest neighbors. Therefore, it is sufficient to define the switching rate functions $R_m^+(x)$ and $R_m^-(x)$, which represent the switchings $m \to m+1$ and $m \to m-1$, respectively.

Each states described by the variable m has its corresponding potential energy, $U_m(x)$. The Langevin dynamics reads

$$\Gamma \dot{x} = f_{\text{ext}} - U'_m(x) + \sqrt{2\Gamma k_{\text{B}} T}\xi(t). \tag{2-5-1}$$

where we wrote $U'_m(x) := \partial U_m(x)/\partial x$. We have in mind the case where the external force f_{ext} is externally applied to the probe of interest, through an optical tweezer with feedback or electric field [16]. The total stochastic process, concerning both x and m could be written by

$$\begin{aligned}\frac{\partial P_t(x,m)}{\partial t} = \frac{\partial}{\partial x}\left\{\left[U'_m(x) - f_{\text{ext}}\right]P_t(x,m) + \frac{k_{\text{B}}T}{\Gamma}\frac{\partial}{\partial x}P_t(x,m)\right\} \\ + R^+_{m-1}(x)P_t(x,m-1) + R^-_{m+1}(x)P_t(x,m+1) - [R^+_m(x) + R^-_m(x)]P_t(x,m)\end{aligned} \tag{2-5-2}$$

The first line in the right hand side of Eq. (2-5-2) corresponds to the usual Fokker-Planck dynamics (see Sect. 2.4), and the second line corresponds to the switching of m.t

We assume that there is a steady-state in this stochastic dynamics, meaning that if a periodic boundary condition set in both x and m, the density function $P_t(x,m)$ will converge to $P_{\text{st}}(x,m)$ after a sufficiently long time.

2.5.2 Energetics of model

The average of the energy difference between the time interval τ after the system has fallen into a steady-state is

$$\langle \Delta U \rangle_{\text{st}} = \left\langle U_{m(\tau)}(x(\tau)) - U_{m(0)}(x(0)) - f_{\text{ext}}\int_0^\tau dt \dot{x}(t)\right\rangle_{\text{st}} \tag{2-5-3}$$

$$= -f_{\text{ext}} v_{\text{st}} \tau \tag{2-5-4}$$

Here, the steady-state average denoted by $\langle\rangle_{\text{st}}$ is the average taken over (x,m) with the density $P_{\text{st}}(x,m)$ and the transition probability. The steady-state average velocity is $v_{\text{st}} := \langle \dot{x}(s)\rangle_{\text{st}}$. Equation (2-5-4) can also be decomposed as

$$\langle \Delta U \rangle_{\text{st}} = \tau \int dx \sum_m \Lambda_m(x)\left[U_{m+1}(x) - U_m(x)\right] - \left\langle \int_0^\tau dt[f_{\text{ext}} - U'_{m(t)}(x(t))] \circ \dot{x}(t)\right\rangle_{\text{st}} \tag{2-5-5}$$

$$= \langle W \rangle_{\text{st}} - \langle Q \rangle_{\text{st}}. \tag{2-5-6}$$

The two terms in the right hand side of Eq. (2-5-5) have distinct physical meanings from the point of view of the system's energy exchange with the thermal bath. The first term corresponds

to W in Eq. (2-2-6); it is the energy shift that accompanies the switching of m, defined using the steady-state switching position density

$$\Lambda_m(x) := P_{\rm st}(x,m)R^+_m(x) - P_{\rm st}(x,m+1)R^-_{m+1}(x). \tag{2-5-7}$$

The the second term of the right hand side of Eq. (2-5-5) is the energy that flows through the one-dimensional Brownian motion (Langevin heat).

Whether or not to call W in Eq. (2-5-5) as work or heat depends on the physical mechanism behind the switching of m. If we consider an external macroscopic system that drives m deterministically, it is natural to call the energy required to switch the potentials $U_m(x)$ as work. If on the other hand, there is no external system that drives the motion in this system apart from the thermal bath, we must assume

$$\frac{R^+_m(x)}{R^-_{m+1}(x)} = \exp\left[\frac{U_m(x) - U_{m+1}(x)}{k_{\rm B}T}\right], \tag{2-5-8}$$

which is the detailed balance condition. This implies that the switching of potentials is itself a stochastic thermodynamic phenomena. Setting $f_{\rm ext} = 0$ together with the condition Eq. (2-5-8), we have an equilibrium dynamics with no current, $v_{\rm st} = 0$ and $\langle W\rangle_{\rm st} = Q_{\rm st} = 0$.

In the case of molecular motors, the switching of m is indeed a stochastic process which follow a similar detailed balance condition, but with an external supply of chemical free energy. Such situation may be realized by combining the detailed balance Eq. (2-5-8) with the bias in the chemical reaction:

$$\frac{R^+_m(x)}{R^-_{m+1}(x)} = \exp\left[\frac{U_m(x) - U_{m+1}(x) + \Delta\mu_{m\to m+1}}{k_{\rm B}T}\right] \tag{2-5-9}$$

Here, $\Delta\mu_{m\to m+1}$ is the free energy difference caused in the chemical reaction that accompanies the switching $m \to m+1$, which makes the additional bias, $\exp[\Delta\mu_{m\to m+1}/k_{\rm B}T]$. If for instance $\Delta\mu_{m\to m+1}$ is positive for all m, and the minimal position x of the potentials $U_m(x)$ is an increasing function of m, then the nonequilibrium unidirectional chemical reaction will drive motion in x (i.e.,$\langle\dot{x}\rangle_{\rm st}$), even when $f_{\rm ext} = 0$ or even $f_{\rm ext} < 0$. Note that the full stochastic dynamics which takes in to account the transition of x and m is consistent with the picture of stochastic thermodynamics [Eq. (2-3-4)] if we take into account the contribution of $\Delta\mu_{m\to m+1}$ in the heat entropy production. This case, which is of most interest in this thesis, will be explained in detail for the model of F_1-ATPase in Sect. 3.4.

Another type of dynamics we can consider is the switching of the value of diffusion constant, more specifically Γ. The reason for unidirectional motion under such setup is less trivial compared with the potential switching scheme, although it can be understood as a nonequilibrium phenomenon through the knowledge on stochastic differential equations presented in Sect. 2.4. This will be the main topic when considering the model for cytoplasmic motors in Chapter 4.

2.6 Nonequilibrium fluctuation response relations

Here we briefly review the nonequilibrium fluctuation response relations (FRR) in the nonequilibrium models. Although one of the main motivation of this research topic was to quantify heat

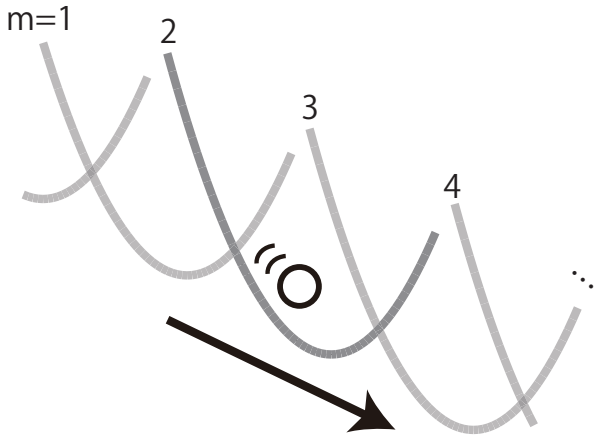

Fig 2.1: Example of the Brownian motion model with chemically-induced potential switching. Each integer m has its corresponding potential. Such model appear in the model of F_1-ATPase, discussed in the next chapter.

dissipation in molecular motors [40], there has been considerable progress in the pure-theoretical side. This is one of the research fields where the practical problems of biophysics motivated the investigation of fundamental problems in statistical physics.

2.6.1 Quantifying heat through the violation of FRR

Even if we assumed the phenomenological model for molecular motors as described in the previous section, we do not know the potential form $U_m(x)$, the applied external force f, or the switching rate functions, $R_m^{\pm}(x)$. Then, the question we address is follows: is it possible to quantify the steady-state heat flow $\langle \dot{Q} \rangle_{\rm st}$ through experimental observation, under the constraint that we do not know the detail of the model parameters?

In this direction, a remarkable idea was presented by Harada and Sasa in 2005 [41]. The authors focused on the fluctuation dissipation relation, which is a macroscopic relation that is accessible in experiment, and proposed a way to utilize the violation of this relation to quantify the heat dissipation. Here we present a simple proof of their theorem, based on the discussions in [42, 43].

Consider the velocity autocorrelation function, and the velocity response function:

$$C(t) := \langle [\dot{x}(s) - v_{\rm st}][\dot{x}(t+s) - v_{\rm st}] \rangle_{\rm st} \tag{2-6-1}$$

$$R(t) := \frac{\delta \langle \dot{x}(s+t) \rangle_{\epsilon}}{\delta \epsilon(s)}. \tag{2-6-2}$$

Their Fourier transforms are defined as

$$\widetilde{C}(\omega) := \int_{-\infty}^{\infty} dt e^{i\omega t} C(t) \tag{2-6-3}$$

$$\widetilde{R'}(\omega) := \mathrm{Re}\left[\int_{-\infty}^{\infty} dt e^{i\omega t} R(t)\right] = \int_{-\infty}^{\infty} dt e^{i\omega t} \frac{R(t) + R(-t)}{2}. \tag{2-6-4}$$

The average denoted by $\langle\rangle_\epsilon$ in Eq. (2-6-2) is also a steady-state average, but for a modified dynamics with a small time-dependent perturbative force $\epsilon(t)$:

$$\Gamma \dot{x} = f_{\mathrm{ext}} + \epsilon(t) - U_m'(x) + \sqrt{2\Gamma k_{\mathrm{B}} T}\xi(t). \tag{2-6-5}$$

Note that $C(t), R(t)$, and v_{st} do not depend on the reference time s because of the time-translational invariance of the steady-state ensemble. We may consider the natural extension of the following results to the case of transient ensembles, nevertheless we stick to the steady-state case since it is most accessible

It is natural to compare the fluctuation and response defined as Eqs. (2-6-1) and (2-6-2), since $\epsilon(t)$ is the conjugate force of the flow $\langle \dot{x} \rangle$. By preparing an equilibrium dynamics with the detailed balance condition Eq. (2-5-8) and $f_{\mathrm{ext}} = 0$, we may prove

$$R(t) = \begin{cases} C(t)/k_{\mathrm{B}}T & t \geq 0 \\ 0 & t < 0 \end{cases}, \tag{2-6-6}$$

which is equivalent to

$$\widetilde{C}(\omega) = 2k_{\mathrm{B}}T\widetilde{R'}(\omega). \tag{2-6-7}$$

Eqs. (2-6-6, 2-6-7) are the fluctuation response relations.

As we have done in Eq. (2-3-6), it is convenient to consider the time-discretized dynamics of the stochastic process. The stochastic variables (x, m) follows the path $(\boldsymbol{x}_N, \boldsymbol{m}_N)$, where N is a sufficiently large integer. Let us replace s and t by $n'\Delta t$ and $n\Delta t$, respectively $(n + n' < N, 0 \leq n, n')$. The transition probability for a single time step (Δt) should be written as

$$W_n^\epsilon(x', m'|x, m) = \begin{cases} W_{n,m}^\epsilon(x'|x) \propto \exp\left\{-\dfrac{\left[\Gamma(x'-x) - \left(f_{\mathrm{ext}} + \epsilon_n - U_m'(x)\right)\Delta t\right]^2}{4\Gamma k_{\mathrm{B}} T \Delta t}\right\} & (\text{if } m = m') \\ R_m^+(x)\Delta t & (\text{if } x' = x \;\&\; m' = m+1) \\ R_m^-(x)\Delta t & (\text{if } x' = x \;\&\; m' = m-1) \\ 0 & (\text{else}) \end{cases} \tag{2-6-8}$$

where the explicit time-dependence through n is due to the perturbative force $\epsilon_n = \epsilon(t)$. The normalization factor for the first line in Eq. (2-6-8) is determined so as to satisfy the condition $\int dx' \sum_{m'} W_n^\epsilon(x', m'|x, m) = 1$.

The right hand side of Eq. (2-6-2) is now written as

$$\frac{\delta\langle\dot{x}(s+t)\rangle_\epsilon}{\delta\epsilon(s)} = \frac{d}{d\epsilon_{n'}}\int d\boldsymbol{x}_N \sum_{\boldsymbol{m}_N} P^\epsilon(\boldsymbol{x}_N,\boldsymbol{m}_N)\frac{x_{n+n'+1}-x_{n+n'}}{\Delta t} \tag{2-6-9}$$

$$= \lim_{\epsilon_{n'}\to 0}\frac{1}{\epsilon_{n'}}\int d\boldsymbol{x}_N \sum_{\boldsymbol{m}_N} P^{\epsilon=0}(\boldsymbol{x}_N,\boldsymbol{m}_N)\left[\frac{P^\epsilon(\boldsymbol{x}_N,\boldsymbol{m}_N)}{P^{\epsilon=0}(\boldsymbol{x}_N,\boldsymbol{m}_N)}-1\right]\frac{x_{n+n'+1}-x_{n+n'}}{\Delta t}, \tag{2-6-10}$$

with the path probability defined as

$$P^\epsilon(\boldsymbol{x}_N,\boldsymbol{m}_N) := P_{\rm st}(x_0,m_0)\prod_{n=0}^{N-1} W_n^\epsilon(x_{n+1},m_{n+1}|x_n,m_n). \tag{2-6-11}$$

We here use = in the sense of equality obtained in the limit $\Delta t \to 0$ without remark. Since the perturbative force does not affect the transition probability of m, the ratio between the path probabilities is

$$\frac{P^\epsilon(\boldsymbol{x}_N,\boldsymbol{m}_N)}{P^{\epsilon=0}(\boldsymbol{x}_N,\boldsymbol{m}_N)} \simeq \exp\left\{\prod_{n=0}^{N-1}\frac{\epsilon_n}{2\Gamma k_{\rm B}T}\left[\Gamma\frac{x_{n+1}-x_n}{\Delta t} - f_{\rm ext} + U'_{m_n}(x_n)\right]\right\}, \tag{2-6-12}$$

up to the smallest order in ϵ. Therefore,

$$R(t) = \int d\boldsymbol{x}_N \sum_{\boldsymbol{m}_N} P^{\epsilon=0}(\boldsymbol{x}_N,\boldsymbol{m}_N)\frac{1}{2\Gamma k_{\rm B}T}\left[\Gamma\frac{x_{n'+1}-x_{n'}}{\Delta t} - f_{\rm ext} + U'_{m_{n'}}(x_{n'})\right]\frac{x_{n+n'+1}-x_{n+n'}}{\Delta t} \tag{2-6-13}$$

Noticing that

$$\frac{1}{2\pi}\int_{-\infty}^{\infty} d\omega\widetilde{C}(\omega) = \lim_{t\to 0}\frac{C(t)+C(-t)}{2} \tag{2-6-14}$$

$$\frac{1}{2\pi}\int_{-\infty}^{\infty} d\omega\widetilde{R}'(\omega) = \lim_{t\to 0}\frac{R(t)+R(-t)}{2}, \tag{2-6-15}$$

we now arrive at

$$\dot{Q}_{\rm st} = \Gamma v_{\rm st}^2 + \frac{\Gamma}{2\pi}\int_{-\infty}^{\infty} d\omega\left[\widetilde{C}(\omega) - 2k_{\rm B}T\widetilde{R}'(\omega)\right]. \tag{2-6-16}$$

The theorem Eq. (2-6-16) has a clear interpretation that the two quantities which value the extent of nonequilibrium, the steady heat dissipation and the violation of the fluctuation response relation, are linked in the most simplest manner.

For a tilted periodic potential model [Eq. (2-2-7)], i.e., when there is no switching in m, we can easily prove from Eq. (2-2-8) that $\dot{Q}_{\rm st} \geq \Gamma v_{\rm st}^2$, with the equality obtained for the case where $U'(x) = 0$. Therefore, the integral term in Eq. (2-6-16) appears as a consequence of the inhomogeneity in space of the force experienced by the probe.[14]

[14]This led to the definition of Stokes efficiency [44]. In the existence of the switching variable m, however, the inequality $\dot{Q}_{\rm st} \geq \Gamma v_{\rm st}^2$ does not hold in general; it is even possible for $\dot{Q}_{\rm st}$ to become negative. Such situation does not contradict with the Second Law, since the total irreversible entropy production, which includes the dissipation from the dynamics of m, is always positive [Eq. (2-3-12)]. Such compensation of entropy production from a sub-system for another is deeply related to the problem of Maxwell's demon [45, 7, 8], which is beyond the scope of this thesis.

The integrals taken in Eq. (2-6-14) diverges to infinity if taken separately. Firstly, $C(t \to 0) = \langle \dot{x}^2 \rangle \simeq 2D\delta(t \to 0)$. Second, since the left hand side of Eq. (2-6-16) is finite in ordinary situations, this divergence means that the integral in Eq. (2-6-15) will also diverge. Note that in the high frequency regime, the correlation and response functions should converge:

$$\widetilde{C}(\omega), 2k_{\mathrm{B}}T\widetilde{R}'(\omega) \xrightarrow{\omega\to\infty} \frac{2k_{\mathrm{B}}T}{\Gamma}, \tag{2-6-17}$$

since for a very small time-scale, the fluctuation term dominates in the Langevin dynamics, and the effective dynamics is dominated by the free Brownian motion, Eq. (2-1-1).

Apart from its physical meaning, what is most significant about Eq. (2-6-16) is that the quantities in the right hand side can be measured by macroscopic experiments, in the sense that the long time average can be effectively taken without the knowledge of the functional forms of $U_m(x)$ or the values of f_{ext}. In fact, we need not to assume anything about the discrete variable m in the data analysis; the relation (2-6-16) does not depend on the type of dynamics introduced through λ, as far as there exists a steady-state in the total stochastic dynamics. Thus, Eq. (2-6-16) was utilized in exploring the heat dissipative feature of the molecular motor F_1-ATPase, which will be discussed as a main topic in Chapter 3.

2.6.2 FRR, model estimate, and entropy-frenesy correspondence

Since the fluctuation response relation is one of the most fundamental equations in statistical physics, considerable efforts have been devoted to the research on its extension to nonequilibrium situations. For example, Speck and Seifert argued that there is a natural extension of the fluctuation response relation for the nonequilibrium steady-state setup [46]. In the case of tilted periodic potential setup [Eq. (2-2-7)], they obtained

$$R(t) = \begin{cases} C_{\mathrm{lc}}(t)/k_{\mathrm{B}}T & t \geq 0 \\ 0 & t < 0 \end{cases}, \tag{2-6-18}$$

where the new correlation function is defined as

$$C_{\mathrm{lc}}(t) = \langle [\dot{x}(s) - v(x(s))][\dot{x}(t+s) - v(x(t+s))] \rangle_{\mathrm{st}} . \tag{2-6-19}$$

The quantity denoted by $v(x)$ is the local velocity:

$$v(x) = \frac{v_{\mathrm{st}}}{LP_{\mathrm{st}}(x)}. \tag{2-6-20}$$

where J_{st} is the steady-state flow [see Eq. (2-4-18)] and L is the length of the periodically bound region.

The reason for the simple relation Eq. (2-6-19) comes from the equality

$$\dot{Q}_{\mathrm{st}} = \Gamma \langle v(x)^2 \rangle_{\mathrm{st}}, \tag{2-6-21}$$

which can be generalized for the non-steady-state case as Eq. (2-4-38). We can directly use Eq. (2-6-21) to quantify the heat dissipation; all we need to measure is the steady-state velocity $v_{\rm st}$ and the precise steady-state density $P_{\rm st}(x)$.

Apart from the general difficulty to measure the precise form of $P_{\rm st}(x)$, especially at the points where $1/P_{\rm st}(x)$ gives large contribution in the ensemble, there is a practical reason why we cannot use Eq. (2-6-21) to estimate the heat dissipation for the case of the stochastic switching model introduced in Sect. 2.5. In experiment, the typically observed variable is the position of the Brownian particle, x, and thus the information on m is not, in general, accessible. This means that we can only measure the steady-state density

$$P_{\rm st}(x) := \sum_m P_{\rm st}(x,m). \tag{2-6-22}$$

However, in order to quantify the steady heat dissipation in this setup, we also need to observe the variable m since the local velocity requi

$$\dot{Q}_{\rm st} = \Gamma \langle v(x,m)^2 \rangle_{\rm st} = \Gamma \left\langle \frac{v_{\rm st}^2}{L^2 P_{\rm st}(x,m)^2} \right\rangle_{\rm st}. \tag{2-6-23}$$

Indeed, it has been confirmed in experiment for the rotary molecular motor F_1-ATPase, (S. Toyabe, private communication, 2012) that Eq. (2-6-18) does not hold if one defines $v(x)$ using the naive steady-state density, Eq. (2-6-22). This means that the dynamics of F_1-ATPase cannot be modeled by a tilted-periodic potential setup, and the chemical degree of freedom, m, needs to be taken into account explicitly.

Another branch of theories were studied by Baiesi, Wynants, and Maes [47, 48, 49]. They focused on the quantity named frenesy. Before we explain their works, let us note on the interesting aspect behind the structure of Eqs. (2-6-16) and (2-6-18). Under the setup of tilted periodic potential $F(x) = f - dU(x)/dx$, we may prove two equalities:

$$\frac{\Gamma}{2\pi}\int_{-\infty}^{\infty} d\omega \left[\widetilde{C}(\omega) - \frac{2k_{\rm B}T}{\Gamma} \right] + \Gamma v_{\rm st}^2 = 4k_B T \langle \lambda(x) \rangle_{\rm st}, \tag{2-6-24}$$

$$\frac{\Gamma}{2\pi}\int_{-\infty}^{\infty} d\omega \left[2k_B T \widetilde{R}'(\omega) - \frac{2k_{\rm B}T}{\Gamma} \right] = -\frac{(k_B T)^2}{\Gamma} \left\langle \left(\frac{P_{\rm st}'(x)}{P_{\rm st}(x)} \right)^2 \right\rangle_{\rm st}. \tag{2-6-25}$$

We introduced the frenesy as

$$\lambda(x) := \frac{F(x)^2}{8\Gamma k_{\rm B}T} + \frac{1}{4\Gamma}\frac{dF(x)}{dx}, \tag{2-6-26}$$

which has the dimension of time^{-1}. Note that because of Eq. (2-6-17), it is consistent that the right hand sides of Eqs. (2-6-24) and (2-6-25) are both finite.

The frenesy [Eq. (2-6-26)] has a physical meaning as the escape rate from site x. To see this, we consider the Langevin equation in continuous time and discretized space to consider

the corresponding Markov jump process. Assuming that the positions x, x' are placed on lattice points, we define the jump rate from site x to site x' as

$$R(x \to x') = w(x' - x) \exp\left\{ \frac{U(x) - U(x') + f(x' - x)}{2k_{\rm B}T} \right\}. \tag{2-6-27}$$

To obtain the Langevin description from Eq. (2-6-27) through the Kramers-Moyal expansion [18], we require $\sum_r rw(r) = 0$, $\sum_r r^2 w(r) = 2k_{\rm B}T/\gamma$, and that the higher order moments are negligible. Now, the escape rate is defined and calculated as

$$\sum_{x' \neq x} R(x \to x') \simeq \sum_{r \neq 0} w(r) \left[1 + \frac{\beta r}{2}[U'(x) - f] - \frac{\beta r^2}{4} U''(x) + \frac{\beta^2 r^2}{8}[U'(x) - f]^2 \right] \tag{2-6-28}$$

$$\simeq \sum_{r \neq 0} w(r) + \frac{1}{4\gamma} \left[F'(x) + \frac{F(x)^2}{2k_{\rm B}T} \right]. \tag{2-6-29}$$

We find that the x-dependent part of the escape rate is obtained as Eq. (2-6-26).

It has been claimed that frenesy plays important roles in Markov dynamics without detailed balance (=nonequilibrium). For example, it has been found to appear in the variational formula of the cumulant-generating functions [50], extension of the minimum entropy principle [51], and large deviation functions [52]. What we find interesting is that these relations, formulated in Markov jump dynamics, have the counterpart formulae that can be re-derived for the case of Langevin equations, with all the frenesy terms exchanged to the irreversible entropy production [50, 53].

The structure behind such exchange of frenesy and irreversible entropy production is a consequence of the formula satisfied in the Langevin dynamics:

$$\left\langle \dot{\Sigma}(t) \right\rangle_t - k_B T \langle \lambda(x) \rangle_t = \frac{(k_B T)^2}{\Gamma} \left\langle \left(\frac{P_t'(x)}{P_t(x)} \right)^2 \right\rangle_t, \tag{2-6-30}$$

which may be proved easily from Eq. (2-4-38). This relation indicates that under a fixed density function, the irreversible entropy production and frenesy are essentially equivalent in Langevin systems.

Given the equality (2-6-30), it is now interesting to interpret it as the generalized fluctuation response relation. This is obtained by simply substituting Eqs. (2-6-24) and (2-6-25) into Eq. (2-6-30); remarkably, we recover the Harada-Sasa equality, Eq. (2-6-16).

What Eq. (2-6-25) is claiming is that the response function at time $t = 0$ does not include any information about the nonequilibrium feature of the dynamics. Thus, the Harada-Sasa equality can be understood as simply quantifying the heat dissipation by $\langle \dot{Q} \rangle_{\rm st} \sim \Gamma \langle \dot{x}^2 \rangle_{\rm st}$ but by subtracting the convergent term and the contributions from the spacial inhomogeneity through the corresponding response function term.

2.7 Objectivity in the definition of heat

Up to here, we have discussed the theoretical ideas which allow us to quantify heat dissipation in small stochastic systems. The basic idea is that we do not need to directly measure the energy

transfer in such systems in order to obtain the thermodynamic quantities; they can be estimated through the observation of the motion of the probe beads, possibly with some applied perturbations. Nevertheless, since the actual calorimetric heat is inaccessible in such small systems, there is a general concern that the presented framework of stochastic thermodynamics is missing some level of heat dissipation that we are not aware of. Here we make a couple of remarks related to this problem.

For instance, the free energy that dissipates in chemical reactions [Eq. (2-1-6)], and the potential $U(x)$ in the Langevin description (cf. Sect. 2.2), may include non-energetic components. For the chemical reaction, the free energy change is composed of an energetic part $\Delta\mu_0$ and the concentration dependent part [cf. Eq. (2-1-6)], where the latter obviously has no interpretation as energy transfer or heat dissipation. The force obtained through $U(x)$ in the Langevin model does not distinguish between potential force and entropic force, since in most cases it is only the effective force that is introduced to match the dynamics with the experimental observation.

These issues are the natural consequence of our phenomenological model description. When we introduced the modes as Markov processes, the physics behind the hidden degrees of freedom were only taken into account through the transition probabilities. Since there are infinitely many physical systems that produce mathematically equivalent Markov processes, it is, in general, impossible to estimate the thermodynamic quantities through just the observation of the stochastic dynamics.

Such possibilities of different physical origins of the given dynamics may be narrowed down if we were able explicitly take into account the hidden degrees of freedom. Thus, the general problem can be formulated as follows: is there a proper way to quantify heat dissipation in an effective model-independent manner? For example, in the case of an entropic spring, the Langevin heat (coarse-grained scale) is non-zero, whereas the heat dissipation quantified at the scale where we could see the degrees of freedom in the spring (fine-grained scale) is zero, which is the case that we failed to quantify heat dissipation in an objective manner.

There is a fairly general work around to this problem; when we consider the irreversible entropy production, i.e., if we add the entropy of the system to the heat entropy production, the objectivity with respect to the change of the level of descriptions, is recovered. This is because, for the example case of an entropic spring, the entropy of the spring will contribute to the irreversible entropy production at the level of fine-grained scale [54], which will account for the Langevin heat dissipation observed in the coarse-grained scale.

Thus, if we are interested in the irreversible entropy production, or the steady-state heat dissipation $\langle \dot{Q} \rangle_{\rm st}$ which is essentially equivalent to the irreversible entropy production [cf., Eq. (2-3-13)], we do not need to worry about the physical interpretation of heat or its objectivity. Even if the potentials were not purely mechanical, and there is doubt in calling the estimated Langevin heat as heat dissipation, at least what we are measuring through the application of stochastic thermodynamics it is the most important quantity related to the Second Law.

There are, however, cases that even the irreversible entropy production takes different values depending on the scale of description. In the works presented in [35, 55], we proposed the concept of hidden entropy production, which is the difference in the irreversible entropy production that

appears in the coarse-graining procedure of nonequilibrium dynamics[15]. Under the existence of such hidden entropy production, there seems to be no general way to experimentally estimate the "correct" dissipative feature, apart from considering the excess part of entropy production [55]. Thus, it is left for future studies to consider a more general framework to resolve the existence of of hidden entropy production, or at least prove a non-existence theorem under specific setups of bio-molecular experiments.

[15]This is the main topic of Dr. Yohei Nakayama's thesis (in Japanese, 2015).

Chapter 3

Rotary motors
-Asymmetric switching rule in F_1-ATPase-

In this chapter, we describe the current theoretical understanding on the motion and thermodynamics of the molecular motor F_1-ATPase (or F_1). After giving a brief historical overview, we discuss the correspondence of the dynamics of F_1 motor to the model description explained in the previous chapter. Then we will focus on the recent experimental finding that the dissipative heat inside the F_1 motor is very small, irrespective of the velocity of rotation and energy transport. We claim that the totally asymmetric allosteric model (TASAM), where ATP binding to F_1 is assumed to have low dependence on the angle of the rotating shaft, produces significantly consistent results with the experimental data. The key features of the model is understood through the time scales appearing in the singular perturbation analysis. We explain how the proposed model gives predictions on the heat dissipative feature in the ATP synthetic rotation of F_1.

3.1 Introduction

The detailed chemistry and energetics of F_1-ATPase (or F_1) has attracted special attention due to its outstanding role in the endpoint of the metabolic network. In eukaryotic cells, the F_oF_1 complex in the inner membrane of the mitocondrion is responsible for the generation of more than 90% of the ATP consumed in the cell. Since ATP is the most fundamental currency of energy in biological systems, the thermodynamic feature of F_1 in terms of efficiency and speed is of critical matter to the whole cellular process.

The brief mechanism of ATP generation (reformation) in the mitochondrion is described as as follows [56, 57]. The electron transport chain functions as a consequence of the metabolic reactions, and generates a large proton gradient across the inner plasma membrane of mitochondria. The F_o complex, which is embedded in the membrane, sits as a pathway for the protons to flow through the membrane (Fig. 3.1, left). Upon this transport of protons, the F_o component generates torque on the γ subunit, which is the elongated shaft-like protein that links the F_o and F_1 complexes. The F_1 complex holds three nucleotide binding sites (called catalytic sites in some context) corresponding to the three pairs of α and β subunits aligned in a circle (Fig. 3.1). The unidirectional rotation of the shaft induced by F_o stimulates the F_1 complex to induce the otherwise unfavorable chemical reaction ADP + Pi $\rightarrow$ ATP in these binding sites. In such manner, the chemical free energy corresponding to the proton gradient across the membrane is first translated into a mechanical potential that induces the rotary motion of the shaft, and then converted into the chemical free energy of ATP.

The uniqueness of F_1 lies in its feature of reversibility. In 1997, Kinosita and Yoshida's group reported that the F_1 not only works as an ATP synthesizer, but can also act as an ATP consuming rotor [58]. In their experiment, the minimal components of F_1, the α,β, and γ subunits, were placed on a coated bead to observe the dynamics of the γ shaft, through a probe filament attached to the end of it (Fig. 3.1, right). Strikingly, the live fluorescent images showed the unidirectional rotation of F_1 (anti-clockwise, viewed from above), with clear evidence of 120° stepwise motion [59]. The observed steps were immediately related to the three-fold symmetric structure of F_1, which had been known from the biochemical [60] and crystal structure analyses [61].

Rotational motion of the F_1 motor is roughly explained as follows: the $\alpha\beta$ subunits change their conformations following the events of the binding of ATP, the hydrolysis reaction ATP $\rightarrow$ ADP + Pi, and the release of Pi and ADP. These chemical-reaction coupled conformation changes induce the γ subunit to rotate 120° per single ATP input and ADP + Pi output. The fact that the 120° step corresponds to the hydrolysis of a single ATP was confirmed through various setups of experiment [62, 63]. Thus, the F_1motor is not only the smallest known rotary motor, but it is also a tightly-coupled efficiency-maximized motor (see Sect. 3.3.1).

The key in the rotational motion of F_1 is in the strong correspondence between the chemical states of the nucleotide binding sites in $\alpha\beta$ and the rotational position of the γ shaft. Observation of motion using smaller probes [64] showed that the 120° step is actually composed of substeps with 80° and 40° of rotation. The two-step motion was related to the chemical reaction steps in the ATP hydrolysis reaction [65] (see Fig. 3.8). These observations led to the so-called γ shaft

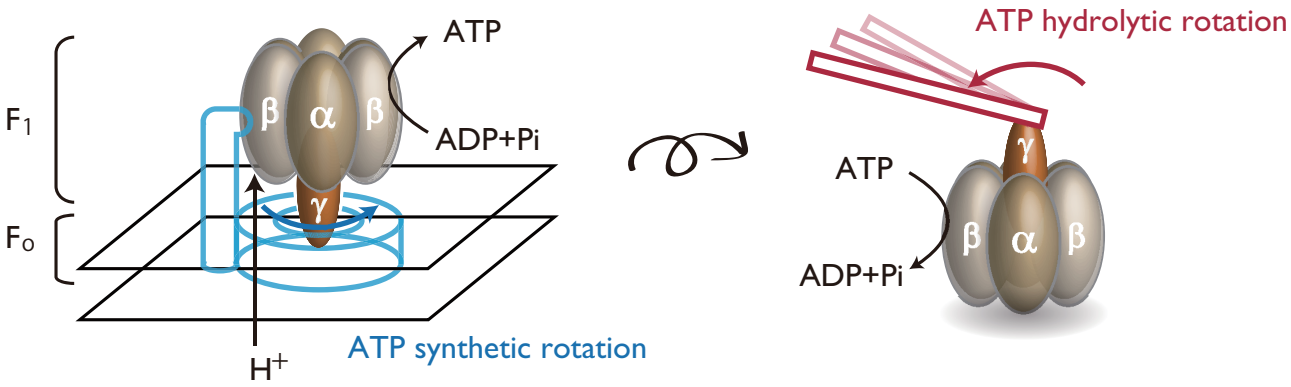

Fig 3.1: (Left) The F_oF_1 complex embedded in the plasma membrane of the mitocondria. The large chemical potential corresponding to the proton concentration gradient across the membrane is converted to the free energy of ATP, through the rotation of the γ shaft forced by the F_o. (Right) Minimal component of F_1 placed on a bead or a cover slip, upside down from the left figure. F_1 functions as a motor in such situation; it consumes the free energy of ATP hydrolysis to rotate the γ shaft unidirectionally, as was observed through the fluorescent image of the probe filament (red). Notice that the direction of rotation with respect the $\alpha\beta$ subunits is opposite in the two cases.

dominator model [66].[1] Indeed, external torque applied to the γ shaft in the clockwise direction induced the *in vitro* synthesis of ATP by F_1 [68, 62]. This means that the angular position of the γ shaft with respect to the $\alpha\beta$ subunits is a single variable that is sufficient to control the whole chemical process involved in the reaction, ATP $\leftrightharpoons$ ADP + Pi.

From the experimental point of view, a rotary molecular motor has its definite advantage over linear motors in the sense of statistical analyses. The motion of the same single molecule can be traced for a long time for a rotary motor, whereas linear motors will detach from the rail during the observation, especially upon application of external force for instance by optical tweezers. In [12], for example, the state specific forms of the effective potential of F_1 was calculated from the high-resolution trajectory data of a single-molecule. Such work is taking advantage of the fact that the probe particle gets trapped by the same effective potential over and over again during the rotational motion. From the data obtained in these manners, it is becoming possible to compare the detail of the phenomenological models to the actual physical aspects of F_1 with high precision.

Speaking of theoretical modeling, numerical calculations on the modeled motion of F_1 have been conducted from right after the initial observations of the *in vitro* rotation. In [69], Wang and Oster introduced a chemical switching-induced Brownian model, which is a rather complicated model that takes into account the many possibilities of the different nucleotide states in all three ATP binding sites. The mechanism of motion in such model, no matter how complex, is the directional bias induced by the chemical reactions as described in Sect. 2.5.1, which is referred to as the chemical ratchet [11, 27, 70]. A model considering the ATP synthetic rotation of F_1

[1] There is however, an interesting report [67] that the γ shaft is not required for the ATP hydrolysis reaction, and the $\alpha\beta$ subunits move in a similar manner as it rotates the γ shaft, even without the γ shaft. Nevertheless, the rate of "rotation" in such setup was found to be significantly lower than the usual setup with the γ shaft.

induced by F_o was also proposed in [71].

3.2 Aim of research

Given that the basic features behind the motion of F_1 have been elucidated, the next goal is to understand and describe the design principle of this reversible motor as precisely as possible. Indeed, data obtained by experiments have gone further beyond the simple toy modeling. At the time of the proposal of the initial models [69], the detailed properties such as the chemical reactions considering substeps [64, 65], rotational velocity modulation with respect to the external torque [63], or the precise shape of the effective potential [12] were all unknown.

Although the heat dissipative feature in the rotational motion was first estimated by assuming linear relation for the dissipation [15], it was not until recently [16] that the nonlinear component and its precise dependence on physical parameters was quantified. The striking result reported in [16] was that, in the absence of external load, the chemical energy consumption of F_1 is made almost 100% through the rotational motion, irrespective of the value of the velocity of rotation $\Delta\mu$. As we shall explain, the heat measured in this experiment was the Langevin heat, which corresponds to the heat dissipation through the Brownian motion of the bead ($Q_{\rm ext}$ in Fig. 3.2). The outcome in experiment is that the internal dissipation ($Q_{\rm int}$ in Fig. 3.2), which is the energy transfer between the motor and the thermal bath (water) during the chemical reaction occurring in the $\alpha\beta$ subunits, is very close to zero.

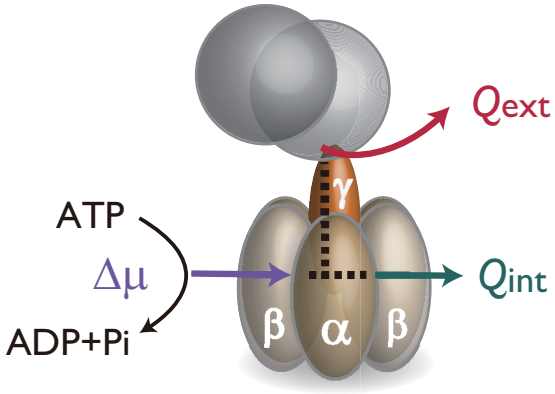

Fig 3.2: Summary of the energy income and outflow of F_1 in the ATP hydrolysis rotation in the absence of external load. Free energy of the chemical fuel $\Delta\mu$ is dissipated through the rotary motion of the γ shaft ($Q_{\rm ext}$), or through the $\alpha\beta$ complex where the reactions take place ($Q_{\rm int}$).

This highly suggestive result provokes us to consider the hidden rules that govern molecular motors. In fact, the established theories in stochastic thermodynamics, for instance the fluctuation theorem [4, 5, 30] and the Second Law (Sect. 2.3), can only explain the positivity of the total irreversible entropy production, which in this case, is the trivial $\Delta\mu \geq 0$. This means that in the

general theory of Markov processes, there are no restrictions which rule the individual values of Q_{ext} and Q_{int}.

Motivated by this situation, we here reconsider the features of F_1 at the level of the phenomenological model, where only the rotary degree of freedom of the γ shaft and the nucleotide state of the $\alpha\beta$ subunits are taken into account. We focus on the interesting fact that the chemical reactions, which are the main source of the rotational motion, are itself controlled by the rotary position of the γ shaft [72, 73]. Such correlation between the apparently far apart domain in protein complexes is a feature known as allosterism [74]. The amount of internal/external dissipation in a model may be manipulated by setting various types of γ angular dependence of the chemical reactions. Specifically, we introduce the totally asymmetric allosteric model (TASAM, Fig. 3.3) in order to explain the internal dissipation-free nature of F_1.

The key assumption in our model is that the ATP binding to the motor, which is the limiting slow process, is allowed with equal probability over the γ shaft angle. The motor thus passively waits and lets the ATP to bind freely, and decides whether or not to release this ATP depending on the angle of the γ shaft. As we shall see (Fig. 3.9), numerical results in our model show remarkable consistency with experiment in terms of the heat dissipative feature. We identify the crucial role of two time scales in the TASAM, which explains the universal mechanism in the model to produce the internal dissipation-free feature. Moreover, we analyze the nucleotide concentration dependence on the torque-velocity relation (Fig. 3.14), and find that a certain asymmetric pattern observed in experiment is also reproduced by the TASAM.

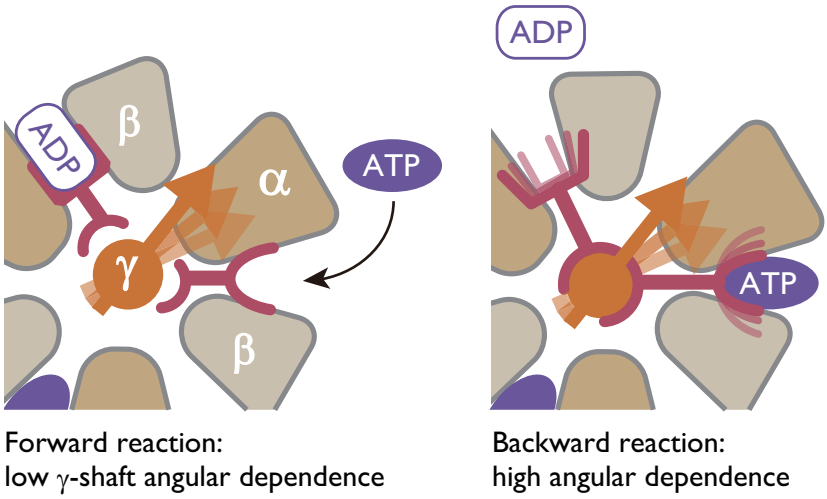

Fig 3.3: Schematic of the totally asymmetric allosteric model. When the motor is waiting for the ATP to bind (left), the binding site is free from the control by the γ shaft rotary angle. Conversely, once the ATP is bound to the motor and the ADP release has proceeded (right), the affinity of the binding sites to the nucleotides strictly depends on the γ shaft angle.

3.3 Phenomenological model description of F_1

3.3.1 Chemical coupling model and high efficiency

Let us first consider the coarse-grained description of the motion of F_1, where we only focus on the discrete steps of 120°. We model the switching of the discrete variable m by a Markov process with the transition probabilities $R^+\Delta t$ and $R^-\Delta t$ (transition rates R^+ and R^-), corresponding to the motion in the forward and backward directions, respectively (see Fig. 3.4). Here, $m = 0, \pm 1, \pm 2, ...$ may be thought of as the angular position of the γ shaft in the units of 120°, or the number of ATP consumed through the rotary motion. Note that the transition probabilities are assumed to be independent of m because of the translational symmetry of F_1 in the rotational direction. Considering that the forward (backward) step is coupled to the hydrolysis (synthesis) of ATP, the ratio between the transition rates should satisfy

$$\frac{R^+}{R^-} = \exp\left[\frac{\Delta\mu - FL}{k_B T}\right]. \tag{3-3-1}$$

Here, F is the externally applied torque (corresponding to $-f_{\rm ext}$ in Sect. 2-5-1) and L is the size of the step, which is 120° in the case of F_1. Equation (3-3-1) can be viewed as the local detailed balance of this simple system [cf., Eq. (2-3-4)], where the log of the right hand side corresponds to the dissipation per step in the + direction, since FL is the work done by the motor against the external torque.

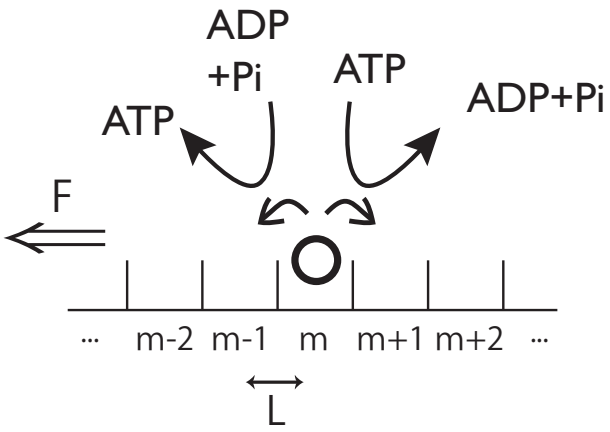

Fig 3.4: Coarse-grained stochastic model of the dynamics of F_1. Each step in m corresponds to the 120° steps of the γ subunit, which is accompanied by the hydrolysis of ATP ($m \to m + 1$) or the synthesis of ($m \to m - 1$).

For Eq. (3-3-1) to be satisfied, there are several conditions to be met from the point of view of real bio-molecules. Firstly, the degree of freedom in the dynamics must be effectively captured by the single variable, m. Since F_1 is a complex molecule with many degrees of freedom in principle, it is nontrivial that applying torque on the probe bead will ideally affect the dynamics

following such simple local detail balance law. Secondly, it must be that each stepping motion is accompanied by the chemical reaction of exactly one molecule of ATP. For instance, when torque is applied to the backward direction (i.e., $F > 0$), it is possible that the motor may make a backward step without synthesizing an ATP, which may be thought of as a slip[2]. In such case, the bias by the chemical potential will be smaller than $\exp[\Delta\mu/k_{\rm B}T]$, which will lead to a smaller stall torque than the ideal value,

$$F_{\rm stall} = \frac{\Delta\mu}{L}. \tag{3-3-2}$$

Although the experiments verifying the in vitro ATP synthesis [62] provided indirect evidence that these two conditions were satisfied for F_1, it came to a surprise when Eq. (3-3-1) was verified quantitatively using the rotary electric field [63]. Indeed, the stall torque only depended on the value of $\Delta\mu$ following Eq. (3-3-2), and not on the absolute values of [ATP], [ADP], and [Pi] under the condition that [ATP][H_2O]/[ADP][Pi] was fixed [cf., Eq. (2-1-6)].

Such outstanding feature of F_1, that the transition of the switching is perfectly coupled to the chemical reaction of ATP, is referred to as the tight-coupling. This remarkable character indicates that the thermodynamic efficiency is maximized for such chemical coupling dependent motor; when stall force is applied, the motor conducts work against the load with 100% efficiency with the rotational speed 0 Hz, corresponding to the quasi-static operation of a thermodynamic system.

3.3.2 Brownian motion

Knowing that the property of the stepwise motion of F_1 is well-characterized by the ideal transition rates satisfying Eq. (3-3-1), we next focus on the Brownian motion of the probe bead, with the motivation to consider the significance of the experimental results presented in [16].

The overdamped Brownian motion of the probe is characterized by the mechanical (yet effective) potentials $U_m(x)$, which trap the rotational degree of freedom x of the probe attached to the tip of the γ subunit. Each potential is created by the interaction between the γ subunit and the $\alpha\beta$ subunits [12, 76], and the joint between the γ subunit and the probe bead [77]. Due to the translational symmetry of the motor (Fig. 3.2), the potentials are assumed to be translationally identical $U_m(x) = U_0(x - mL)$.

Although the detailed version of the model should take into account the substeps (Fig. 3.8), the hydrolysis dwell potentials can be effectively included in $U_m(x)$, since the substeps corresponding to the hydrolysis/synthesis reaction + releasing/binding of Pi is fast [64]. Thus, our model with the effective potentials $U_m(x)$ has the ATP binding followed by ADP release as the rate-limiting step (Fig. 3.6). By assuming that the ATP binding dwell and the hydrolysis dwell potentials are harmonic with the same spring constants k, which has been observed in experi-

[2] In the case of conventional kinesin, which will be described in the next chapter, the motor was found to hydrolyze ATP even in the event of backward stepping [75].

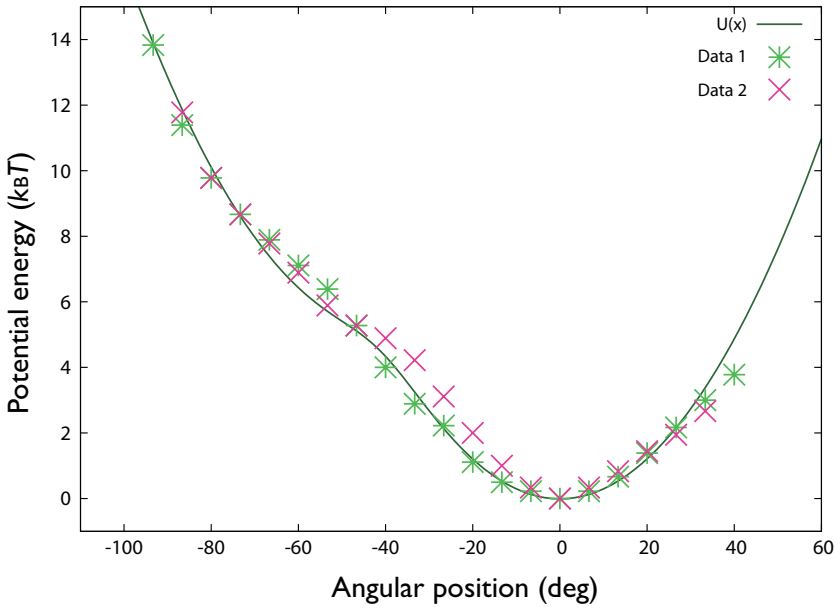

Fig 3.5: Estimate of the effective potential, $U_0(x)$ (red line). Two data of the effective potential obtained in experiment [12] (green asterisks and pinc crosses) are plotted. The functional form obtained in Eq. (3-3-3) was used to fit Data 1, where we obtained $k = 0.0061$ deg^{-2} and $\widetilde{\Delta\mu} = 5.2k_BT$.

ment [72], the form of $U_0(x)$ is estimated as an effective potential,

$$U_0(x) = k_{\rm B}T\left\{\frac{1}{2}kx^2 - \log\left[e^{-klx} + e^{\widetilde{\Delta\mu}/k_{\rm B}T + kl^2/2}\right]\right\}. \tag{3-3-3}$$

Here, $l = 40^\circ$ is the angle of the substep, and $\widetilde{\Delta\mu}$ is the free energy difference between the ATP hydrolysis dwell state and the binding dwell state. By fitting the data in [12] as shown in Fig. 3.5, we obtained $k = 0.0061$ deg^{-2} and $\widetilde{\Delta\mu} = 5.2k_BT$, which are in good agreement with previous independent observations [64, 72, 77]. Derivation of $U_0(x)$ is given in the next subsection.

The angular position of the probe bead, x, undergoes an overdamped Brownian motion inside each effective potential:

$$\Gamma\dot{x} = -\frac{\partial}{\partial x}U_m(x) - F + \sqrt{2\Gamma k_{\rm B}T}\xi_t, \tag{3-3-4}$$

where ξ_t is the Gaussian white noise with unit variance, F is the applied external torque as introduced in Eq. (3-3-1), Γ is the friction coefficient determined by the size of the probe bead, and T is the temperature of the water (i.e., the heat bath).

The potentials are switched according to chemical-reaction induced Poissonian transitions (Fig. 3.7). The switching between the effective potentials are governed by the switching rates denoted by $R_m^+(x)$ and $R_m^-(x)$, for the forward direction ($m \to m+1$) corresponding to the ATP binding + ADP release reaction, and the backward ($m \to m-1$) direction corresponding to the

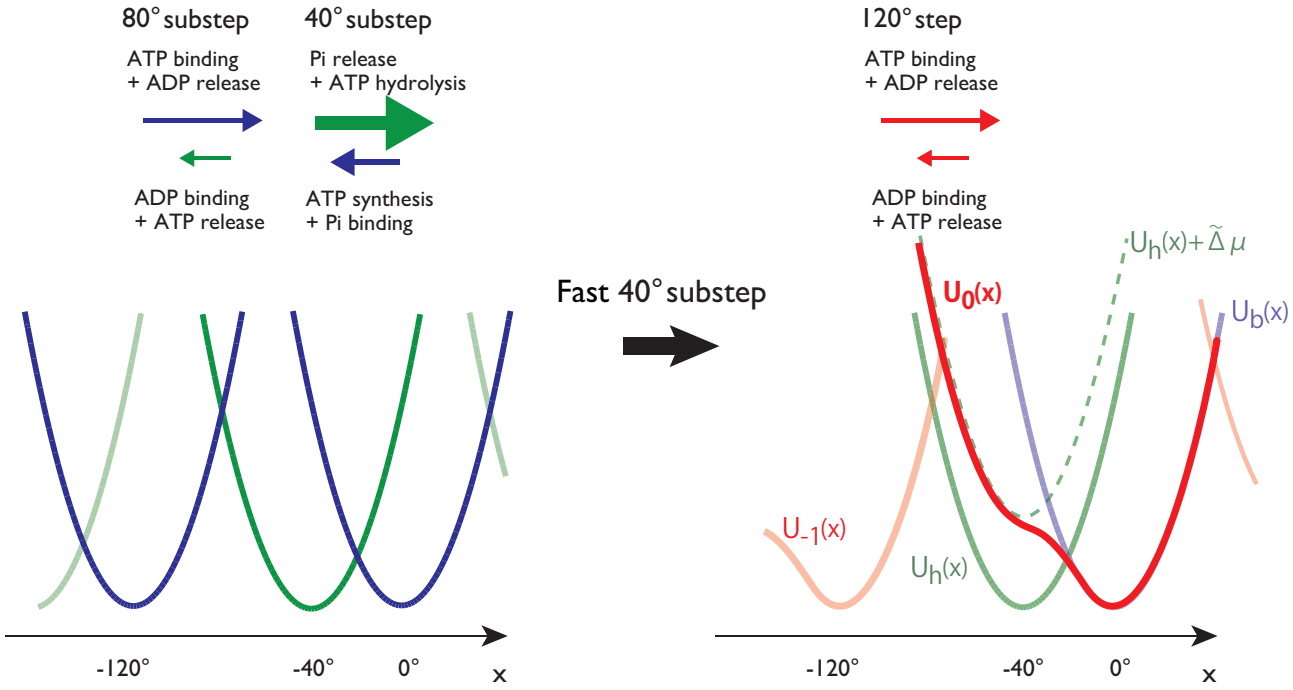

Fig 3.6: Left: Mechanical potentials and chemical reactions corresponding to the substeps. Right: In the limit of the fast 40° substep, the two potentials, $U_{\rm h}(x)$ and $U_{\rm b}(x)$, corresponding to the ATP hydrolysis dwell and the ATP binding dwell, respectively, will be merged into one effective potential, $U_0(x)$. When $U_{\rm h}(x)$ and $U_{\rm b}(x)$ are assumed to be harmonic with the same spring constant (as observed in [72]), $U_0(x)$ is given by Eq. (3-3-3) (see also Fig. 3.5).

ADP binding + ATP release, respectively. The switching rate functions depend on the angular position x, which reflect the allosteric mechanism. We assume $R_m^{\pm}(x) = R_0^{\pm}(x - mL)$. The switching rate functions satisfy the local detailed balance condition (Fig. 3.7)

$$\frac{R_m^+(x)}{R_{m+1}^-(x)} = \exp\left\{\frac{1}{k_{\rm B}T}\left[U_m(x) - U_{m+1}(x) + \Delta\mu\right]\right\}. \tag{3-3-5}$$

Note that we have incorporated the tight coupling condition explained in the previous section, thus the stall torque for this model is $F_{\rm stall} = \Delta\mu/L$.

The schematic of the two-dimensional process (concerning x and m) is described in Fig. 3.8. Let us here note on the requirement to introduce our potential switching model. Although it has been clarified that the discrete position of the gamma subunit $(0°, 80°, 120°...)$ is coupled strongly to the nucleotide state and conformation of the alpha-beta subunits [59, 76, 64], what is happening in between these discrete angles is a question with yet no concrete answer. In fact, it has been clarified in [72, 73] that the chemical reactions do not necessarily occur precisely at a certain angle of the γ shaft, meaning that the timing of chemical reaction is indeed a stochastic phenomena with respect to the angular position. Furthermore, it was shown in [12] that there exist separate potentials corresponding to the discrete positions with a certain extent of overlap. This

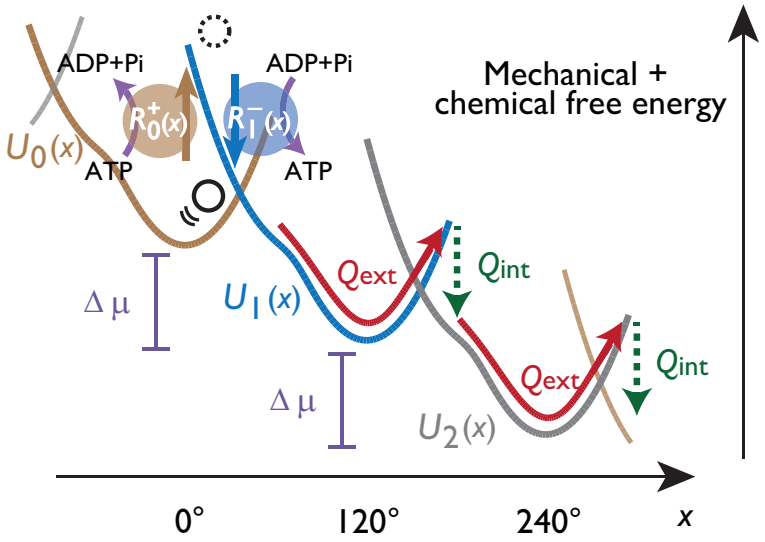

Fig 3.7: Potential switching model and schematic of the heat dissipation for the hydrolysis-driven rotation of F_1 in the absence of applied external torque ($F = 0$). The black circle represents the angular position of the probe bead attached to the γ subunit. The kinetics of x is described by an overdamped Brownian motion inside each potential. Potentials are switched according to the angular position dependent rates $R_m^{\pm}(x)$.

is consistent with the fact that the relation introduced in Eq. (2-6-18) was not satisfied in the F_1 dynamics (S. Toyabe, private communication, 2012), meaning that the model with all the effective potentials merged together (tilted periodic potential setup) fails to describe this molecular motor. Taking these facts together, it is required to adopt our model depicted in Fig. 3.7 to reproduce the experimentally observed kinetics and energetics of the F_1 motor.

3.3.3 Derivation of effective potential

The effective potential $U_0(x)$ is obtained as follows. We first consider that there are two potentials (Fig. 3.6), $U_{\rm h}(x)$ and $U_{\rm b}(x)$, corresponding to the ATP hydrolysis dwell (centered at $x = -l = -40^\circ$) and the ATP binding dwell ($x = 0$). To neglect the slow switching (80° step), we assume that the probe is contained in either of the potential for the time scale of interest. We assume that the potential energy is large compared with the thermal energy, $U_{\rm h}(0), U_{\rm b}(-l) \gg k_{\rm B}T$, which is the case observed in experiment [72]. Let $P_{\rm h}(x)$ and $P_{\rm b}(x)$ be the probability density functions of finding x inside each potentials, and the switching rates from h to b and b to h defined as $X f_h(\tilde{x})$ and $X f_b(\tilde{x})$, respectively. Here, X is the inverse of the typical time-scale involved in the ATP hydrolysis and the Pi releasing reaction. The local detailed balance should be satisfied by $f_h(\tilde{x})$ and $f_b(\tilde{x})$:

$$\frac{f_{\rm h}(x)}{f_{\rm b}(x)} = \exp\left\{\frac{1}{k_{\rm B}T}[U_{\rm h}(x) - U_{\rm b}(x) + \widetilde{\Delta\mu}]\right\}. \tag{3-3-6}$$

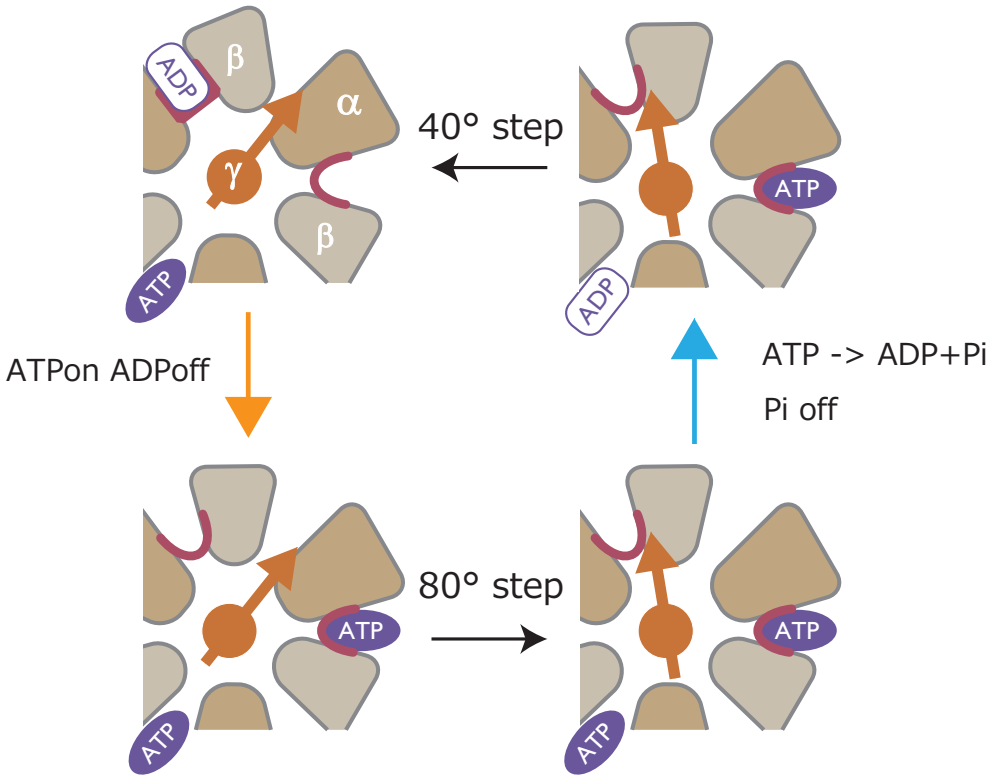

Fig 3.8: Schematic illustration of the 120° step of the F_1 motor. The vertical axis corresponds to the chemical reactions that take place in the $\alpha\beta$ subunits: the ATP binding + ADP release step (left) and the ATP hydrolysis + Pi release step (right). The horizontal axis corresponds to the Brownian motion of the γ shaft, which follows Eq. (3-3-4). One cycle in the figure corresponds to an anticlockwise rotation of 120° with one ATP input and a pair of ADP and Pi output. In the transition from the right top to the left top, the figure should be rotated 120° in the clockwise direction.

The Fokker-Planck equations corresponding to the overdamped Langevin equations with the potentials $U_{\rm h}(x)$ and $U_{\rm b}(x)$ read

$$\frac{\partial}{\partial t}P_i^{\tilde{t}}(x) = \frac{k_{\rm B}T}{\Gamma}\frac{\partial}{\partial x}\left[\frac{dU_i}{dx}P_i^{\tilde{t}}(x) + \frac{\partial}{\partial x}P_i^{\tilde{t}}(x)\right] + X f_j(x)P_j^{\tilde{t}}(x) - X f_{\rm i}(x)P_i^{\tilde{t}}(x), \tag{3-3-7}$$

where i and $j \neq i$ are h or b. By introducing $\tilde{t} = Xt$, $\tilde{x} = x/l_v$, and $\widetilde{U}_i(x) = U_i(x)/k_{\rm B}T$, we obtain the normalized equation:

$$\frac{\partial}{\partial \tilde{t}}P_i^{\tilde{t}}(\tilde{x}) = \epsilon\frac{\partial}{\partial \tilde{x}}\left[\frac{d\widetilde{U}_i(\tilde{x})}{d\tilde{x}}P_i^{\tilde{t}}(\tilde{x}) + \frac{\partial}{\partial \tilde{x}}P_i^{\tilde{t}}(\tilde{x})\right] + f_j(\tilde{x})P_j^{\tilde{t}}(\tilde{x}) - f_{\rm i}(\tilde{x})P_i^{\tilde{t}}(\tilde{x}). \tag{3-3-8}$$

Here we introduced

$$\epsilon := \frac{k_{\rm B}T}{\Gamma X l_v^2} = \frac{1}{\tau_v X}. \tag{3-3-9}$$

As we shall see, the typical length scale l_v should be chosen as that of $E(x) := [U_{\rm h}(x) - U_{\rm b}(x) + \widetilde{\Delta\mu}]/k_{\rm B}T$. The important time scale in this analysis is τ_v:

$$\tau_v := \frac{\Gamma l_v^2}{k_{\rm B}T}. \tag{3-3-10}$$

Assuming fast reaction ($X \to \infty$) corresponds to taking ϵ as the small parameter. The following derivation of the effective dynamics in the limit $\epsilon \to 0$ is given through a method called singular perturbation.

Let us calculate $P_i^t(x)$ in the form, $P_i^t(x) = P_i^{(0)}(x) + \epsilon P_i^{(1)}(x) + O(\epsilon^2)$. We obtain from the 0-th order equations in Eq. (3-3-8):

$$P_i^{(0)}(x) = Q^t(x) P_i^*(x), \tag{3-3-11}$$

where we defined

$$P_{\rm h}^*(x) := \frac{1}{1+\exp[E(x)]} \tag{3-3-12}$$

$$P_{\rm b}^*(x) := \frac{1}{1+\exp[-E(x)]} = 1 - P_{\rm h}^*(x). \tag{3-3-13}$$

It is required to adopt the length scale of $E(x)$ as l_v in Eq. (3-3-8), since this is the length scale which characterizes $P_{\rm h,b}^*(x)$.

The solvability condition for the 1st order equations in Eq. (3-3-8), which is obtained by taking the sum over i in both hand sides, determines the dynamics of $Q^t(x)$:

$$\frac{\partial}{\partial t} Q^t(x) = \frac{1}{\Gamma}\frac{\partial}{\partial x}\left[\sum_{i={\rm h,b}} P_i^*(x)\frac{dU_i(x)}{dx} Q^t(x) + k_{\rm B}T\frac{\partial}{\partial x}Q^t(x)\right], \tag{3-3-14}$$

which is equivalent to the one-dimensional overdamped Langevin equation with the effective force

$$-\frac{dU_0(x)}{dx} = -\sum_{i=h,b} P_i^*(x)\frac{dU_i(x)}{dx}, \tag{3-3-15}$$

where the effective potential is obtained by

$$U_0(x) := \int_c^x dx' \sum_{i=h,b} P_i^*(x')\frac{dU_i(x')}{dx'}, \tag{3-3-16}$$

with an arbitrary fixed constant c. The schematic explaining the effective potential is given in Fig. 3.6

Assuming that the two potentials $U_b(x)$ and $U_h(x)$ are harmonic with the same spring constants, $U_b(x) = U_h(x+l) = kx^2/2 \times k_{\rm B}T$ [72], we have

$$U_0(x) = \int_c^x dx' \left[\frac{kx}{1+\exp[-klx - \widetilde{\Delta\mu}/k_{\rm B}T - kl^2/2]} + \frac{k(x-l)}{1+\exp[klx + \widetilde{\Delta\mu}/k_{\rm B}T + kl^2/2]}\right] \tag{3-3-17}$$

which may be calculated as Eq. (3-3-3) by neglecting the constant.

We find, from the obtained parameters through fitting (Fig. 3.5), that the value of τ_v is of order < 1 msec in the case of the given diffusion constant of the probe in the experiment. This is consistent with the fast substep (ATP hydrolysis step) characterized by X, which is known to be difficult to observe with the frame rate lower than 1000 Hz.[3]

3.3.4 Steady-state and parameters in numerical analyses

In the following sections, we will show numerical results obtained for the steady-state of the described model, Eq. (3-3-4), under the various conditions. In practice, we utilize the translational symmetry to merge the different states corresponding to different m's into one ($m = 0$), and consider the steady-state condition:

$$\frac{\partial}{\partial x}\left\{\left[U_0'(x)+F\right]P_{\rm st}(x)+\frac{k_{\rm B}T}{\Gamma}\frac{\partial}{\partial x}P_{\rm st}(x)\right\} + R_0^+(x+L)P_{\rm st}(x+L)+R_0^-(x-L)P_{\rm st}(x-L)-[R_0^+(x)+R_0^-(x)]P_{\rm st}(x)=0. \quad (3\text{-}3\text{-}18)$$

Here we denoted the steady-state density as $P_{\rm st}(x) \propto P_{\rm st}(x, m = 0)$ and used the translational symmetry $P_{\rm st}(x, m) = P_{\rm st}(x - mL)$ and $R_m^{\pm}(x) = R_0^{\pm}(x - mL)$. We set the normalization condition as $\int_{-\infty}^{\infty} dx P_{\rm st}(x) = 1$ for later convenience. By discretizing in space and taking the system size sufficiently larger than L, Eq. (3-3-18) may be solved as a problem of linear algebra.

For the parameters in the numerical analysis, we used the diffusion constant $k_{\rm B}T/\gamma L^2 = 3.3$ sec^{-1} which was noted in [12]. The chemical free energy $\Delta\mu$ was set as 18.3 $k_{\rm B}T$ in Figs. 3.9, 3.14, 28 $k_{\rm B}T$ in Fig. 3.10 and 16.5 $k_{\rm B}T$ in Fig. 3.12, corresponding to the different experiments ([16], [79], and [12]).

3.4 Measured heat in the model of F_1

In the stochastic dynamics of our model described by Eq. (3-3-4), there are two paths for the motor to exchange energy with the surrounding water (Fig. 3.2). One is through the change of rotational position, which corresponds to the external dissipation, since this energy flows out from the γ shaft. The other is through the change of mechanical potential, which is the internal dissipation corresponding to the energy used to change the conformation of $\alpha\beta$.

Corresponding to the framework introduced in Sect. 2.5, we may characterize these quantities by introducing

$$\Lambda(x) = P_{\rm st}(x)R_0^+(x) - P_{\rm st}(x-L)R_0^-(x-L), \quad (3\text{-}4\text{-}1)$$

[3] Recently, however, it was claimed that the substep is observable even for such relatively large probe, depending on the quality of the motor [78]. If the effective potential picture should be modified and the substep should be explicitly taken into account in the model, it may cause additional internal dissipation, although in experiment it is not observed. It shall be interesting to measure the dissipative feature of F_1 in the presence of large concentration of ATPγS, which makes the rate limiting step to be the ATP hydrolysis step instead of the ATP binding. Such experiment will enable us to access to the information of $f_{\rm h}(x)$ and $f_{\rm b}(x)$ (which in fact, has been estimated though a different method in [72]).

which is the steady-state switching rate that characterizes the switching position. The first term in the right-hand side corresponds to the probability density of the position at which the forward switching ($m \to m+1$) occurs, and the second term corresponds to that of the backward switching ($m+1 \to m$). By integrating Λx, we obtain the net transport rate from potential 0 to 1,

$$v := \frac{1}{3}\int_{-\infty}^{\infty} dx \Lambda(x), \tag{3-4-2}$$

which is equivalent to the steady-state rotational velocity.[4] The factor three is due to the three steps of 120° corresponding to one rotation.

The heat dissipations $Q_{\rm int}$ and $Q_{\rm ext}$ in the model are defined as the steady-state average of the internal and external heat dissipation per 120° step, respectively (Fig. 3.7). $Q_{\rm int}$, the energy dissipation accompanying the switching of m, is calculated by

$$Q_{\rm int} := \frac{1}{3v_{\rm st}}\int dx \Lambda(x)\left[U_0(x) - U_1(x) + \Delta\mu\right]. \tag{3-4-3}$$

Notice that the term $U_0(x) - U_1(x) + \Delta\mu$ corresponds to the total energy shift (=heat exchange with the thermal bath and chemical bath) upon the potential switching $m = 0 \to 1$ at position x, which appears inside the exponential in the local detailed balance equation (3-3-5), . $Q_{\rm ext}$, the dissipation through the spatial motion of x, is the difference between the total dissipation and the internal one:

$$Q_{\rm ext} := |\Delta\mu - FL| - Q_{\rm int}. \tag{3-4-4}$$

Here, FL is the work performed by the motor against the external torque per forward step, and therefore $|\Delta\mu - FL|$ corresponds to the total dissipation per step [cf., Eq. (3-3-1)]. We take the absolute value since the average stepping direction changes its sign at $FL = \Delta\mu$.

In terms of Sect. 2.5.1, we may write $Q_{\rm int} = \Delta\mu - \langle\dot{W}\rangle_{\rm st}/3v_{\rm st}$ and $Q_{\rm ext} = \langle\dot{Q}\rangle_{\rm st}/3v_{\rm st}$. Therefore, it is possible to quantify $Q_{\rm ext}$ by measuring the extent of the violation of the fluctuation response relation, as explained in Sect. 2.6. Results from the experiment conducted by Toyabe et al. [16] for the F_1 motor is shown as cross-points in Figs. 3.9 and 3.10. Remarkably, the external dissipation was very close to $\Delta\mu$ in the absence of external torque for all the conditions of $\Delta\mu$ and rotational velocity (controlled by changing [ATP] and [ADP] with fixed $\Delta\mu$). This means that $Q_{\rm int}$ is very small, irrespective of the velocity of the rotational motion (horizontal axis in figures). We shall explain what this means from the standpoint of model analysis in the following sections.

3.5 Fast chemical reaction

First, we consider the case where [ATP] and [ADP] are set high under a fixed ratio [ATP][H_2O]/[ADP][Pi]. We show in the model that the steady-state rotation rate $v_{\rm st}$ converges to a finite maximum velocity $v_{\rm max}$, and the external dissipation $Q_{\rm ext}$ converges to $\Delta\mu$.

[4] We abbreviate the steady-state velocity $v_{\rm st}$ as v in this chapter.

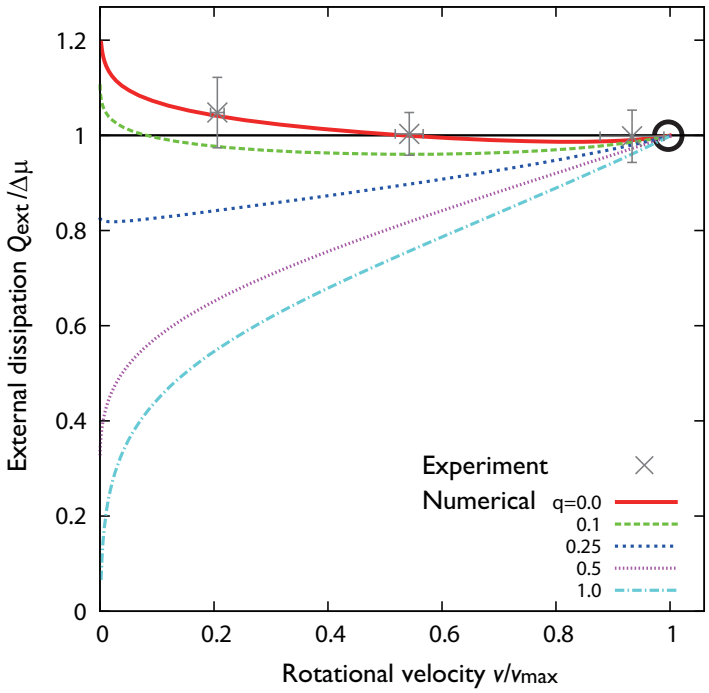

Fig 3.9: Steady-state rotational velocity v versus the external heat dissipation per step $Q_{\rm ext}$ in the case of $\Delta\mu = 18.3k_{\rm B}T$. The red line is the case of the TASAM ($q = 0$), and the other lines correspond to various $q \neq 0$ models introduced by Eq. 3-6-1. Experimental data were obtained from [16] (errorbars: standard error of mean). The black circle indicates the high ATP concentration limit.

To see this, let us write $R_n^{\pm}(x) = W f_n^{\pm}(x)$. Here, W is the rate characterizing the chemical reaction, and $f_n^{\pm}(x)$ are dimension-less functions which do not explicitly depend on [ATP], [ADP], or [Pi] but only depend on the ratio [ATP][H_2O]/[ADP][Pi] through $\Delta\mu$. Note that the nucleotide concentration condition set by [ATP] and [ADP] may be described using the two parameters, W and $\Delta\mu$.

Under a fixed $\Delta\mu$, the high [ATP] and [ADP] situation is represented by large W. In our model which consists of potentials $U_m(x)$ and switching rates $R_m^{\pm}(x)$, the high ATP concentration limit can be treated in a similar method used to obtain the effective potentials in Sect. 3.3.3.

We consider the limit $W\tau_{\rm v} \gg 1$, where $\tau_{\rm v}$ is defined by Eq. (3-3-10). $l_{\rm v}$ used in the definition of $\tau_{\rm v}$ is the length scale of $[U_m(x) - U_{m+1}(x) + \Delta\mu]/k_{\rm B}T$. The dynamics in the limit is described by

$$\Gamma\dot{x} = F(x) + \sqrt{2\Gamma k_{\rm B}T}\xi_t. \tag{3-5-1}$$

The effective force $F(x)$ is given by

$$F(x) = -\sum_{m=-\infty}^{\infty} P_m^*(x)\frac{dU_m(x)}{dx}, \tag{3-5-2}$$

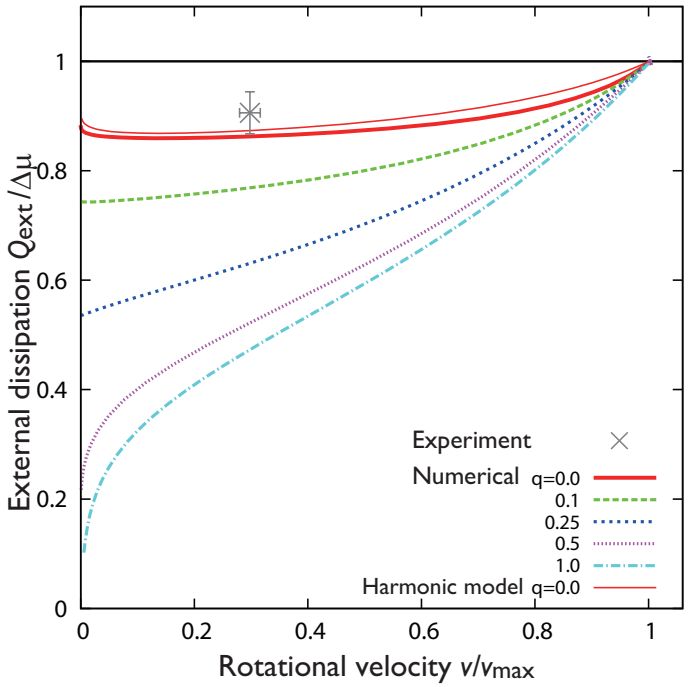

Fig 3.10: Steady-state rotational velocity v versus the external heat dissipation per step $Q_{\rm ext}$ in the non-harmonic potential model [using Eq. (3-3-3) for $U_0(x)$] and the harmonic potential model, in the case of $\Delta\mu = 28k_{\rm B}T$. The experimental result was obtained from [16] (error bar: standard error of mean). In this large $\Delta\mu$ setup, the intersection point becomes $x_c < 0$ in the non-harmonic and harmonic potentials, which is beyond our analytical understanding presented in the Appendix. Nevertheless, the numerical result for $q = 0$ shows consistent value with the experiment.

with $P^*_m(x)$ defined similarly to the previous case as

$$P^*_m(x) := \frac{\exp\{-[U_m(x) - n\Delta\mu]/k_{\rm B}T\}}{\sum_{m=-\infty}^{\infty}\exp\{-[U_m(x) - m\Delta\mu]/k_{\rm B}T\}}. \tag{3-5-3}$$

The force in Eq. (3-5-2) corresponds to a tilted periodic potential, where the energy difference per 120° step is $\Delta\mu$ (Fig. 3.11, bottom). Since this energy difference is dissipated through the rotational motion of the probe, we immediately find

$$Q_{\rm ext} = -\int_0^{120^\circ} F(x)dx = \Delta\mu. \tag{3-5-4}$$

This result indicates that when W is sufficiently large, the dynamics becomes independent of the form of $f^{\pm}_m(x)$, and the switching of mechanical potentials becomes too fast to be observed as distinct steps. Then, $v_{\rm max}$, which is the steady-state velocity for $W \to \infty$ under fixed $\Delta\mu$, is equivalent to the steady-state velocity for the one-dimensional tilted periodic potential setup

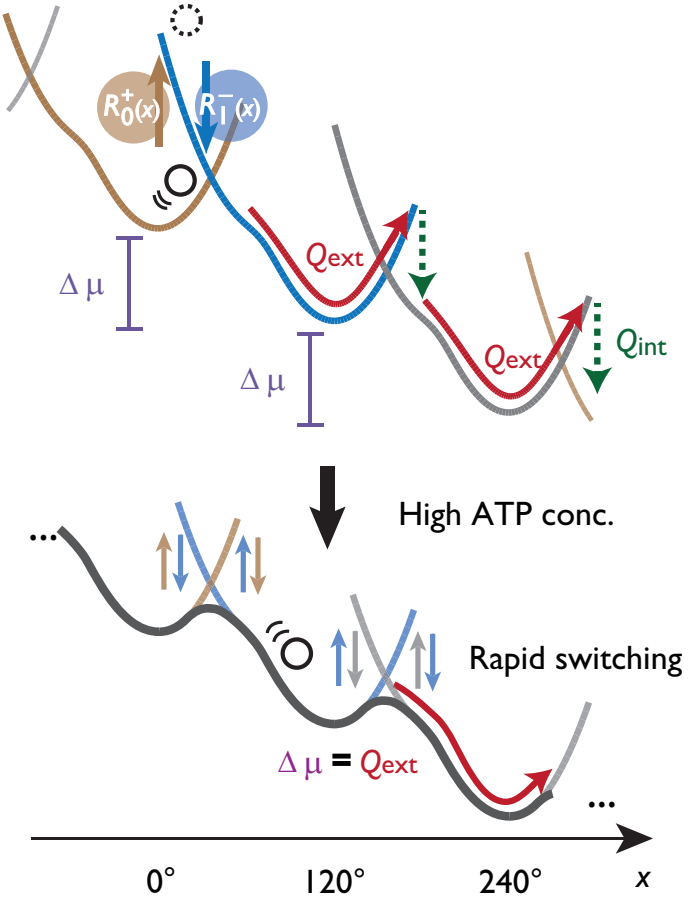

Fig 3.11: Effective potential in the high ATP concentration limit. Since the switching dynamics is fast, the independent potentials become invisible, and the dynamics follows the tilted periodic potential description, irrespective of the form of $R_m^{\pm}(x)$. In this limit, the external dissipation $Q_{\rm ext}$ becomes equal to $\Delta\mu$.

concerning the force $F(x)$[5]. Velocity saturation at high ATP concentration (see also Fig. 3.20 for the harmonic potential model) is a well-known property in molecular motors, which has been phenomenologically understood through the Michaelis-Menten curve [1].

What is happening in this limit is that the potential switching dynamics becomes too fast that the switching governed by $R_m^+(x)$ and $R_m^-(x)$ puts the dynamics of m in equilibrium, under the condition of fixed x. This means that the energy dissipation accounting for the $\alpha\beta$ conformation change is balanced and becomes zero, $Q_{\rm int} = 0$, which is consistent with Eq. (3-5-4), as presented in the right end of Fig. 3.9 in both experiment and numerical analysis with various switching rate functions.

We note that the time scale $\tau_v = \Gamma l_v^2/k_{\rm B}T$ which should be compared with W^{-1} to discuss whether the chemical reactions are fast enough for such limit, is in fact much smaller than the

[5]In order to use Eq. (2-2-8), we decompose the effective force as $F(x) = -\Delta\mu/L - U'_{\rm eff}(x)$ using a periodic potential $U_{\rm eff}(x)$

time scale of equilibration inside the potentials $U_m(x)$, which we denote as τ_p. This difference in the time scale is critical in the internal dissipation-free feature of TASAM, as will be discussed in Sect. 3.6.2.

3.6 Asymmetric model

The torque-free experiment [16] shows that even when [ATP] is low enough and $v < v_{max}$, the external dissipation Q_{ext} is still close to $\Delta\mu$ (Fig. 3.9, crosses). Although we have shown that the feature where $Q_{ext} \sim \Delta\mu$ is achieved for any switching rate function when $v \sim v_{max}$, the external dissipation has a strong dependence on the functional form of $f_m^{\pm}(x)$ in the low velocity regime, since the value of Q_{int} (and consequently, Q_{ext}) is determined by the typical position x at which the switching occurs (Fig. 3.7 top). The experimental observation is striking, since the individual functional forms of $f_m^{\pm}(x)$ are arbitrary as long as the detailed balance condition Eq. 3-3-5 is satisfied; there is no general reason for Q_{ext} to become close to $\Delta\mu$ in the low velocity regime.

3.6.1 Introducing asymmetry through switching rate functions

To see the significance of the experimental result for lower velocities, and introduce the totally asymmetric model, we parameterize the switching rate functions by introducing a parameter q ($0 \le q \le 1$):

$$\begin{aligned} f_m^{+}(x) &= \exp\left\{\frac{q}{k_B T}\left[U_m(x) - U_{m+1}(x) + \Delta\mu\right]\right\}, \\ f_{m+1}^{-}(x) &= \exp\left\{\frac{q-1}{k_B T}\left[U_m(x) - U_{m+1}(x) + \Delta\mu\right]\right\}. \end{aligned} \tag{3-6-1}$$

This q determines the asymmetry in the x-dependence of the forward and backward switching rates, while respecting the detailed balance condition, Eq. (3-3-5). The totally asymmetric allosteric model (TASAM) is the case where the switching rate in the forward direction (ATP binding rate) has no dependence on the γ angle, and therefore, corresponds to $q = 0$. The case of $q = 1$ corresponds to another type of totally asymmetric model that is opposite to the TASAM, where the ATP binding event is strictly controlled by the γ angle, whereas the reverse reaction (ADP binding) is instead independent of the angle. In this manner, q describes the asymmetry in the extent of coordination between the angle of γ subunit and the ATP binding site.

Fig. 3.9 shows the numerically obtained relation between v and Q_{ext} for various q's. The TASAM produces the internal dissipation-free feature ($Q_{ext} \sim \Delta\mu$), which indeed has low dependence on the rotational velocity in the broad range tested in the experiment (Fig. 3.9, red). This feature of the model is preserved for the larger $\Delta\mu$ case (Fig. 3.10). Note that under a fixed functional form of $U_m(x)$, the maximum velocity v_{max} does not depend on q, which is why we may compare Q_{ext} between various models for the same v/v_{max}. Although all models produce $Q_{ext} = \Delta\mu$ for $v = v_{max}$ (black circle), the values of Q_{ext} for the cases of $q > 0.1$ deviate from $\Delta\mu$ significantly at lower v. Thus, we propose that the internal dissipation-free motor is obtained

only by assuming low coordination ($q \sim 0$) in the ATP free state and high coordination in the ATP bound state.

3.6.2 Bare switching rate and switching position density

As seen in Eq. (3-4-3), the value of $Q_{\rm int}$ is determined by the typical switching position. We compare $\Lambda(x)$ for the various models in the low velocity regime in Fig. 3.12. Although the steady-state distribution of the γ angle [$P_{\rm st}(x)$] has a peak at the potential minimum point in this low velocity regime (Fig. 3.12B, black dotted line), the peak of $\Lambda_0(x)$ in the $q = 0$ model is positioned close to the point $x = x_c$ where $U_1(x_c) - U_0(x_c) - \Delta\mu = 0$, which we shall refer to as the potential intersection point.

The mechanism which produces this behavior is that, although the ATPs most likely approach the motor when the γ angle is around the potential minimum point, the bound ATP is almost always kicked out instantaneously, due to the large energy difference required to switch the potential at such points, $U_{m+1}(x) - U_m(x) - \Delta\mu \gg k_{\rm B}T$ (Fig. 3.12). The switching would inevitably occur at positions close to x_c, resulting in low energy dissipation in the potential switching (low $Q_{\rm int}$). $\Lambda(x)$ of the TASAM (Fig. 3.12) agrees with the estimated distribution presented in [12] whereas the $q = 0.5$ and 1 cases (schematic shown in Fig. 3.13) have peaks clearly shifted more toward the forward direction than the intersection point.

On theoretical grounds, the low velocity dependence of $Q_{\rm ext}$ could be understood through the existence of two time scales, $\tau_{\rm v}$ and $\tau_{\rm p}$. As we have seen in Sect. 3.5, $\tau_{\rm v}$ is the small time scale which determines the rotational velocity saturation and the single tilted potential description (Fig. 3.11). In contrast, $\tau_{\rm p}$ is the time scale of the angular position to relax inside a single potential, which is relatively large. There is a separation of order between $\tau_{\rm v}$ and $\tau_{\rm p}$; if we substitute the effective potential with a harmonic potential, $U_0(x) = Kx^2/2$, then the separation can be explicitly obtained as $\tau_{\rm p}/\tau_{\rm v} = U(L)/k_{\rm B}T$, which is the order of $10 \sim 100$ [cf. Eq. (3-9-4)].

We have numerically verified that in the $q = 0$ model, it is $\tau_{\rm p}$ that determines the minimal value of W which the model presents the internal dissipation-free feature. The large separation between the values of $\tau_{\rm p}$ and $\tau_{\rm v}$ causes the experimentally accessible region of the value of W (corresponding to the ATP concentration) to fit inside the inequality $\tau_{\rm p}^{-1} < W \leq \tau_{\rm v}^{-1}$, and the internal dissipation-free feature is observed at all velocity conditions as a consequence. In more practical words, our theory shows that when the actual motor adopts the TASAM , $Q_{\rm ext} \sim \Delta\mu$ holds if [ATP] is as large as 0.1 μM for the 0.3 μm probe bead case [16, 79]. Since the velocity saturation occurs at [ATP] > 5 μM under this condition [64], this lower bound concentration to observe $Q_{\rm ext} \sim \Delta\mu$ is significantly small.

3.7 Asymmetry in macroscopic features

Up to here, we have claimed that the TASAM draws consistent result with the F_1 in terms of the external heat dissipation. We next consider how other features of the TASAM appear in measurable quantities.

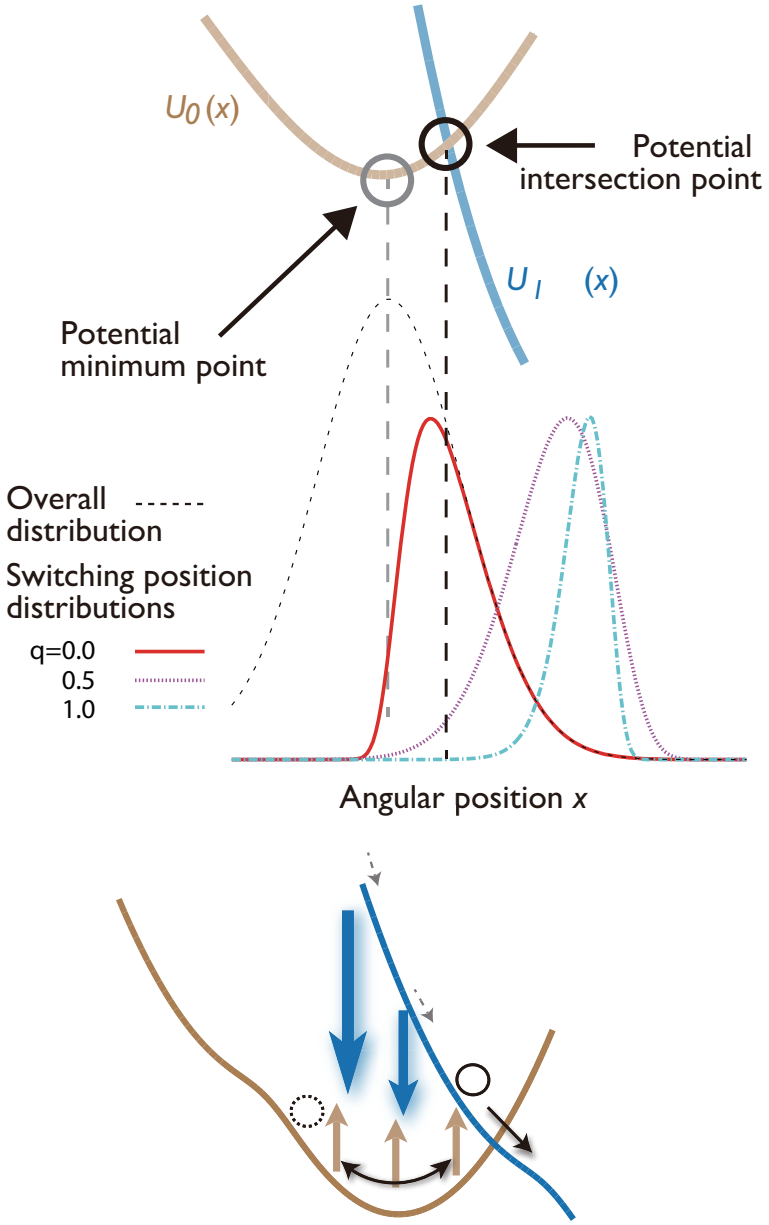

Fig 3.12: Switching position distribution of the TASAM in the case of $\Delta\mu = 16.5k_BT$. (Top) Distribution of the switching angular position at the slow rotation rate condition. Numerically obtained switching position distribution in the $q = 0$ (red), 0.5 (pink), and 1 (light blue) models, compared for the same rotational rate $v = 2$ Hz (low velocity). The vertical axis is arbitrarily scaled. Although the steady-state distribution of the $q = 0$ model (black dotted line) has a peak at the minimum point of $U_m(x)$, the switching position density clearly has a peak around the intersection point, which is consistent with experiment [12]. (Bottom) Mechanism behind the internal dissipation-free feature of the TASAM. The potential switching may occur at any angle in the TASAM (brown arrows), while the backward switching of the potential follows instantaneously if the energy required for the forward switching was too large (blue arrows). Suppression of switching at high energy difference positions lets the switching to occur only around the potential intersection point, leading to the $Q_{\rm int} \sim 0$ feature.

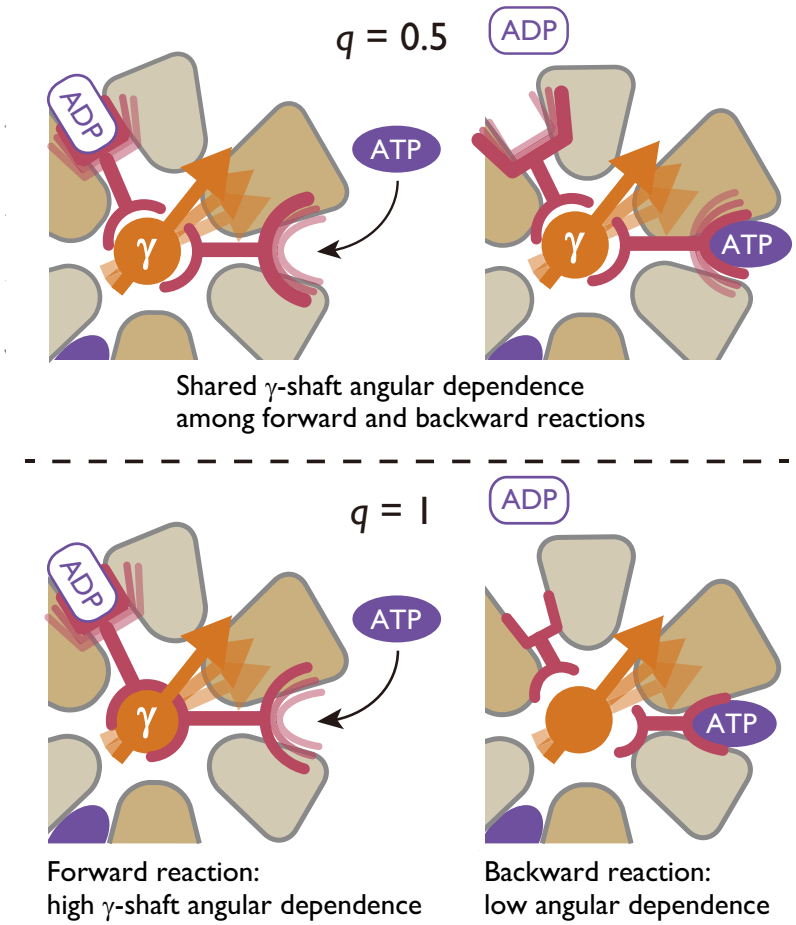

Fig 3.13: Schematic of the $q = 0.5$ and $q = 1$ models. In the $q = 0.5$ model, the coordination between the γ shaft and the nucleotide binding sites are equally present in the forward and backward reactions. On the other hand, the γ shaft and the nucleotide binding sites are only coordinated in the forward step in the $q = 1$ model, which is completely opposite to the case of $q = 0$ model (Fig. 3.3). As shown in Fig. 3.9, 3.10, 3.12, and 3.14, these models fail to reproduce the internal dissipation-free and asymmetric velocity feature of F_1.

3.7.1 Torque dependence of rotational velocity

We first consider how the rotational velocity depends on applied external torque in models with various q (Fig. 3.14). For the sake of schematic explanation, let us consider that the mechanical potentials are harmonic, $U_0(x) = K(x/L)^2/2$ (Fig. 3.16, top). Then, the potential switching model would be symmetric about the change of parameters and coordinate, $(F, q, x) \to (2\Delta\mu/L - F, 1 - q, -x)$. It follows from this symmetric property that in the case of $q = 0.5$ (symmetric model, Fig. 3.16, middle), the torque dependence of the steady-state rotational velocity, $v(F)$, would show an anti-symmetric curve with respect to the $F = \Delta\mu/L$ line. Indeed, this property is observed even when we assume the non-harmonic and realistic form of $U_0(x)$, as shown

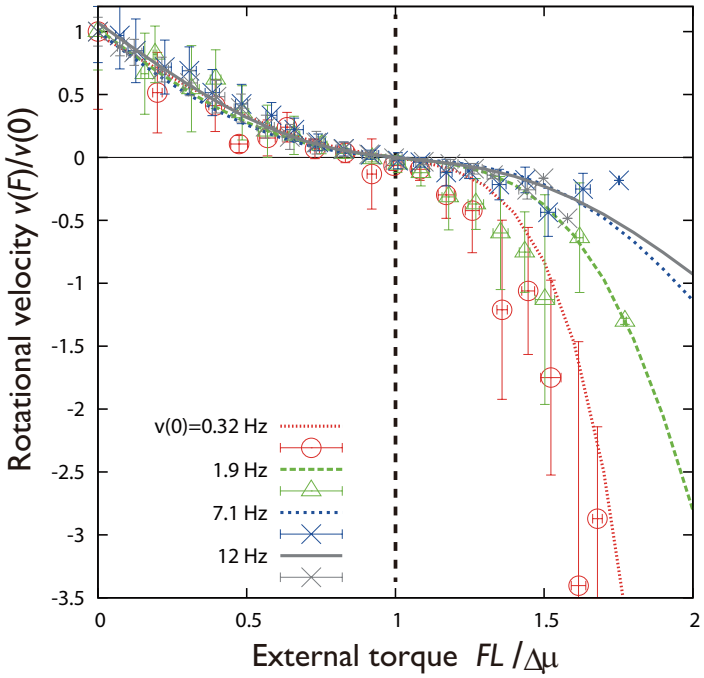

Fig 3.14: External torque dependence of the rotational velocity in the TASAM (numerical, solid lines) and the corresponding values obtained from experiment (lines and points, kindly provided by S. Toyabe, [63]) in the case of $\Delta\mu = 18.3 k_{\rm B}T$. Velocity is normalized using its value at $F = 0$, which is shown as the title of each lines. The $v = 0.32, 1.9, 7.1$, and 12 Hz cases correspond to $W = 1.7, 15, 120$ and 1000 sec^{-1} in the model, respectively, with the other parameters fixed.

in Fig. 3.15. On the contrary, in the TASAM ($q = 0$, Fig. 3.16, bottom), this feature is lost especially at low W, and the torque dependence of the velocity becomes sharper at $F > \Delta\mu/L$ than at $F < \Delta\mu/L$ [$v(0) = 0.32, 1.9, 7.1$ Hz lines in Fig. 3.14]. Remarkably, this feature of the TASAM matches with the experimental observation [63] (line points in Fig. 3.14).

Both in experimental and numerical data shown in Fig. 3.14, the asymmetry seems to become explosively large for low W for the TASAM. In fact, we may calculate the extent of asymmetry in the limit $W \ll \tau_{\rm p}^{-1}$ by assuming harmonic potential. The switching position density in this limit can be calculated by the approximation of the steady-state density as the equilibrium density

$$P_{\rm st}(x) \simeq P_{\rm eq}(x) = \frac{1}{Z} \exp\left[-(U_0(x) + Fx)/k_{\rm B}T\right]. \tag{3-7-1}$$

Using Eq. (3-4-2), the external torque dependence of steady-state velocity can be obtained as

$$v(F) \quad \propto \quad \exp[-qFL/k_{\rm B}T]\{1 - \exp\left[(FL - \Delta\mu)/k_{\rm B}T\right]\}. \tag{3-7-2}$$

Thus, the dependence of the asymmetry on q is very sharp, and in the case of $q = 0$, the asymmetry $v(F)/v(0)$ amounts to $\exp[\Delta\mu/k_{\rm B}T]$, which is extremely large.

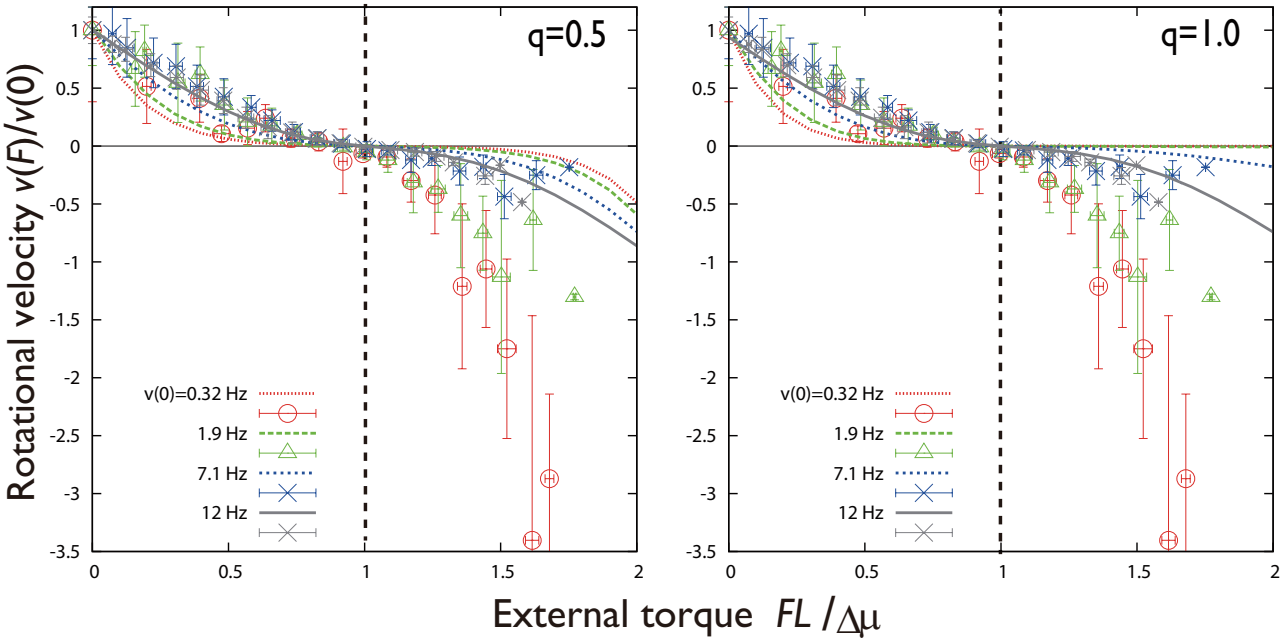

Fig 3.15: External torque dependence of the rotational velocity in the $q = 0.5$ (left) and 1.0 (right) models, plotted with the experimental data [63] (kindly provided by S. Toyabe). For each numerical lines, W was chosen and fixed in order to reproduce the values of $v(0)$ of the corresponding experimental data.

3.7.2 Alternative model: intersection switching

For comparison with the TASAM, let us consider the intersection switching model. Instead of the form we introduced in Eq. 3-6-1, we here define the switching rate functions to have a sharp peak at the position of the potential intersection point. In such model, the peak position of $\Lambda(x)$, which is confined around the intersection point, would be independent of W, and the velocity independent feature of $Q_{\rm int} \sim 0$ would be trivially obtained. We set

$$\begin{aligned} f_0^+(x) &= \exp\left\{-\frac{(x-x_c)^2}{2\sigma^2} + \frac{q}{k_{\rm B}T}\left[U_0(x) - U_1(x) + \Delta\mu\right]\right\}, \\ f_1^-(x) &= \exp\left\{-\frac{(x-x_c)^2}{2\sigma^2} + \frac{q-1}{k_{\rm B}T}\left[U_0(x) - U_1(x) + \Delta\mu\right]\right\}. \end{aligned} \tag{3-7-3}$$

Here, x_c is the intersection point between the two potentials introduced in Sect. 3.6.2, and σ is a parameter which controls the typical width of the window of the angle at which the switching is allowed.

If σ is sufficiently small, this model would become internal dissipation-free for a wide range of W, which seems to be consistent with the experimental data on the external dissipation. This is because the switching of the mechanical potential only occurs at angles satisfying $U_{m+1}(x) - U_m(x) - \Delta\mu \sim 0$ in this model. However, if σ is too small, the torque dependence of the velocity becomes anti-symmetric with respect to the $F = \Delta\mu/L$ line for all q even at small W (Fig. 3.17,

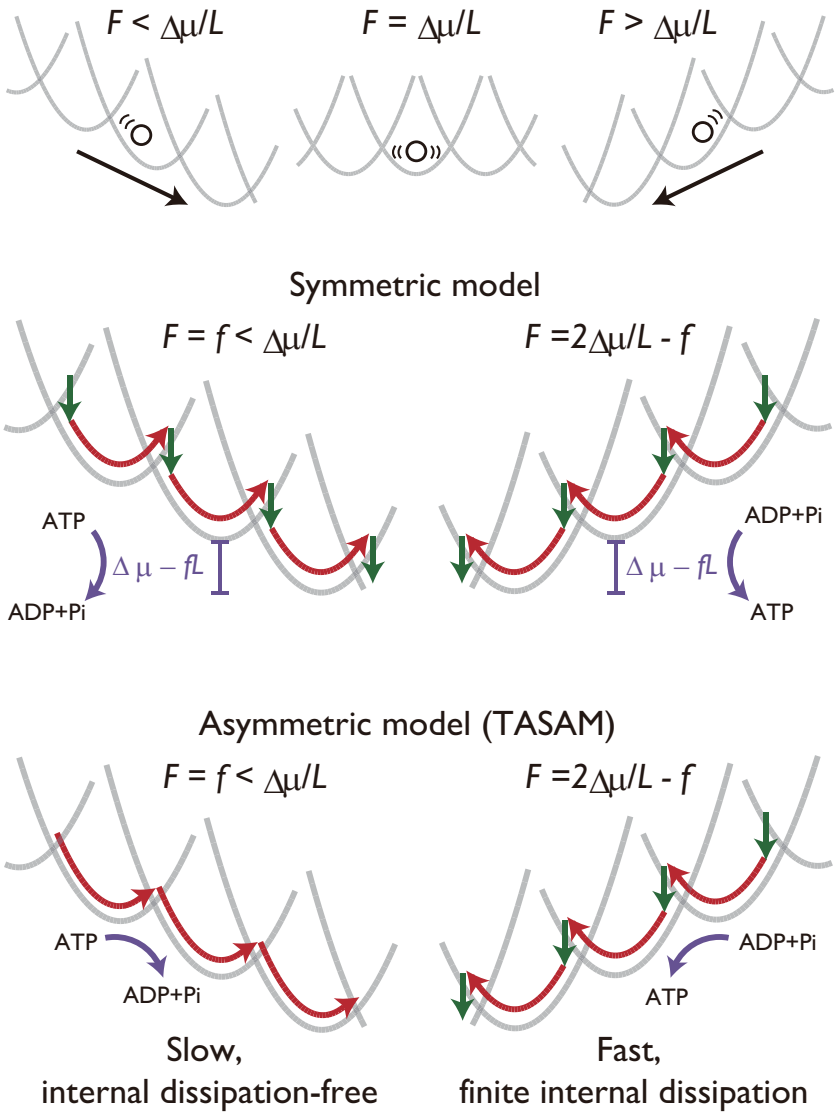

Fig 3.16: Property of the potential switching model under application of external force. (Top) Schematic of the torque F dependence of the potential switching model. When the mechanical potential is harmonic, the model becomes symmetrical about the change $(F, q, x) \to (2\Delta\mu/L - F, 1 - q, -x)$. (Middle) ATP hydrolysis and synthetic rotation in a model with $q = 0.5$. The absolute velocity and the balance between the internal/external dissipations become equivalent in the two cases, $F = f$ and $2\Delta\mu/L - f$. (Bottom) TASAM, especially at the low nucleotide concentration condition. In contrast to the symmetric model (middle), the absolute velocity and the value of internal dissipation are different in the $F = f$ and $2\Delta\mu/L - f$ cases.

left), which is inconsistent with the experimental observations. When σ is sufficiently large (Fig. 3.17, right), the torque-velocity curve would depend on q, which shows that adopting $q \simeq 0$ is critical even in the intersection switching model to reproduce the feature of F_1.

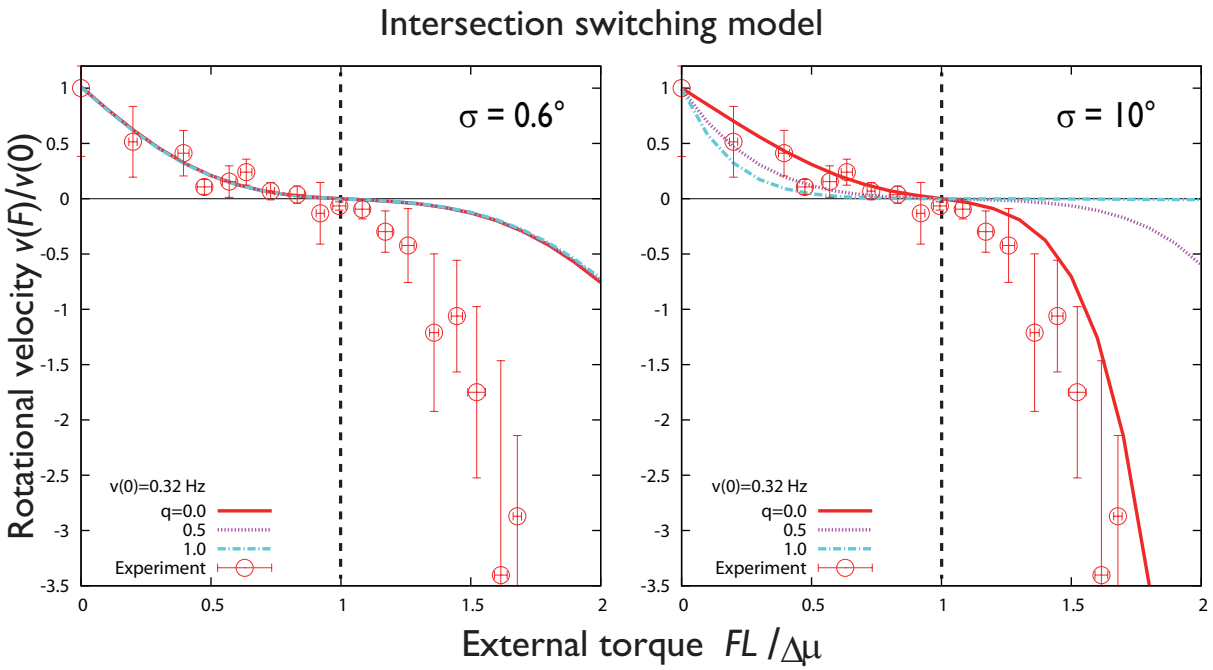

Fig 3.17: External torque dependence of the rotational velocity for the intersection switching model [see Eq. (3-7-3)]. When σ is small and the switching is only allowed in a narrow range around the potential intersection point (left), the torque-velocity curve becomes anti-symmetric with respect to the $FL = \Delta\mu$ line. When σ is set larger (right), the q-dependence appears. For each numerical lines, W was chosen and fixed in order to reproduce the values of $v(0) = 0.32$Hz.

3.7.3 Heat dissipation in the ATP synthetic rotation

We predict that similar difference between the torque-free and torque-applied cases would be observed in the internal dissipation, if the TASAM is adopted in the F_1 motor. In fact, Fig. 3.18 shows that the internal dissipation-free nature of the TASAM is lost, especially when large torque $F > \Delta\mu/L$ is applied in the model. The low torque dependence of $Q_{\rm int}$ at high nucleotide concentration has recently been measured and reported [79], which is consistent with the case of $v(0) = 12$ Hz in Fig. 3.18. The validity of our model can be checked by further measuring $Q_{\rm int}$ in the low nucleotide concentration condition, which are the $v(0) = 0.32, 1.9$ and 7.1 Hz cases in Fig. 3.18.

The character of the torque dependence of TASAM could be understood through the property of the potential switching model discussed above. The dynamics of the TASAM at the presence of large applied torque, for instance $F = 2\Delta\mu/L$, becomes equivalent to that of the $q = 1$ model

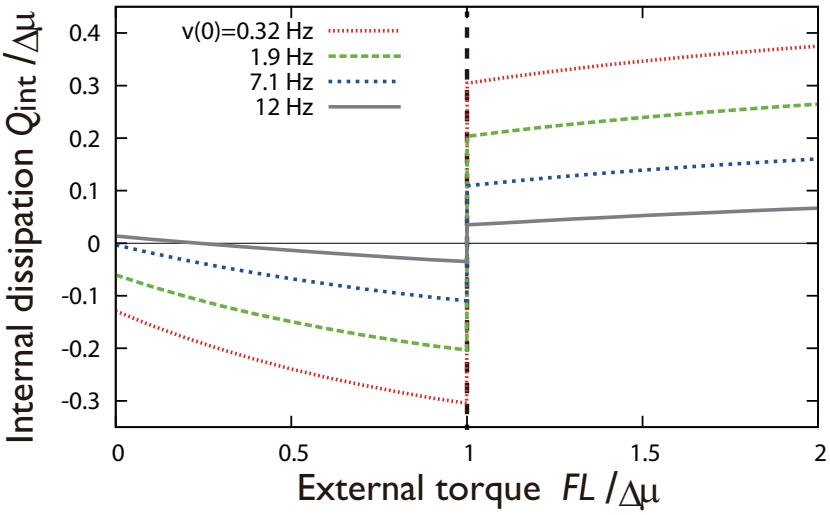

Fig 3.18: (B) External torque dependence of the internal dissipation $Q_{\rm int}$ in the TASAM. At low nucleotide conditions (small W), $Q_{\rm int}$ significantly deviates from zero at the presence of large torque.

with $F = 0$ with opposite velocity. As we have seen, the internal dissipation is large in the $q = 1$ case, which explains why we observe large internal dissipation in the presence of torque in the TASAM at low W. In this sense, adopting the TASAM in the forward step mechanism (ATP hydrolysis) is equivalent to adopting the $q = 1$ model in the backward step (ATP synthesis, see Fig. 3.9). The absolute velocity at low nucleotide condition becomes faster at $F = 2\Delta\mu/L$ than at $F = 0$ in the TASAM (Fig. 3.14), which is suggestive since the F_1 is forced to rotate in the ATP hydrolysis direction in biological conditions. It shall be interesting to quantify how asymmetric the thermodynamic quantities and force-velocity relations are in other molecular motors.

3.8 Comparing with other experiments

One way to verify our model is to directly measure the switching rate functions in the F_1 experiments. Recently, two groups have reported the angular position dependence of chemical reaction rates in the F_1 motor. Iko et al. [80] indirectly estimated the angular dependence of the ATP binding rate, which we refer to as $k_{\rm on}^{\rm ATP}(x)$. This was done by comparing the forced rotation speed dependence of the ATP consumption rate with model simulations. Watanabe et al. [72] tweezed the magnetic probe bead at a defined angle with respect to the ATP binding dwell, and measured the probability of the forward and backward stepping as a function of the angle and the tweezing time, from which $k_{\rm on}^{\rm ATP}(x)$ and also $k_{\rm off}^{\rm ATP}(x)$ was estimated. Adachi et al. [73] used nucleotides with fluorescent dyes to directly observe the binding events during the forced rotation of the probe bead. This also led to the estimation of the various rates including $k_{\rm on}^{\rm ATP}(x)$.

To compare our proposal with these experiments, let us consider again the harmonic potential model, $U_0(x) = K(x/L)^2/2$, with $K = 50k_{\rm B}T$. This value of K was determined to match the steady-state velocity of the model with experiment (see Appendix). Note that in this model, the

angular position dependence of the forward switching rate has a simple form,

$$R_m^+(x) \propto \exp\left[\frac{qKLx}{k_B T}\right], \tag{3-8-1}$$

By assuming that the $k_{on}^{ATP}(x)$ measured in the above reports correspond to the forward switching rate in our model, $R_m^+(x)$, we obtain $q = 0.07 \sim 0.12$ for [80], [72], and [73], respectively. These values are consistent with our model, suggesting that q should be close to zero in order to explain the internal dissipation-free and asymmetric velocity features of the F_1 motor.

We predict that if the direct measurement of $R_m^-(x)$ is possible, one should find a large dependence on the angle, since $0 \sim q < 1 - q \sim 1$. Note that $R_m^-(x)$ corresponds to the combination of the ADP binding and ATP release reaction, thus it is different from $k_{off}^{ATP}(x)$ obtained for example in [72] and [73]. In [73], there is data presented for $k_{on}^{ADP}(x)$ which does not seem to have the expected large dependence on x, although it is difficult to give conclusion since the experiment is conducted in the ultra-low nucleotide condition.

3.9 Remarks and conclusion

In summary, we showed in this chapter that the Brownian motion + switching scheme introduced to model F_1 is internal dissipation-free, but only when the chemical fuel concentration is high enough for the motor to reach maximum velocity. The TASAM was introduced in order to explain the internal dissipation-less feature of F_1 at the small velocity condition. We showed the consistency of the model with the experimentally observed feature in rotational velocity and the angular dependent chemical reactions, and further discussed on the possibility of large internal dissipation in the ATP synthetic rotation to be observed in future experiments.

Our stochastic model is based on confirmed properties of F_1, such as the discrete steps [76, 64], mechanical potentials [12], and large stall force [63] with all the real parameters. However, we did not refer to the microscopic interactions, for example, at the amino acid residue level, which is typically required in molecular dynamic simulations. Nevertheless, the key feature of the F_1 energetics and dynamics seem to be well reproduced by the simple one-dimensional description. The existence of such consistent description encourages us to consider the fundamental design principle behind molecular machines, since at this coarse-grained scale, comparison between different bio-motors and blueprints of artificial nanomotors is possible.

The significant picture we obtained through the analysis of F_1 is the relationship between the heat dissipative feature and the asymmetric switching rule of the motor. From the viewpoint of optimization, we are at this point uncertain about whether the internal dissipation-free feature or the characteristic torque-velocity curve is more important in the design principle of F_1. In one end, the motor might be desiring to minimize the internal dissipation in the motor rotation even in the situation of low chemical fuel concentration (low W), which makes us imagine that F_1 was build as a motor and not an ATP generator in its primitive age of evolution. In the other end, we may regard the asymmetric torque response curve at low ATP concentration as an important message, and consider the larger response to ATP generating direction of torque to be the ultimate goal that F_1 has achieved for its function as an efficient ATP generator.

Such ambiguous thoughts on the origin of the design principle of F_1 may be tested to some extent by looking at different molecular motors. For instance, the V-ATPase, which is another membrane embedded protein complex which resembles the F-ATPase with respect to its components and structures, is known to be functioning as an ion pump in cells. In particular, the V_1-ATPase (or V_1) is the rotor part of the complex, which is an ATP catalyst. It shall be of great interest to investigate the heat dissipative feature and the asymmetric torque-response curve for V_1, and compare it with F_1; depending on which direction of asymmetry appears, if any, we may be able to assign the design principle of F_1 to its feature as the motor or the generator.

Appendix: Analysis of the harmonic potential model

We consider in this appendix the simplified harmonic potential case, $U_m(x) = K(x - mL)^2/2$, where $L = 120°$. Although this simplified case is still not solvable, we can obtain analytical understandings to some extent.

In Fig. 3.19, we show the numerical results of $Q_{\rm ext}$ in this model. Under the condition that the diffusion coefficient $D = k_{\rm B}T/\Gamma$ as $D/L^2 = 3.3{\rm sec}^{-1}$ [12], and the chemical potential as $\Delta\mu/k_{\rm B}T = 19$ [16, 63], the value of K was determined as $KL^2/k_{\rm B}T = 50$ by setting the maximum average velocity to fit with that obtained in experiment. The characteristic feature of q dependence is similar to the case of Fig. 3.9, where the potential estimated through experiment was used in the calculation.

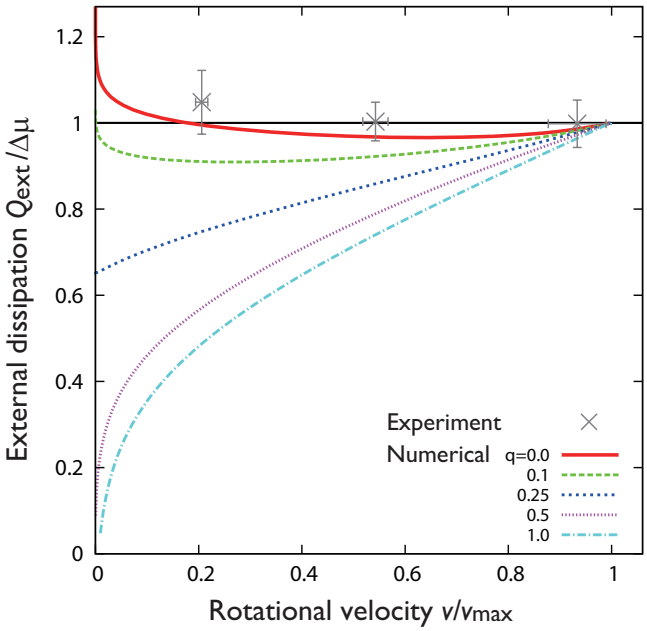

Fig 3.19: Rotational velocity v versus the external heat dissipation per step $Q_{\rm ext}$ in the harmonic potential model. Parameters are given in the text. The experimental results were obtained from [16] (error bar: standard error of mean).

Let us first consider the large W limit (high ATP concentration). The length scale of potentials $U_m(x) = K(x - mL)^2/2$ and that of $U_m(x) - U_{m\pm1}(x) = \mp KLx$ are $\sqrt{k_{\rm B}T/K}$ and $k_{\rm B}T/(KL)$, respectively. Since the potential energy is sufficiently large $KL^2/k_{\rm B}T \gg 1$, the smallest length scale in this model is

$$l_v = \frac{k_{\rm B}T}{KL}. \tag{3-9-1}$$

This length defines the time scale [cf. Eq. (3-3-10)]

$$\tau_v = \frac{\Gamma k_{\rm B}T}{(KL)^2}, \tag{3-9-2}$$

which determines the typical W (ATP concentration) that allows the effective force description of the model, and consequently the velocity saturation. Let us also define

$$\tau_{\rm p} := \frac{\Gamma}{K}, \tag{3-9-3}$$

which corresponds to the time scale of equilibration inside a single potential. Notice that

$$\frac{\tau_{\rm p}}{\tau_{\rm v}} = \frac{KL^2}{k_{\rm B}T} \gg 1, \tag{3-9-4}$$

Significance of the time scale $\tau_{\rm v}$ is numerically verified through seeing how the velocity dependence of W in the model changes according to the spring constant K. In Fig. 3.20, we show the results for the case where K and $\Delta\mu$ are parameterized by d $(= -1, 0, 1, 2, 3, 4, 5)$ as

$$KL^2/k_{\rm B}T = 50 \times 2^d \tag{3-9-5}$$

$$\Delta\mu/k_{\rm B}T = 19 \times 2^d. \tag{3-9-6}$$

Clearly, the value of W at which the velocity saturates is scaled by $\tau_{\rm v}$ $(\propto K^{-2})$ and not by $\tau_{\rm p}$ $(\propto K^{-1})$, when d is sufficiently large.

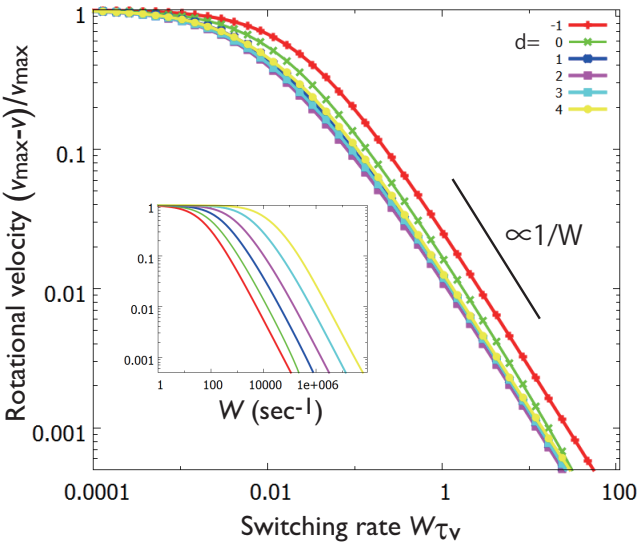

Fig 3.20: W dependence of velocity for the harmonic potential model with $q = 0$ (numerical). Different colors correspond to different d's, which changes the set of spring constant K and hydrolysis free energy $\Delta\mu$ in the model according to Eqs. (3-9-5) and (3-9-6). Results from models with different d are plotted by scaling W by $\tau_{\rm v}^{-1}$. Inset shows same data without scaling W.

To understand the limit $W \to 0$ of the model, we focus on the switching dynamics between potentials $U_0(x)$ and $U_1(x) - \Delta\mu$, since the dynamics between two neighboring potentials are

equivalent in steady-state. Our aim is to estimate the probability density of the position where the switching from $U_0(x)$ to $U_1(x) - \Delta\mu$ takes place:

$$\lambda(x) := \frac{\Lambda(x)}{W} = P_{\rm st}(x) f_0^+(x) - P_{\rm st}(x-L) f_1^-(x). \tag{3-9-7}$$

$P_0^{\rm ss}(x)$ and $P_1^{\rm ss}(x)$ are the steady-state densities of x under the condition that n is 0 and 1, respectively. The first term in the right-hand side of Eq. (3-9-7) corresponds to the probability density of the switching at x, whereas the second part is that of the switch back (1→0). When $\Lambda(x)$ is obtained, the internal heat dissipation may be calculated as

$$Q_{\rm int} = \frac{1}{Z}\int dx \lambda(x) \left[U_0(x) - U_1(x) + \Delta\mu\right], \tag{3-9-8}$$

where $Z = \int dx \lambda_0(x)$ is the normalization factor.

For $W \ll \tau_{\rm p}^{-1}$, the steady-state probability density of x is close to the equilibrium density inside each potential

$$P_{\rm st}(x) \simeq P_{\rm eq}(x) \propto \exp\left[-\frac{U_0(x)}{k_{\rm B}T}\right]. \tag{3-9-9}$$

Although this assumption is valid in estimating the first term in the right-hand side of Eq. (3-9-7), it fails to capture the feature of the second term at $W > 0$, since the small but finite switching makes $P_{\rm st}(x)$ deviate from $P_{\rm eq}(x)$ at around the peak point of $P_{\rm st}(x) f_0^+(x)$, where $f_1^-(x)$ may take a significantly large value.

We focus on the model with $q < x_c/L$, where

$$x_c := \frac{KL^2/2 - \Delta\mu}{k_{\rm B}TKL} \simeq 14^\circ \tag{3-9-10}$$

is the intersection point between the two potentials, $U_0(x_c) - U_1(x_c) + \Delta\mu = 0$. In this region of q, $P_0^{\rm eq}(x) f_0^+(x)$ has a peak at $x < x_c$. In order to phenemenologically take into account the effect of switch back, we consider the conditional probability that after the switching occurs at x, the potential stays as $U_1(x) - \Delta\mu$ and is not switched back to $U_0(x)$:

$$D_0(x) \;:=\; \frac{\exp[-\tau_v/\tau_{\rm leq}(x)] + \exp[E_0(x)]}{1 + \exp[E_0(x)]}. \tag{3-9-11}$$

We have introduced the local equilibrium time scale

$$\tau_{\rm leq}(x) := \frac{1}{R_0^+(x) + R_1^-(x)} = \frac{1}{W[f_0^+(x) + f_1^-(x)]}, \tag{3-9-12}$$

which is the typical time required for equilibration between $U_0(x)$ and $U_1(x) - \Delta\mu$ at a fixed position x. Using $D_0(x)$, we assume that the switching position probability density is given by

$$\tilde{\lambda}(x) := P_{\rm eq}(x) f_0^+(x) D_0(x). \tag{3-9-13}$$

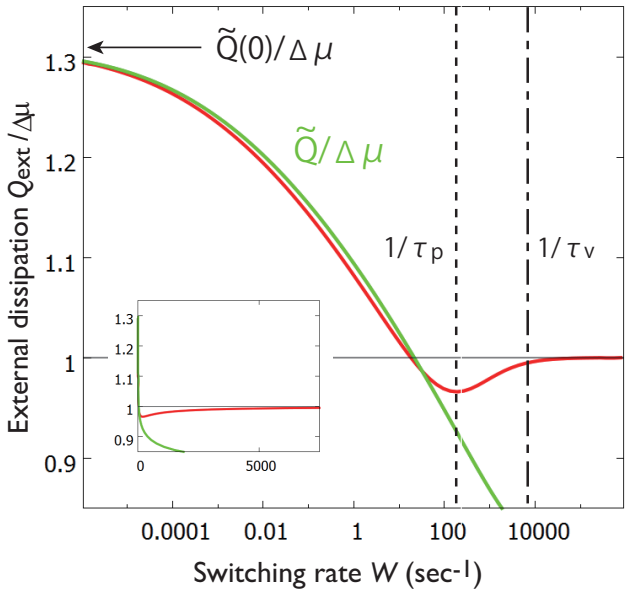

Fig 3.21: Numerically obtained $Q_{\rm ext}$ (red) and the theoretical $\tilde{Q}$ (green) obtained from Eq. 3-9-15 in the $q = 0$ model. Starting from $\tilde{Q}(0)$ at the limit $W \to 0$, $Q_{\rm ext}$ drops sharply in a manner $\propto -\log W$ at low but finite W. $Q_{\rm ext}$ stops dropping at $W \sim \tau_p^{-1}$, and converges to $\Delta\mu$ at $W > \tau_v^{-1}$. Inset shows same data with linear-scale W.

This is justified since the main contribution from the $P_1^{\rm ss}(x) f_1^-(x)$ term in Eq. 3-9-7 is the switch back which occurs right after the switch 0→1, and the probability that the probe spontaneously climbs the potential $U_1(x)$ in the backward direction for the switch back to occur is negligibly small.

As shown in Fig. 3.21, the external heat dissipation theoretically obtained as

$$\widetilde{Q}(W) := \Delta\mu - \frac{1}{Z}\int dx \tilde{\lambda}(x)\,[U_0(x) - U_1(x) + \Delta\mu] \tag{3-9-14}$$

$$= \frac{1}{2}KL^2 - \frac{KL}{Z}\int dx \tilde{\lambda}(x) x, \tag{3-9-15}$$

captures the feature of $Q_{\rm ext}$ at small W. Note that in the limit $W \to 0$, we find

$$Q_{\rm ext} = \widetilde{Q}(0) = (1/2 - q)KL^2, \tag{3-9-16}$$

since in this limit the switching position probability density becomes $P_{\rm eq}(x) f_0^+(x) \propto \exp[-K(x - qL)^2/2k_{\rm B}T]$, a Gaussian distribution with peak at $x = qL$. For finite W, the value of $Q_{\rm int}$ deviates drastically from $\widetilde{Q}(0)$ in a manner $\propto -\log W$, which is observed as a sharp drop when W or v is linear scaled (Fig. 3.21 inset, Fig. 3.19). Physically, this corresponds to the fact that very little ADP concentration is sufficient to prevent switching to occur at energetically unfavorable positions $[U_1(x) - U_0(x) - \Delta\mu \gg k_{\rm B}T]$.

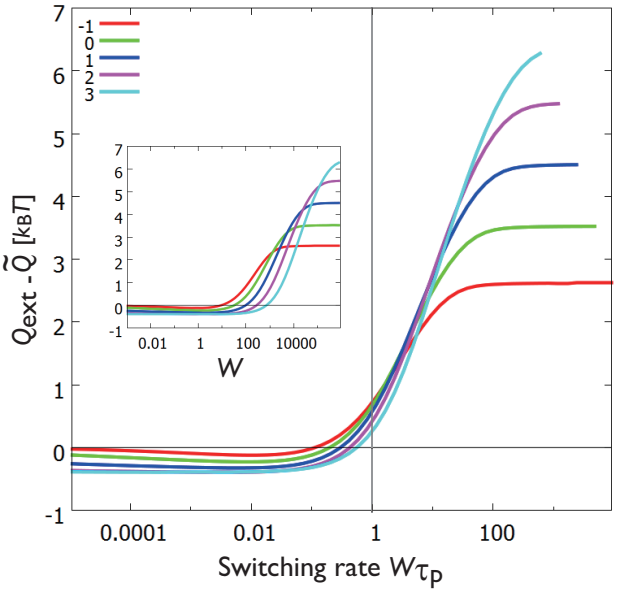

Fig 3.22: Deviation of $Q_{\rm ext}$ from the theoretically obtained $\tilde{Q}(W)$ from Eq. 3-9-15. Different colors correspond to $d = -1, 0, 1, 2, 3, 4, 5$ in the model parameterized by Eqs. 3-9-5) and 3-9-6. Inset shows same data without scaling.

$\lambda_0(x) \simeq \tilde{\lambda}_0(x)$ is valid when $W \ll \tau_{\rm p}^{-1}$, and should fail when $W > \tau_{\rm p}^{-1}$ since Eq. 3-9-9 used to evaluate the first term of Eq. 3-9-7 is violated in this region. The $Q_{\rm ext}$ therefore deviates from the sharp theoretical curve at around $W \sim \tau_{\rm p}^{-1}$ (Fig. 3.22). As shown in Fig. 3.21, the value of $\tilde{Q}(W)$ is sufficiently close to $\Delta\mu$ when $W \sim \tau_{\rm p}^{-1}$, which could be understood as follows. Assuming $D(x) \simeq \exp[-\tau_v/\tau_{\rm leq}(x)]$, the peak position $x = x_c - \delta$ of $\Lambda_0(x)$ at $W = \tau_{\rm p}^{-1}$ satisfies

$$\frac{KL(x_c - qL)}{k_{\rm B}T} = \frac{KL\delta}{k_{\rm B}T} - q\exp\left[-\frac{qKL\delta}{k_{\rm B}T}\right] + (1-q)\exp\left[\frac{(1-q)KL\delta}{k_{\rm B}T}\right]. \tag{3-9-17}$$

Using the δ obtained in Eq. 3-9-17, $\tilde{Q}(W = \tau_{\rm p}^{-1})$ is estimated as $\simeq \Delta\mu + KL\delta$. At large $A := KL^2/k_{\rm B}T$ and $B := \Delta\mu/k_{\rm B}T = O(A)$, the value of δ satisfying Eq. 3-9-17 scales as $A\delta/L \propto \log A$. Therefore, $\tilde{Q}(W = \tau_{\rm p})/\Delta\mu = 1 + O(\log A/A)$, which means that $\tilde{Q}(W = \tau_{\rm p}) \simeq \Delta\mu$ is satisfied with a small error term under $A \gg 1$.

To sum up, in the potential switching model with the switching rates Eq. (3-6-1) and $q < x_c/L$, $Q_{\rm ext}$ becomes sufficiently close to $\Delta\mu$ at $W \sim \tau_{\rm p}^{-1}$, when the condition $KL^2, \Delta\mu \gg k_{\rm B}T$ is satisfied. Since $\tau_{\rm p} = \tau_v KL^2/k_{\rm B}T$, there exists a time scale separation $\tau_{\rm p} \gg \tau_v$, hence at $W \sim \tau_{\rm p}^{-1}$ the velocity is still smaller than the maximum velocity, $v < v_{\rm max}$. This means that if $KL^2/k_{\rm B}T = 50$, which is the case where the maximum velocity is close to the real F_1, the model shows the $Q_{\rm ext} \sim \Delta\mu$ behavior even when [ATP] is as low as 1/50 of the velocity saturating concentration. Persistent $Q_{\rm ext} \sim \Delta\mu$ for the broad range of $W > \tau_{\rm p}^{-1}$ allows the low dependence of $Q_{\rm ext}$ on v, which explains the internal dissipation-free feature of F_1 observed in experiment. For the case

of models with $q > x_c/L$, it is confirmed that there exists a significant difference between Q_{ext} and $\Delta\mu$ for $W = \tau_{\text{p}}^{-1}$, even when d is as large as 5 in the parameterization given by Eqs. 3-9-5 and 3-9-6. It is left for future studies to theoretically understand the $q > x_c/L$ models (including $q = 0.5$ and 1, Fig. 3.13).

Chapter 4

Linear motors
-Cooperativity of cytoplasmic motors-

In this chapter, we discuss the model for linear molecular motors, which are motor proteins that typically function in the cytoplasm of eukaryotic cells. Our focus here is on the cooperativity of the molecular motors; unlike the F_1-ATPase, linear motors usually work in dimers or in multiple molecules sharing the same cargo. After reviewing the facts on the previously obtained experimental results on myosin, kinesin, and dynein proteins, we give a simple phenomenological understanding of the design principle in the single molecule of these motors. We then propose a scheme that allows diffusive and bidirectional elements to produce unidirectional transport through collective interaction. The key idea is that the force-sensor is coupled to the diffusive mode through the chemical state of each motor molecule. Further analysis considering the degree of freedom of the cargo is given.

4.1 Cytoplasmic motors

Linear motors are protein molecules that work typically in the cytoplasm of the cells with the roles for instance in cargo transport and cell division [1, 81]. These motor proteins function along pseudo-one-dimensional rails of microtubules or actin filaments, called cytoskeletons, in a unidirectional manner with the aid of the nonequilibrium free energy source, ATP. Intense studies on the mechanical properties of cytoplasmic motors have aroused interest from physicists as well as biologists. Not only that these motors touch so many aspects of cell- and developmental biology, it also provides rigorous examples to elucidate the design principles required in making such super-nanomachines.

Although cytoplasmic transport had been observed in plants from early as the 18th century, specific research on molecular motors are said to have originated by the studies on the acto-myosin (refering to actin + myosin) complex [82]. Acto-myosin is the main player in the muscle contraction dynamics [83, 84, 85]; myosin motors are themselves ATP hydrolyzing enzymes, which, in relative motion to the actin filament, extract force to make displacement at the single head levels. Myosin involved in muscle contraction, which is now classified as myosin II (or conventional myosin), forms a bundle to interact with the actin filament, and the dynamics of many single heads adds up to the contraction in the macro scale.

It was discovered later that there exist individual myosin motors that function as dimers, called processive myosins[1]. These myosins, for example myosin V [86] and myosin VI [87], have the capability to move along the actin filament without forming a bundle, and can transport cargoes even by a single molecule [88] in a robust and unidirectional manner. Although the functional roles and even the direction of transport is different among the myosins [89], the basic mechanism that govern the motion seems to be surprisingly preserved among the species.

Conventional kinesin, or kinesin-1, is similar to myosin V or VI in the sense that it is a processive motor which transports unidirectionally the cargos. It was originally found as the motor responsible for the fast axonal transport in the giant neuron of squid [90, 91]. The stage that kinesin acts on is the microtubule, which is a cytoskeleton with higher stiffness than actin filaments. Like myosin, there exists a super family of kinesins, with some moving in different directions [92] and some even functioning in monomers [93].

Single molecular level experiments [94, 95] have uncovered the high efficiency of these unidirectional motors [96]. Similarly to the F_1-ATPase, these cytoplasmic motors undergo stepwise motion with the step sizes corresponding to the length scale embedded in the cytoskeleton (Fig. 4.1), for example, 8 nm for conventional kinesin and 32 nm for myosin V. The stepwise motions were found to be the consequence of the hand-over-hand dynamics [97, 98] of these dimerized molecular motors; identical molecules are tied together through a linker, thus forming a dimer, which become the feet for the molecules to literally walk along the rails.

Recently, there is large attention devoted to another complex cytoplasmic motor, called dynein [99]. In comparison to the large family of kinesin and myosin, there is only one gene that encodes dynein (cytoplamic dynein 1), although it is responsible for most of the transport to the minus

[1] "Processive" is a technical term that refers to the ability of the molecular motor to attach to the rail (cytoskeleton) for a certain amount of time in a functional manner, typically showing unidirectional motion.

end of the microtubule in the cell. Dynein has a long history of research after its first discovery [100]. Nevertheless, it was not until recently that purified complexes of cytoplasmic dynein could be obtained to explore its biochemical properties, including the structure of motor domains and linkers [101].

The observed dynamics of single molecule cytoplasmic dyneins has proved to be unique. Dyneins, also dimerized molecular motors, produced uncoordinated stepping (yeast,[102, 103]) or diffusive motion (human,[104]) on the microtubule (Fig. 4.3, left). It was reported that the unidirectional motion of human cytoplasmic dyneins can be recovered [105, 106] however with the requirement of subcomplexes such as dynactins attached to the molecule.

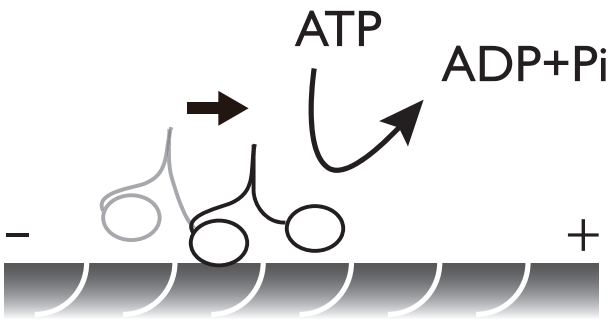

Fig 4.1: Conventional kinesin as an example of dimerized molecular motor with discrete step size. The step size is 8 nm, corresponding to the minimal components of microtubules (the pair of $\alpha\beta$ tubulin) which form a lattice-like structure in the one-dimensional direction. The microtubule has polarity, thus kinesin knows which way it should step to (plus end, right in figure). A single molecule of ATP is consumed in one forward step of kinesin, resembling the stepwise dynamics of F_1. The major difference, however, is in the reversibility of the dynamics; there is no evidence that kinesin synthesizes ATP when the probe is pulled backward with respect to the direction of motion, and instead it may be even hydrolysing ATP upon the backstep [75].

4.1.1 Mechanism of motion

We describe in Fig. 4.2 the simplified schematic of the relation between the chemical states and the dynamics in conventional kinesin and myosin V. The key in the design principle in these molecules is how they incorporate the directionality; the motor heads of these dimers should know whether or not they are in the front or in the back, and proceed their chemical reactions with the rates controlled by these notions. Since in these motors the heads are separated and only linked through protein chains, it is unnatural to assume that one molecule knows the precise chemical state of the other molecule. In contrast, it should be possible for the molecule to sense the force from the other, through the conformational change of its own caused by the interaction of the molecules through the pushing or pulling by the linker.

Indeed, such force-sensor mechanism has been elucidated in single head experiments for myosin and kinesin [110]. In [111], for example, it was shown that the single headed myosin molecules have a preference of direction in the binding dynamics; it has a larger time scale

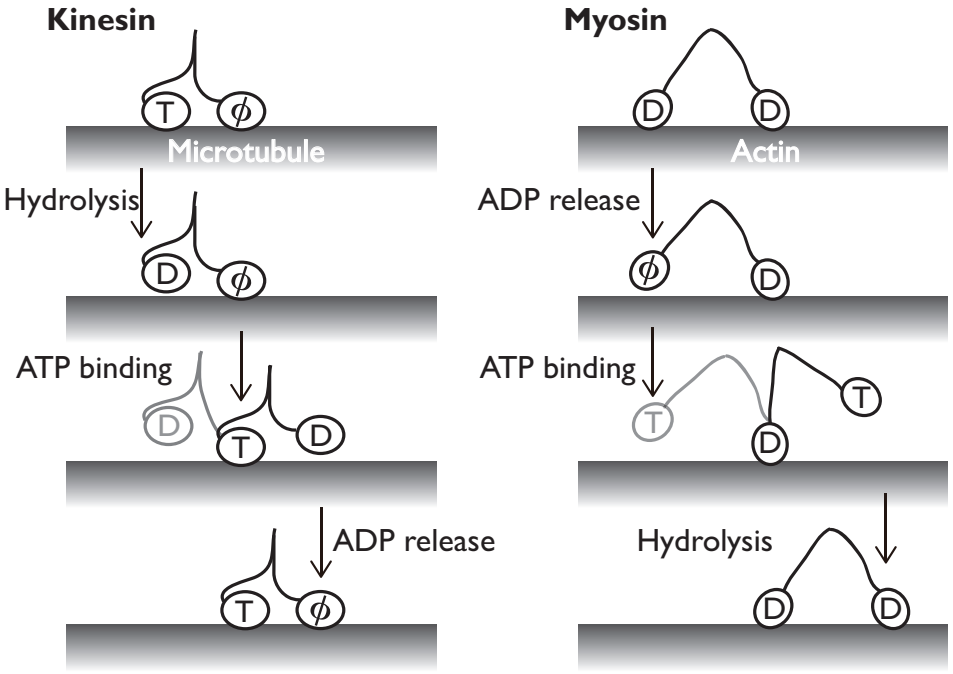

Fig 4.2: Simplified schematics of the stepwise motion of molecular motors [107, 108]. T: ATP, D: ADP, and ϕ: no nucleotides (apo). Although some states described as D in the figure should be substituted by ADP+Pi, we omitted Pi for the sake of simplicity. (Left) Hand-over-hand motion of conventional kinesin. The tightly bound state and the weakly bound state (released state) in the single motor head correspond to "T or ϕ" and "D", respectively. (Right) Hand-over-hand motion of Myosin V. The step size is 32 nm corresponding to half of the pitch size in the actin rail. The tightly bound state and the weakly bound (released state) correspond to "D" and "T or ϕ", respectively. The mechanism is very similar for the case of myosin VI [109], only with the polarity switched to the opposite direction.

to be stuck on the actin rail when it is pulled backward with respect to the directional motion, compared with when pulled forward. The strongly bound state of myosin to the actin corresponds to the chemical state with ADP or ADP+Pi bound to the motor head. Thus, the experimental result indicates that the switching of the state in myosin from the tightly bound to the detached (corresponding to the nucleotide free state), is less likely to occur when the head is in the back, rather than when in the front (Fig. 4.2, right).

Such preference of direction embedded in the chemical reaction rate has also been found in single monomer dynein experiments [104, 112]. In the case of dynein, although large heterogeneity has been observed in the feature of motion and stall force among the molecular species, it seems common that there are also two states of conformation, named in some context, pre-power-stroke and post-power-stroke [113]. The two states, corresponding to the ATP binding state and the ADP or apo (nucleotide null) state (Fig. 4.4), presumably have different interaction with the microtubule according to the recent data [104].

Experimental techniques have further allowed systematic analyses on the effect of coordination in the motor protein dynamics. Since the force-sensing mechanism is relying on the proper

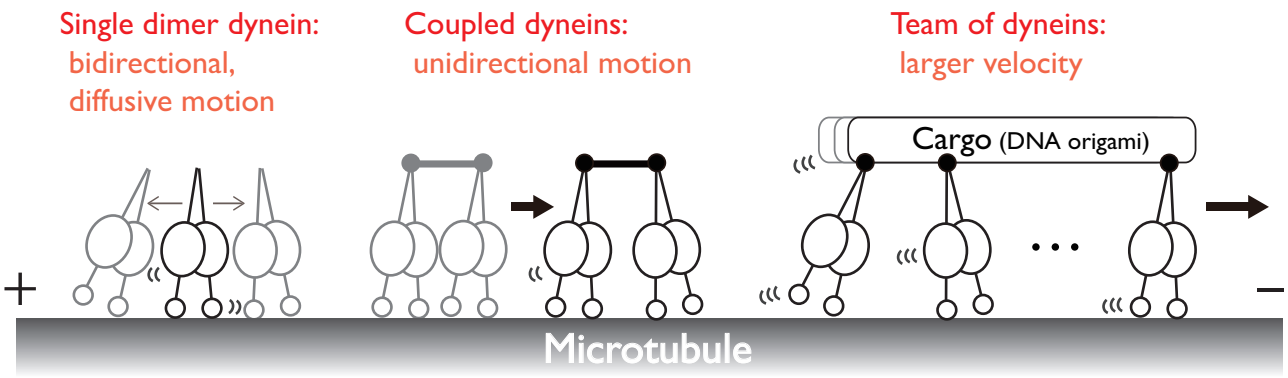

Fig 4.3: Schematic of the experimental results on human cytoplasmic dynein. Single dimers of full-length dynein were observed to undergo bidirectional diffusive motion. When two or more of the dimer dynein molecules where tied together by double strand DNA (middle) or through an artificial cargo made of DNA origami (right), unidirectional motion appeared.

interaction between the molecular motor heads, it is natural to consider that the artificial manipulation of motors will lead to perturbations in their functions. In [107], the linker of kinesin heads, which is a region of protein chain called neck-linkers, were controlled by adding extra residues. Although some properties such as speed and ATP hydrolysis rate where changed, the motors were able to perform unidirectional motion, suggesting that the information transmitted through the linker does not rely on the specific conformation of the linkers.

In [104], Torisawa et al. reported that the motion of human cytoplasmic dynein changes from bidirectional and diffusive (Fig. 4.3, left) to unidirectional (Fig. 4.3, middle, right) only by putting multiple molecules in interaction through cargo. The simple scheme presented here motivates us to consider the fundamental mechanism behind unidirectional motion of cytoplasmic motors.

Another key feature apart from the head-head interaction of these motors is the multiple states of diffusive motion. The highly diffusive motion, as observed even in dimeric cytoplasmic dyneins, may be a general physical feature for molecules weakly interacting with the microtubule [114], since similar motion has been observed for the monomer kinesin (KIF1A) [93], myosin on microtubules [115] and even in the case of electro-statically bound silica bead [116]. Such weak confinement in one-dimension is considered to be caused by the negatively charged flexible tails of the microtubules, which attract the positively charged protein molecules and effectivly trap them inside a certain length scale around the microtubule.

The other state of diffusivity is the tightly bound state. As depicted in the cases of myosin and kinesin (Fig. 4.2), the single motor heads attach strongly to the rail in some nucleotide state, which is in contrast to the highly diffusive state that is essentially liberated from the rail or at least in low interaction with it. The two diffusive modes can thus be assigned to two chemical states of the motors. Large diffusion constant appears for the chemical (nucleotide) state which induces weaker binding to the rail, where as smaller (or effectively zero) diffusive constant corresponds to the nucleotide state coresond to the tightly bound state.

The switching between these different states themselves may play crucial roles other than the powerstroke mechanism. In the powerstroke picture, for instance the lever arm model of the

myosin, it is assumed that typical high free energy consuming reactions have one-to-one correspondence with the force generating step. On the contrary, if the switching of the interaction with the rail is operated under a well-designed rule, for example the biased switching, merely the thermal force is sufficient to explain the motion of the motors. There is discussion on whether the direct force generation (powerstroke) or the biased switching is important in molecular motors [111, 117]; it is possible that the balance between them vary between the motor species.

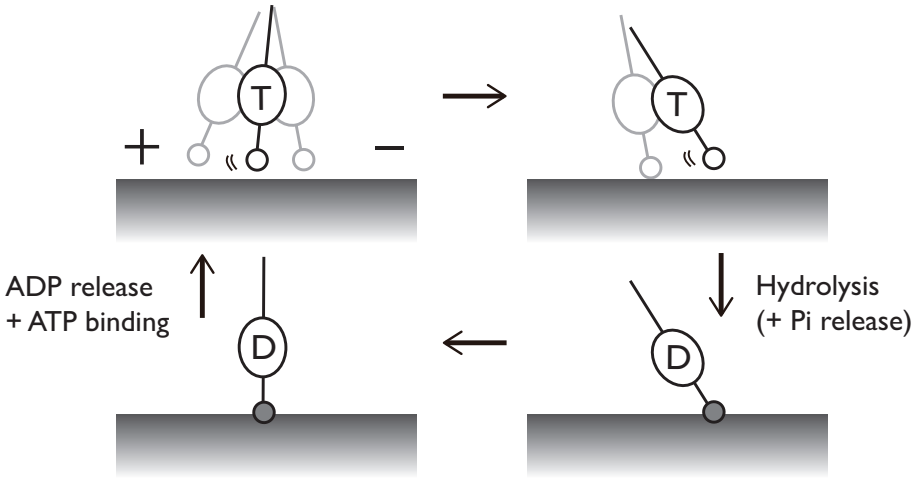

Fig 4.4: Possible mechanism behind the asymmetric interaction between the dynein motor and the microtubule. When dynein is free of load, or is pulled toward the minus end direction, it is likely to stay in the ATP state (with the mark "T"), which is thought to have weak interaction with the microtubule (left top). On the other hand, when dynein is pulled backward (toward the plus end direction), it is likely to transition into the ADP (or apo) state (with the mark "D"), that has stronger interaction with the rail (right bottom). Switching between the states should be accompanied by the chemical reaction steps, for which one cycle of transition amounts to a single molecule ATP hydrolysis.

4.2 Aim of study

In light of the development in the understanding of the design principles behind the motion of cytoplasmic motors, we here aim to propose a simple mechanism that allows the emergence of unidirectional motion through the collective interaction of individually bidirectional molecules.

We introduce a simple solvable Langevin model of a multi-headed motor, which we call a chemically-driven inchworm. The main concept of this model is that the motion of molecules themselves do not have polarity, but the rule of switching between the two diffusive modes on the rail is breaking the symmetry. Through the analysis of this model, especially from the formula of the steady-state velocity, we clarify the role of nonequilibrium chemical free energy input. The nonequilibrium-ness of the model appears in the interpretation of the multiple in the Langevin description.

Similar schematics of motor protein motion has been discussed with long history ([83, 110, 118, 111], to name a few). The aim in our model, however, is to elucidate the key parameters

that control the extent of cooperativity. To this end, we focus on the force-sensitivity, which is a non-dimensional parameter in the model that measures at what value of potential energy (corresponding to force) the switching rule changes. We find that for the case where the force-sensitivity is high, the motor prefers to be in lower number rather than in large number, when considering the velocity of transport.

To confirm our picture obtained in the simplified model, we extend the model to the case where multiple motors carry the same cargo. We discuss how the force-sensitivity of motor proteins may be reflected in the single dimer molecules, with remarks on the classification of cytoplasmic motors.

4.3 Chemically-driven inchworm

4.3.1 Setup for dimer model

We first consider the dynamics of two Brownian particles that are tied together with a spring. We have in mind the experiment where two cytoplasmic dynein dimers were linked through a double-strand DNA [104].

We assume that the single particles have two states of diffusive motion, a highly diffusive state with diffusion constant D and a less diffusive state with diffusion constant d. In the case of human cytoplasmic dynein, for example [104], it is possible to estimate $D \sim 5 \times 10^4 \mathrm{nm}^2/\mathrm{sec}$ and $d < 8 \times 10^2 \mathrm{nm}^2/\,\mathrm{sec}$ by fitting a double-Gaussian function to the distribution of displacement under fixed time frame. The existence of two states of diffusive modes, with the less diffusive state possibly corresponding to case where the particle is tightly bound to the rail ($d \ll D$), is supposed to model the broad situation of molecular motors, as depicted in Figs. 4.2 and 4.4.

The diffisive modes of the molecules stochastically switch between the two diffusive states, with a switching rule depending on the force applied to the single molecules [114, 115]. This is taken into account in the model by allowing stochastic switching between the two diffusive state, in a force-dependent manner.

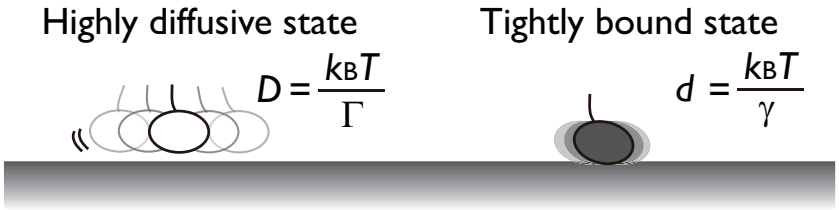

Fig 4.5: Model of the two diffusive modes of the molecular motors. The highly diffusive state corresponds to the chemical state where the rail and the motor protein interact weakly. The tightly bound state corresponds to the state where stronger interaction exists. We introduce the difference between these two states by simply assigning different diffusion coefficients, D and d. The estimated value of D and d for cytoplasmic dynein is 5×10^4 nm^2/sec and $< 8 \times 10^2$ nm^2/sec, respectively [104].

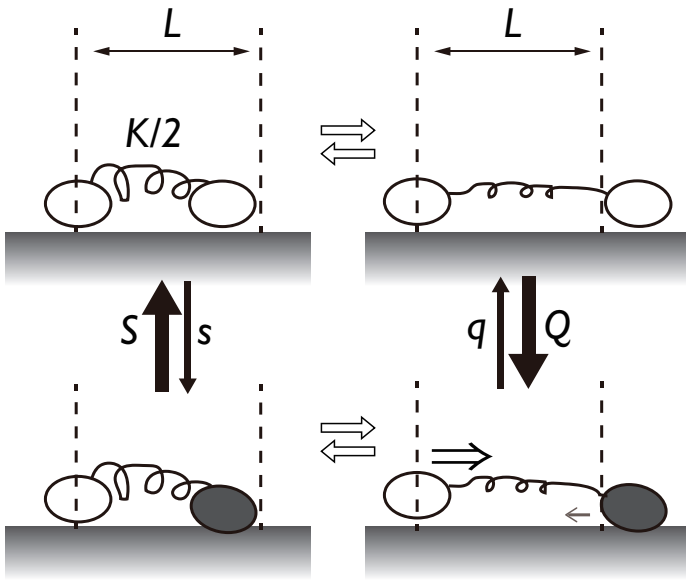

Fig 4.6: Schematic of the chemically-driven inchworm model. The two motor molecules are tied together with a spring. The stochastic switching between the highly diffusive state and the less diffusive state is controlled by a force-sensor; when the potential energy amounts to some value determined by the introduced length scale L, then there is higher probability for the head to switch to a low diffusive state.

The two diffusive molecules are attached to a spring with spring constant $K/2$. Setting x and y as the position of the first and second particles, we have the equation of motion:

$$\gamma_{\mathrm{X}}\dot{x} = -\frac{K}{2}(x-y) + \sqrt{2\gamma_{\mathrm{X}}k_{\mathrm{B}}T}\xi_{\mathrm{X}}(t) \tag{4-3-1}$$

$$\gamma_{\mathrm{Y}}\dot{y} = -\frac{K}{2}(y-x) + \sqrt{2\gamma_{\mathrm{Y}}k_{\mathrm{B}}T}\xi_{\mathrm{Y}}(t). \tag{4-3-2}$$

Here, $\xi_{\mathrm{X}}(t)$ and $\xi_{\mathrm{Y}}(t)$ are independent Gaussian white noises with unit variance. Corresponding to the two diffusive modes, the friction variables γ_{X} and γ_{Y} can take the values of $\gamma := k_{\mathrm{B}}T/d$ and $\Gamma := k_{\mathrm{B}}T/D$. The stochastic dynamics that rule the transition of the variables γ_{X} and γ_{Y} is the Markov jump process. Denoting the rate of the first particle to switch its friction constant from γ to Γ as $R_{\mathrm{X}}(\gamma \to \Gamma|x,y)$, for example, the rates are defined as the function of the interval between x and y:

$$R_{\mathrm{X}}(\gamma \to \Gamma|x,y) = \begin{cases} q & (x-y > L) \\ S & (x-y \le L) \end{cases} \tag{4-3-3}$$

$$R_{\mathrm{X}}(\Gamma \to \gamma|x,y) = \begin{cases} Q & (x-y > L) \\ s & (x-y \le L) \end{cases} \tag{4-3-4}$$

$$R_{\mathrm{Y}}(\gamma,\Gamma \to \Gamma,\gamma|x,y) = (\text{same as above with } x \leftrightarrow y) \tag{4-3-5}$$

Setting $\gamma > \Gamma$ ($D < d$) and $Q/q, S/s > 1$, these transition rates imply that the leading particle tends to switch to the less diffusive mode (with diffusion constant d) when $|x-y| > L$, but otherwise

both molecules prefer to stay in the highly diffusive mode (D). Schematic of the switching rates is described in Fig. 4.6.

4.3.2 Derivation of steady-state velocity

To confirm that the simple model shows unidirectional motion, let us consider the Master equation corresponding to Eqs. (4-3-1) and (4-3-2), and solve for the case where the chemical reactions are fast compared with the Brownian motion. This assumption is valid when the chemical reactions are sufficiently fast; in experiment, this corresponds to is the case where diffusion rather than the reaction is the limiting factor, which is when the velocity has saturated as the function of ATP concentration.

The time evolution of the probability density function $P_t(x, y, \gamma_X, \gamma_Y)$ follows

$$\begin{aligned}\frac{\partial}{\partial t}P_t(x,y,\gamma_X,\gamma_Y) &= \left[\frac{\partial}{\partial x}\frac{K}{2\gamma_X}(x-y)+\frac{\partial}{\partial y}\frac{K}{2\gamma_Y}(y-x)+\frac{\partial^2}{\partial x^2}\frac{k_BT}{\gamma_X}+\frac{\partial^2}{\partial y^2}\frac{k_BT}{\gamma_Y}\right]P_t(x,y,\gamma_X,\gamma_Y)\\ &+R_X(\bar{\gamma}_X\to\gamma_X|x,y)P_t(x,y,\bar{\gamma}_X,\gamma_Y)+R_Y(\bar{\gamma}_Y\to\gamma_Y|x,y)P_t(x,y,\gamma_X,\tilde{\gamma}_Y)\\ &-\left[R_X(\gamma_X\to\bar{\gamma}_X|x,y)+R_Y(\gamma_Y\to\bar{\gamma}_Y|x,y)\right]P_t(x,y,\gamma_X,\gamma_Y). \qquad (4\text{-}3\text{-}6)\end{aligned}$$

which is the Fokker-Planck equation. We introduced the notation $\bar{\gamma}_X, \bar{\gamma}_Y$, which flips the value of the friction constant:

$$\bar{\gamma}_{X,Y} := \begin{cases}\gamma & (\text{if } \gamma_{X,Y}=\Gamma)\\ \Gamma & (\text{if } \gamma_{X,Y}=\gamma).\end{cases} \qquad (4\text{-}3\text{-}7)$$

The first line in the right hand side of Eq. (4-3-6) corresponds to the ordinary Orenstein-Urlenbeck process with the instantaneous friction constants $\gamma_X and \gamma_Y$. The second and third lines correspond to the Markov jump switching of the friction constants.

Let us introduce the time scale of the chemical reactions, W^{-1}, and the non-dimensional functions, $f(\gamma_{x,y}\to\bar{\gamma}_{x,y}|x,y)$, to normalize the stochastic jump rates:

$$R_{X,Y}(\gamma_{X,Y}\to\bar{\gamma}_{X,Y}|x,y) = W f_{X,Y}(\gamma_{X,Y}\to\bar{\gamma}_{X,Y}|x,y). \qquad (4\text{-}3\text{-}8)$$

By considering the case where W is sufficiently large [see similar analysis conducted in Sect. 3.3.3], the probability density function may be written as a product of a time-dependent density of x, y and the time-independent conditional probability of γ_X, γ_Y:

$$P(x,y,\gamma_X,\gamma_y) = P_t(x,y)P_{eq}(\gamma_X,\gamma_Y|x,y) \qquad (4\text{-}3\text{-}9)$$

Here, $P_{eq}(\gamma_x,\gamma_y|x,y)$ is the solution to the equations

$$f_X(\bar{\gamma}_X\to\gamma_X|x,y)P_{eq}(\bar{\gamma}_X,\gamma_Y|x,y) - f_X(\gamma_X\to\bar{\gamma}_X|x,y)P_{eq}(\gamma_X,\gamma_Y|x,y) = 0 \qquad (4\text{-}3\text{-}10)$$

$$f_Y(\bar{\gamma}_Y\to\gamma_Y|x,y)P_{eq}(\gamma_X,\bar{\gamma}_Y|x,y) - f_Y(\gamma_Y\to\bar{\gamma}_Y|x,y)P_{eq}(\gamma_X,\gamma_Y|x,y) = 0. \qquad (4\text{-}3\text{-}11)$$

Note that we fix $\widetilde{q} := q/Q$, $\widetilde{s} := s/S$, and $\theta := (S+s)/(Q+q)$ while taking $Q, q, S, s \to \infty$ corresponding to $W \to \infty$.

Substituting Eq. (4-3-9) into Eq. (4-3-6) and taking the summation over $\gamma_{\mathrm{X,Y}} = \gamma, \Gamma$, we have

$$\frac{\partial}{\partial t}P_t(x,y) = \left[\frac{\partial}{\partial x}\frac{K(x-y)}{2\widetilde{\gamma}_{\mathrm{X}}(x,y)} + \frac{\partial}{\partial y}\frac{K(y-x)}{2\widetilde{\gamma}_{\mathrm{Y}}(x,y)} + \frac{\partial^2}{\partial x^2}\frac{k_{\mathrm{B}}T}{\widetilde{\gamma}_{\mathrm{X}}(x,y)} + \frac{\partial^2}{\partial y^2}\frac{k_{\mathrm{B}}T}{\widetilde{\gamma}_{\mathrm{Y}}(x,y)}\right]P_t(x,y), \quad (4\text{-}3\text{-}12)$$

with

$$\widetilde{\gamma}_{\mathrm{X,Y}}(x,y) \;:=\; \left[\sum_{\gamma_{\mathrm{X}},\gamma_{\mathrm{Y}}=\gamma,\Gamma}\frac{P^{\mathrm{eq}}(\gamma_{\mathrm{X}},\gamma_{\mathrm{Y}}|x,y)}{\gamma_{\mathrm{X,Y}}}\right]^{-1}. \quad (4\text{-}3\text{-}13)$$

The Langevin equation corresponding to Eq. (4-3-12) is written as

$$\dot{x} = -\frac{K(x-y)}{2\widetilde{\gamma}_{\mathrm{X}}(x,y)} + \sqrt{\frac{2k_{\mathrm{B}}T}{\widetilde{\gamma}_{\mathrm{X}}(x,y)}}\cdot\xi_{\mathrm{X}}(t) \quad (4\text{-}3\text{-}14)$$

$$\dot{y} = -\frac{K(y-x)}{2\widetilde{\gamma}_{\mathrm{Y}}(x,y)} + \sqrt{\frac{2k_{\mathrm{B}}T}{\widetilde{\gamma}_{\mathrm{Y}}(x,y)}}\cdot\xi_{\mathrm{Y}}(t), \quad (4\text{-}3\text{-}15)$$

where $\cdot$ is a multiple that should be interpreted in the Itô sense.

We introduce $\xi = (x+y)/2$ and $\eta = (x-y)/2$. Since the jump rate functions (4-3-3-4-3-5) only depend on η, we are able to define

$$\widetilde{\gamma}(\eta) := \widetilde{\gamma}_{\mathrm{X}}(x,y) = \widetilde{\gamma}_{\mathrm{Y}}(y,x) = \begin{cases} k_{\mathrm{B}}T/\widetilde{d} & (\eta > L/2) \\ k_{\mathrm{B}}T/\widetilde{D} & (\eta \le L/2) \end{cases}, \quad (4\text{-}3\text{-}16)$$

with the effective diffusion constants

$$\widetilde{D} := \frac{SD+sd}{S+s}, \quad \widetilde{d} := \frac{qD+Qd}{q+Q}. \quad (4\text{-}3\text{-}17)$$

From Eqs. (4-3-14) and (4-3-15) we have

$$\dot{\eta} = -\frac{K\eta}{2}\left[\frac{1}{\widetilde{\gamma}(\eta)} + \frac{1}{\widetilde{\gamma}(-\eta)}\right] + \sqrt{\frac{k_{\mathrm{B}}T}{2\widetilde{\gamma}(\eta)} + \frac{k_{\mathrm{B}}T}{2\widetilde{\gamma}(-\eta)}}\cdot\xi'(t). \quad (4\text{-}3\text{-}18)$$

The dynamics described by Eq. (4-3-18) produces no current in η, therefore it is in equilibrium. However, since the multiple in the fluctuation term is interpreted in the Itô sense, the steady-state density deviates from the canonical density. By using Eq. (2-4-31) with $p = 1$, the steady-state average density of η is obtained as

$$P_{\mathrm{ss}}(\eta) \propto \left[\frac{1}{\widetilde{\gamma}(\eta)} + \frac{1}{\widetilde{\gamma}(-\eta)}\right]^{-1}\exp\left[-\frac{K\eta^2}{k_{\mathrm{B}}T}\right]. \quad (4\text{-}3\text{-}19)$$

Using Eq. (4-3-19), the steady-state average velocity, V_2, can now be obtained:

$$V_2 := \langle \dot{\xi} \rangle_{\rm ss} = \int_{-\infty}^{\infty} d\eta P_{\rm ss}(\eta) \left\{ -\frac{K\eta}{2} \left[\frac{1}{\widetilde{\gamma}(\eta)} - \frac{1}{\widetilde{\gamma}(-\eta)} \right] \right\} \tag{4-3-20}$$

$$= -\frac{K}{2} \frac{\displaystyle\int_{-\infty}^{\infty} d\eta \frac{\widetilde{\gamma}(\eta)^{-1} - \widetilde{\gamma}(-\eta)^{-1}}{\widetilde{\gamma}(\eta)^{-1} + \widetilde{\gamma}(-\eta)^{-1}} \eta \exp\left[-\frac{K\eta^2}{k_{\rm B}T} \right]}{\displaystyle\int_{-\infty}^{\infty} d\eta [\widetilde{\gamma}(\eta)^{-1} + \widetilde{\gamma}(-\eta)^{-1}]^{-1} \exp\left[-\frac{K\eta^2}{k_{\rm B}T} \right]} \tag{4-3-21}$$

$$= \widetilde{D} \sqrt{\frac{K}{\pi k_{\rm B}T}} \frac{1-\epsilon}{1+\epsilon+2(1-\epsilon)\Phi\left(\sqrt{E}\right)} e^{-E/2}. \tag{4-3-22}$$

Here we defined the parameter corresponding to the inverse of the sensitivity of force:

$$E := \frac{KL^2}{2k_{\rm B}T}, \tag{4-3-23}$$

and $\epsilon := \widetilde{d}/\widetilde{D}$. We also introduced the function

$$\Phi(a) := \frac{1}{\sqrt{2\pi}} \int_{-\infty}^{a} dx e^{-x^2/2}. \tag{4-3-24}$$

We immediately see from Eq. (4-3-22) that the steady-state velocity is positive when $\epsilon < 1$, which is a satisfied condition as long as $d < D$ and $QS/qs > 1$. The velocity becomes zero if $QS/qs = 1$, irrespective of the values of d, D, which is consistent with the picture that the nonequilibrium cycle depicted in Fig. 4.6 is critical in the motion of the motor. In the words of free energy, one cycle in the clockwise direction presented in Fig. 4.6 should amount to a single ATP hydrolysis reaction. Since we assume that upon stochastic switching there is no change in the mechanical (effective) potential profile as in the case of the model for F_1, we have the simple constraint in the stochastic switching rules,

$$\frac{QS}{qs} = \exp\left[\frac{\Delta\mu}{k_{\rm B}T} \right]. \tag{4-3-25}$$

Thus, $QS/qs > 1$ corresponds to the assumption, $\Delta\mu \geq 0$.

Schematically, the finite steady-state velocity of the two-particle model may be understood as follows. When the two molecules are near each other or feel low tension (Fig. 4.6, left), the two molecules will most likely be in the highly diffusive state, and there is no net transport in the center of mass. However, once the two molecules come apart due to the Brownian motion, the molecule in the front will feel force toward the backward direction, and will likely transition into a tightly bound state, following the rule depicted in the right side of Fig. 4.6. Since in such case there is strong tension between the molecules, the particle in the back, which is likely to be staying in the highly diffusive state, will have larger chance to be pulled forward (Fig. 4.6, right). Thus, the introduced rule on switching lets the center of mass of the molecules to be transported forward on average.

From the more fundamental side, the Itô integral in Eq. (4-3-18) plays the essential role for the model to show nonequilibrium transport. The situation should be compared with the Brownian inchworm model introduced in [119, 120], where the particles with coordinate-dependent friction needed to be shaken by active ($\neq$ thermal) noise in order to produce unidirectional motion. The difference between the models come from the origin of inhomogeneous friction in the models. If the particles passively have the property of inhomogeneous friction, for instance it develops larger friction when pulled backward owing to its non-uniform interaction with the surface, the model is essentially in equilibrium, and the anti-Itô interpretation arises as a natural consequence [cf., Sect. 2.4.3]. On the contrary, what we found in our model is that the Itô interpretation arises when the cause of position dependent friction is due to fast and nonequilibrium chemical reactions.

Remark should be made on our assumption that the typical rate of the chemical reaction, W, is very large. Although it is difficult to obtain the precise value of W in experiment, it should be sensible to estimate from the maximum velocity of F_1-ATPase rotation and kinesin locomotion, which is more than 100 per second. Thus, W can be taken to be the order of 1000 $\sec^{-1}$, considering that the approaching rate of nucleotides do not vary so much in different motor species.

How large W should be in the model determined from the smallest length scale in the system, which in this case, is the length scale inherited in $P_{\rm eq}(\cdot)$, which is zero. In reality, there should be some small length scale that characterizes the position dependence of the switching rates, $l_{\rm s}$, and we should take $W \gg k_{\rm B}T/\gamma l_{\rm s}^2$. Therefore, what we calculated was the case where $W \gg k_{\rm B}T/\gamma l_{\rm s}^2 \gg K/\gamma$. As we shall see, the length scale $l_{\rm s}$ naturally arises in the case where we explicitly consider the motion of cargo (cf., Sect. 4.4).

4.3.3 Extension to multi-molecules

The natural extension of the previous inchworm model to $N > 2$ molecules may be given as follows. Denoting the position of the i-th particle (motor head) as x_i, and the Gaussian white noises with unit variances as $\xi_i(t)$, the overdamped Langevin equation reads

$$\gamma_i \dot{x}_i = -K\,(x_i - \overline{x}) + \sqrt{2\gamma_i k_{\rm B}T}\,\xi_i(t), \tag{4-3-26}$$

We have introduced the frictions γ_i, which stochastically switch between two values, γ and $\Gamma = k_{\rm B}T/D$, similarly to the previous model. We assume that the switching rates are independent for each particle, but depend on the relative position of the motor seen from the average position, $\overline{x} := \sum_i x_i/N$:

$$R_i(\gamma \to \Gamma | x_i, \overline{x}) = \begin{cases} q & (x_i - \overline{x} > L/2) \\ S & (x_i - \overline{x} \le L/2) \end{cases} \tag{4-3-27}$$

$$R_i(\Gamma \to \gamma | x_i, \overline{x}) = \begin{cases} Q & (x_i - \overline{x} > L/2) \\ s & (x_i - \overline{x} \le L/2) \end{cases}. \tag{4-3-28}$$

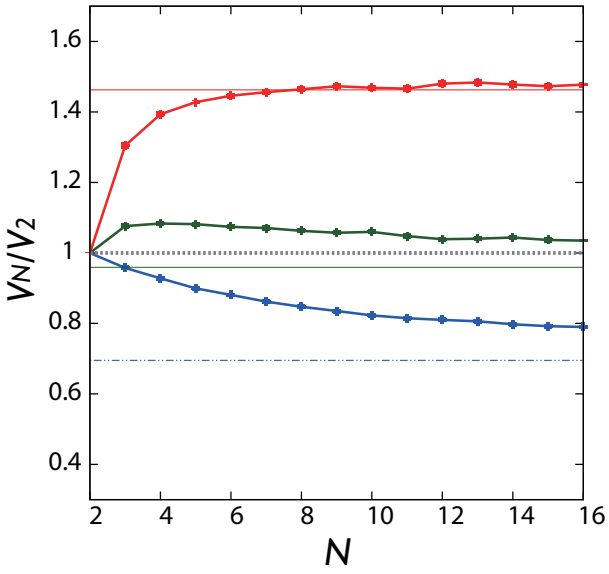

Fig 4.7: Numerical results for the chemically-driven inchworm model, Eq. (4-3-29). $\epsilon := \widetilde{d}/\widetilde{D}$ was fixed at 0.02, as estimated from experiments on dynein . Three cases of $E := KL^2/2k_BT$ were tested: results for $E = 1.3, 0.4$, and 0.1 are plotted in red, green, and blue, respectively. the solid and dotted lines corresponding to the same colors are the analytically obtained values of V_∞/V_2 in the same parameter setups.

It is easily confirmed that the $N = 2$ case is equivalent to the model in Sect. 4.3.1. Again, by assuming the fast chemical reaction limit, we arrive at

$$\dot{x}_i = -\frac{K}{\widetilde{\gamma}(\eta_i)}(x_i - \bar{x}) + \sqrt{\frac{2k_BT}{\widetilde{\gamma}(\eta_i)}} \cdot \xi_i(t), \tag{4-3-29}$$

where $\eta_i := x_i - \bar{x}$, and the effective potential $\widetilde{\gamma}(\eta_i)$ is equivalent to the step function obtained in Eq. (4-3-16). Here, the integral in the fluctuation term is again interpreted in the Itô sense.

The numerical simulation results for two example cases in the general N model is are given in Fig. 4.7. Since the model can be non-dimensionalized and rewritten using ϵ and E apart from the typical time scale, Γ/K, which only changes the velocity by multiples, we fixed ϵ to the experimental data estimated in dynein, $\epsilon = 0.02$ and changed E in the simulations. We observe that for large N, the steady-state velocity converges to a finite value. It is also found that whether the velocity increases or decreases with respect to the molecular number N, depends on the parameters.

Although it is challenging to solve the model with general N, we may consider the case of $N \to \infty$ through the mean field theory, and especially prove the convergence of the steady-state velocity to a finite quantity, V_∞. To this end, we first write the equation of motion for η_i.

$$\dot{\eta}_i = -\frac{K\eta_i}{\widetilde{\gamma}(\eta_i)} + \sqrt{\frac{2k_BT}{\widetilde{\gamma}(\eta_i)}} \cdot \xi_i(t) + \frac{1}{N}\sum_j \left[\frac{K\eta_j}{\widetilde{\gamma}(\eta_j)} - \sqrt{\frac{2k_BT}{\widetilde{\gamma}(\eta_j)}} \cdot \xi_j(t)\right], \tag{4-3-30}$$

Due to the central limit theorem, the fluctuation of the third and forth terms become negligible at $N \to \infty$ compared with that of the second term. Therefore, we may substitute the third term with a constant. Since $\langle \dot{\eta}_i \rangle_{\rm ss} = 0$, this introduced constant should be equal to the steady-state velocity:

$$\dot{\eta}_i = -\frac{K\eta_i}{\widetilde{\gamma}(\eta_i)} + \sqrt{\frac{2k_{\rm B}T}{\widetilde{\gamma}(\eta_i)}} \cdot \xi_i(t) - V_\infty + O\left(\frac{1}{\sqrt{N}}\right) \tag{4-3-31}$$

$$V_\infty := \langle \dot{\tilde{x}} \rangle_{\rm ss} = \langle \dot{x}_i \rangle_{\rm ss} = \left\langle -\frac{K\eta_i}{\widetilde{\gamma}(\eta_i)} \right\rangle \tag{4-3-32}$$

In the limit of $N \to \infty$, equations (4-3-32) and (4-3-31) form the self consistency equation. By fixing the constant V_∞, the steady-state density of η_i reads

$$P_{\rm ss}(\eta_i) = \frac{\exp\left[-K\eta_i^2/2k_{\rm B}T\right]}{Z'} \times \begin{cases} e^{-V_\infty(\eta_i - L/2)/\widetilde{D}}/\widetilde{D} & (\eta_i \le L/2) \\ e^{-V_\infty(\eta_i - L/2)/\widetilde{d}}/\tilde{d} & (\eta_i > L/2). \end{cases}, \tag{4-3-33}$$

where we used Eq. (2-4-31) again.

Notice that the distribution of η_i is independent of $\eta_{j\neq i}$ in this mean field limit $N \to \infty$. The value of V_∞ may be calculated by noticing that the average displacement of molecule i with respect to the mean position

$$\begin{aligned} \langle \eta_i \rangle = \int d\eta P_{\rm ss}(\eta)\eta \propto \frac{1}{\widetilde{D}} \int_{-\infty}^{L/2} d\eta \exp\left[-K\eta_i^2/2k_{\rm B}T - V_\infty(\eta_i - L/2)/\widetilde{D}\right]\eta \\ + \frac{1}{\widetilde{d}} \int_{L/2}^{\infty} d\eta \exp\left[-K\eta_i^2/2k_{\rm B}T - V_\infty(\eta_i - L/2)/\widetilde{d}\right]\eta, \end{aligned}$$

is equal to zero. The result is

$$V_\infty = \widetilde{D}\sqrt{\frac{2K}{k_{\rm B}T}} Q\left(\sqrt{E}/2, \epsilon\right), \tag{4-3-34}$$

where $Q(\chi, \epsilon)$ is a function obtained as the solution to

$$1 - \epsilon = \sqrt{\pi} Q \left[\frac{e^{(\chi + Q/\epsilon)^2}}{\epsilon} \mathrm{erfc}\left(\chi + \frac{Q}{\epsilon}\right) + \epsilon e^{(\chi+Q)^2} \mathrm{erfc}(-\chi - Q) \right]. \tag{4-3-35}$$

Now that we have the analytical solutions to the two cases of the model, $N = 2$ and $N \to \infty$, we may consider the ratio:

$$\frac{V_\infty}{V_2} = \sqrt{2\pi}\left[\frac{1+\epsilon}{1-\epsilon} + 2\Phi\left(\sqrt{E}\right)\right] e^{E/2} Q\left(\sqrt{E}/2, \epsilon\right). \tag{4-3-36}$$

We plotted the values of V_∞/V_2 corresponding to the cases of the parameters simulated in Fig. 4.7. We see good correspondence with the convergence of the results obtained in the stochastic simulation for large N. The ratio clearly captures the feature of whether the transport speeds up

or down upon increasing N. Notice that $|V_N - V_\infty| \sim 1/\sqrt{N}$ for large N, corresponding to the correction from the mean field theory at finite N.

We plotted the dependence of the ratio (4-3-36) as a function of E in Fig. 4.8, left in the case of $\epsilon = 0$. Note that there is no singularity in the $\epsilon \to 0$ limit, since we have

$$V_\infty = \widetilde{D}\sqrt{\frac{2K}{k_\mathrm{B}T}}Q^*\left(\sqrt{E}/2\right), \tag{4-3-37}$$

with $Q^*(\chi)$ satisfying,

$$Q^* - \chi + \sqrt{\pi}Q^{*2}\epsilon e^{(\chi+Q^*)^2}\mathrm{erfc}(-\chi - Q^*) = 0. \tag{4-3-38}$$

Equation (4-3-37) was used in the plot.

From Fig. 4.8, left, we see that for low E, there appears the case where the velocity decreases upon increasing the number of molecules. We call such situations the uncooperative phase, since in such region of the parameter, the molecules prefer to be in dimers rather than forming a larger team like a bundle. The ratio (4-3-36) only depends on the parameters ϵ and E; thus we can calculate the phase diagram concerning whether or not it is larger than 1. V_∞/V_2 as a function of E and ϵ is shown in Fig. 4.8, right.

The concept we find from the analysis is that the cooperativity of the motor molecules can change according to the sensitivity and the ratio of the effective diffusion constant. Significantly, the uncooperative phase ($V_\infty/V_2 < 1$) arises in the model, corresponding to low ϵ and E. Although large number of molecules is advantageous for the effective transport in general cases, if too much portion of the molecules are transitioned into the less diffusive state, it may interfere with the positive direction motion of the molecules in the highly diffusive state. Such case should be observed when the force-sensitivity is large (E is small), thus the uncooperative situation may appear. The parameter ϵ presumably controls the extent of such interference; larger ϵ corresponds to the two diffusive modes becoming close to identical, making the interfering effect smaller.

4.4 Multiple molecules with a cargo

The previous model was somewhat unrealistic in the sense of time-scale separation and the mechanism of sensing the force through the displacement from the mean. To resolve the concern that our phase diagram, especially the existence of the uncooperative phase, may be an artifact of the inchworm model, we here extend the model to the case where multiple motors share a cargo.

We consider the situation depicted in Fig. 4.9. The additional degree of freedom, the position of the cargo, is also considered to undergo the overdamped Langevin motion.

$$\gamma_i \dot{x}_i = -K\left(x_i - C\right) + \sqrt{2\gamma_i k_\mathrm{B}T}\xi_i(t), \tag{4-4-1}$$

$$\gamma_\mathrm{c}\dot{C} = -\sum_i K(C - x_i) + \sqrt{2\gamma_\mathrm{c}k_\mathrm{B}T}\xi_\mathrm{c}(t). \tag{4-4-2}$$

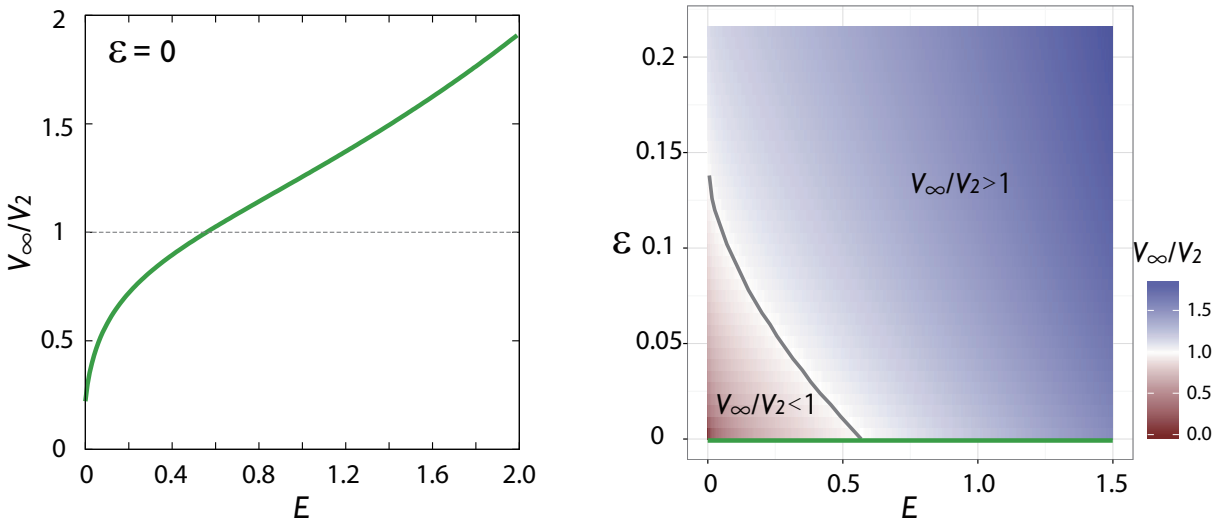

Fig 4.8: Analytical results for the steady-state velocity of the chemically-driven inchworm model. (Left) the ratio Eq. (4-3-36) was plotted as a function of E for fixed $\epsilon = 0$. (Right) Phase diagram of the ratio V_∞/V_2 with respect to the parameters ϵ and E.

Here, Γ_c is the friction constant for the cargo particle. Again, we consider the frictions γ_i to stochastically switch between two values, but now the rule is changed to sense the relative position from the cargo instead of the average position:

$$R_i(\gamma \to \Gamma | x_i, C) = \begin{cases} q & (x_i - C > L/2) \\ S & (x_i - C \le L/2) \end{cases} \tag{4-4-3}$$

$$R_i(\Gamma \to \gamma | x_i, C) = \begin{cases} Q & (x_i - C > L/2) \\ s & (x_i - C \le L/2) \end{cases}. \tag{4-4-4}$$

The time evolution of the density function follows

$$\begin{aligned} \frac{\partial}{\partial t} P_t(\boldsymbol{x}, \boldsymbol{\gamma}, C) &= \sum_i \left[\frac{\partial}{\partial x_i} \frac{K}{\gamma_i} (x_i - C) + \frac{\partial^2}{\partial x_i^2} \frac{k_B T}{\gamma_i} \right] P_t(\boldsymbol{x}, \boldsymbol{\gamma}, C) \\ &+ \left[\sum_i \frac{\partial}{\partial C} \frac{K}{\gamma_C} (C - x_i) + \frac{\partial^2}{\partial C^2} \frac{k_B T}{\gamma_C} \right] P_t(\boldsymbol{x}, \boldsymbol{\gamma}, C) \\ &+ \sum_i \left[R_i(\bar{\gamma}_i \to \gamma_i | x_i, C) P_t(\boldsymbol{x}, \bar{\boldsymbol{\gamma}}^i, C) - R_i(\gamma_i \to \bar{\gamma}_i | x_i, C) P_t(\boldsymbol{x}, \boldsymbol{\gamma}, C) \right], \end{aligned} \tag{4-4-5}$$

where we denoted $\boldsymbol{x} = \{x_1, x_2, ..., x_N\}$, $\boldsymbol{\gamma} = \{\gamma_1, \gamma_2, ..., \gamma_N\}$ and $\bar{\boldsymbol{\gamma}}^i = \{\gamma_1, ..., \gamma_{i-1}, \bar{\gamma}_i, \gamma_{i+1}, ..., \gamma_N\}$.

We consider the case where the diffusive motion of cargo is fast compared with the chemical reactions and the diffusive motion of motor heads. This corresponds to taking the parameter as $NK/\gamma_C \gg \max\{W, NK/\gamma\}$, where W is again the typical rate of the chemical reaction, and NK/γ corresponds to the inverse of the smallest time-scale experienced by the diffusive motion of the

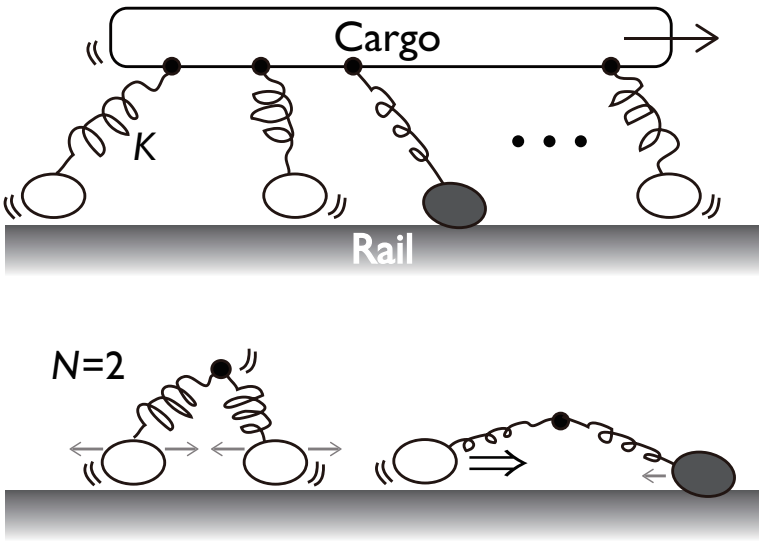

Fig 4.9: (Top) A cargo is attached to N motor molecules through springs. (Bottom) Case of the model with $N = 2$.

motors, as we will find later. In this limit, the second line in Eq. (4-4-5) should become zero, thus

$$P_t(\boldsymbol{x}, \boldsymbol{\gamma}, C) = P_t(\boldsymbol{x}, \boldsymbol{\gamma}) \times \sqrt{\frac{NK}{2\pi k_{\mathrm{B}} T}} \exp\left[-\frac{NK(C-\bar{x})^2}{2k_{\mathrm{B}}T}\right], \tag{4-4-6}$$

where $\bar{x} := \sum_i x_i/N$ is again the average position. Replacing P_t by the right hand side of Eq. (4-4-6) and taking the integral over C in both sides, we have

$$\begin{aligned}\frac{\partial}{\partial t}P_t(\boldsymbol{x}, \boldsymbol{\gamma}) &= \sum_i \left[\frac{\partial}{\partial x_i}\frac{K}{\gamma_i}(x_i - \bar{x}) + \frac{\partial^2}{\partial x_i^2}\frac{k_{\mathrm{B}}T}{\gamma_i}\right] P_t(\boldsymbol{x}, \boldsymbol{\gamma}) \\ &\quad + \sum_i \left[\widetilde{R}_i(\bar{\gamma}_i \to \gamma_i | x_i, \bar{x}) P_t(\boldsymbol{x}, \bar{\boldsymbol{\gamma}}^i) - \widetilde{R}_i(\gamma_i \to \bar{\gamma}_i | x_i, \bar{x}) P_t(\boldsymbol{x}, \boldsymbol{\gamma})\right]. \end{aligned} \tag{4-4-7}$$

Here, the effective switching rates $\widetilde{R}$ were introduced as

$$\widetilde{R}_i(\gamma \to \Gamma | x_i, \bar{x}) = q + (S - q)\Phi\left(-\sqrt{\frac{NK}{k_{\mathrm{B}}T}}(x_i - \bar{x} - L/2)\right) \tag{4-4-8}$$

$$\widetilde{R}_i(\Gamma \to \gamma | x_i, \bar{x}) = Q + (s - Q)\Phi\left(-\sqrt{\frac{NK}{k_{\mathrm{B}}T}}(x_i - \bar{x} - L/2)\right). \tag{4-4-9}$$

We have arrived at a model similar to the previous setup, yet with the switching rates changed from a step function [Eq. (4-3-3)...] to a function with length scale, l_{s}. Following the procedure

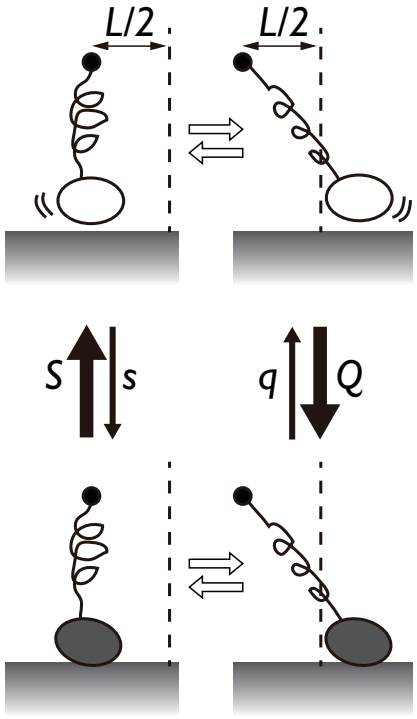

Fig 4.10: Schematic of the switching rates in the cargo model. Difference from the model depicted in Fig. 4.6 is that the force-sensitivity is defined by taking the reference point at the position of cargo (black dot) rather than that of the pair molecule.

of Sect. 4.3.2, we take the fast chemical reaction limit, $W \gg k_{\rm B}T/\gamma l_{\rm s}^2$. Notice that here we have a definite a typical length scale, $l_{\rm s} = \sqrt{k_{\rm B}T/NK}$, therefore the condition is $W \gg NK/\Gamma$. Then we have

$$\frac{\partial}{\partial t}P_t(\boldsymbol{x},\boldsymbol{\gamma}) = \sum_i \left[\frac{\partial}{\partial x_i}\frac{K}{\widetilde{\gamma}(x_i-\overline{x})}(x_i-\overline{x}) + \frac{\partial^2}{\partial x_i^2}\frac{k_{\rm B}T}{\widetilde{\gamma}(x_i-\overline{x})}\right]P_t(\boldsymbol{x},\boldsymbol{\gamma}) \tag{4-4-10}$$

Thus, we finally have the Langevin equation

$$\dot{x}_i = -\frac{K(x_i-\overline{x})}{\widetilde{\gamma}(x_i-\overline{x})} + \sqrt{\frac{2k_{\rm B}T}{\widetilde{\gamma}(x_i-\overline{x})}}\cdot\xi_i(t), \tag{4-4-11}$$

with again, the multiple $\cdot$ interpreted in the Itô sense. The friction as a function of $\eta_i := x_i - \overline{x}$ is

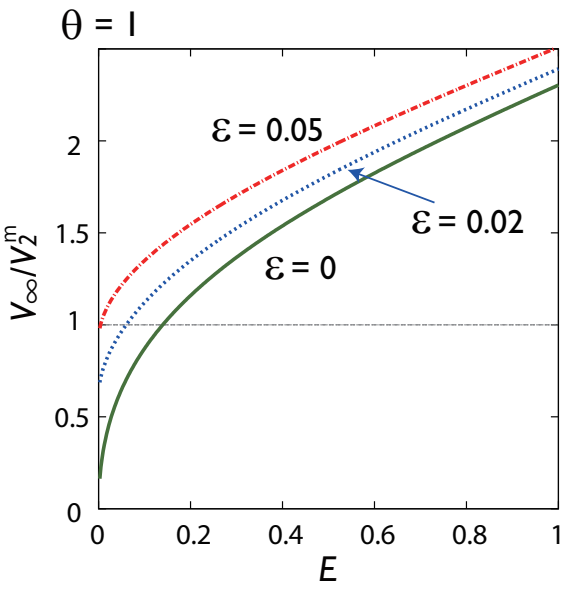

Fig 4.11: Analytical results for the steady-state velocity of the model with cargo with the parameter θ set as 1.

obtained as

$$\widetilde{\gamma}(x) = \frac{Q+q+(S+s-Q-q)\Phi\left(-\sqrt{\frac{NK}{k_BT}}(x-L/2)\right)}{Q/\gamma+q/\Gamma+[(S-q)/\Gamma+(s-Q)/\gamma]\Phi\left(-\sqrt{\frac{NK}{k_BT}}(\eta_i-L/2)\right)} \tag{4-4-12}$$

$$= \frac{1}{\widetilde{D}}\frac{1+(\theta-1)\Phi\left(-\sqrt{\frac{NK}{k_BT}}(x-L/2)\right)}{\epsilon+(\theta-\epsilon)\Phi\left(-\sqrt{\frac{NK}{k_BT}}(\eta_i-L/2)\right)}. \tag{4-4-13}$$

Here, recall the parameter $\theta := (Q+q)/(S+s)$, which did not appear in the previous model after taking the limit $W \to \infty$.

In comparison to the friction obtained in the previous setup, which was a stup function, the effective friction observed in this model with the cargo has a finite length scale, corresponding to that of the switching rates. Since we may reuse the general formula Eq. (4-3-22) by changing the friction function from (4-3-16) to (4-4-13), we may obtain the steady-state of the case $N = 2$, which we denote as V_2^m, by performing the integral numerically.

The length scale of $\gamma(\eta)$ will become zero in the limit $N \to \infty$. This means that the friction obtained as (4-4-13) will converge to the step function (4-3-16) in the limit $N \to \infty$. Thus, the model with cargo will undergo the same dynamics as the case of the inchworm model, in the large molecular number limit. We must be aware, however, that we derived the effective model under the assumption of $NK/\gamma_C \gg W \gg NK/\Gamma$. If the time-scale separation between the three quantities is not large enough for $N \sim 2$, it naturally arises that W will become comparable with NK/Γ for large N.

We show in Fig. 4.11 the ratio $V_\infty/V_2^{\rm m}$. We considered the same value for V_∞ with the previous inchworm model, assuming that the proper time-scale separation condition is met. We find that, although the parameter region for the uncooperative phase is narrower compared with the previous inchworm model, the phase still exists if ϵ is small enough. The reason for the narrower region of uncooperative phase is that the finite length scale in $\gamma(\eta)$ will make the model with $N = 2$ to become slower, owing to the large fluctuation experienced by the cargo, which is the reference point for the motor to determine the switching rule (Fig. 4.9, bottom). Thus, in the cargo model, the increase in the number N has an additional effect to suppress the fluctuation of the cargo.

4.5 Remarks and conclusion

In this chapter, we discussed a simple schematic of coordination between molecular motors, through a solvable Langevin model. The main result obtained from the analysis of this model is the dependence of the extent of cooperativity of motor proteins, which we quantify by the ratio of the velocity at $N = 2$ and $N \to \infty$, on the parameters, ϵ and E. Although the value of the steady-state velocity may depend highly on the functional form of the molecular interactions, we predict that the features such as the dependence of cooperativity on such non-dimensional parameters, may have universality to some extent.

The ratio between the effective diffusivity of two states, ϵ, may be modulated in experiments by changing the balance of concentration in ATP, ADP, and Pi, for example. The force-sensitivity, E, is a parameter somewhat more embedded in the design principle of molecular motors. Nevertheless, it is possible to change E by adding linkers in the artificial setups (cf., Fig. 4.3). Experiments directly corresponding to these situations are now being conducted by our collaborators.

The dependence of the cooperative feature of motors on the force-sensitivity may have correspondence to the duty ratio considered in the model of muscle contraction [1]. The duty ratio quantifies the length of time of the myosin head to be touching the actin filament, relative to the length of time they are detached. Myosins forming filaments can function properly even if the duty ratio is low, where as dimeric myosin must have a high duty ratio, since at least one of the motor heads needs to be attached to the rail for the processive motion. If we interpret the duty ratio as the ratio of molecules in the low diffusive mode, it has a monotonic dependence on E, since higher force-sensitivity (small E) will naturally put larger number of molecules in the less diffusive mode.

For instance, experiments on Myosin VI have shown that the average velocity decreases by linking more than two monomers in the same molecule [121]. There is also a study [122] that addresses the decrease of the velocity of a probe bead upon larger molecular numbers of monomeric kinesins attached to it. These results are different to the case of cytoplasmic dyneins, where the velocity increased as the number of molecules were increased [104, 112]. The processive myosin and conventional kinesin inevitably have large duty ratio and low E, which is needed to achieve the hand-over-hand motion by guaranteeing one head to be always in the tightly On the other hand, dyneins can cooperate in a large number of molecules, such as in the case of cilia and

flagella beating [100], which means that the duty ratio is not necessarily high, as in the case of muscle myosins. The uncoordinated stepping of yeast cytoplasmic dyneins [102, 123] is another hallmark of low duty ratio, thus high E. Through these discussions, it is possible that various types of cytoplasmic molecular motors and their cooperativity, whether they prefer functioning as dimers or act better by forming bundles, may be explained and classified by the uncooperative and cooperative phases predicted in the diagram [Fig. 4.8].

Although we only focused on the average velocity in our analysis, there are more questions that should be answered through our simple model. For instance, how does the stall force and thermodynamic efficiency depend on the number of molecules? What happens if some molecules in the model are inactive compared to others, as in the case where passive molecules like dynactin [105] or inactivated motor heads [124] enhanced the unidirectional motion? Qualitative predictions through answering such questions may motivate quantitative experiments on the effect of cooperativity, thus leading to more detailed models for the dynamics of cytoplasmic motors.

Chapter 5

General conclusion and outlook

In this thesis, we considered the phenomenological modeling of molecular motors. We first reviewed on the basic aspects of stochastic thermodynamics, which is a useful framework in measuring otherwise inaccessible quantities like potential energy and heat dissipation in small thermodynamic systems. Some theoretical ideas behind the framework, with a brief focus on the fluctuation theorem and the generalized fluctuation response relations, were presented.

The modeling of F_1-ATPase, the rotary ATP synthetic/catalytic machine, was described in detail in Chapter 3. Motivated by the precise experimental data on the internal dissipation-free feature of F_1 in the ATP catalytic regime, we investigated the phenomenological model with combined Brownian motion and chemical switching. We found and proposed that a model with totally asymmetric switching rates best matches with all the known experimental data. Our predictions shall be confirmed by future experiments, for example by quantifying the heat dissipative features and angular position dependence reactions in the ATP synthetic reactions.

We next set out to propose a simple model of cooperative transport for cytoplasmic linear motors in Chapter 4. In contrast to the case of F_1, details such as the functional form of the effective potentials and the conformation dependent chemical reaction rates are yet to be experimentally elucidated in these motors. Nevertheless, we stand at the optimistic viewpoint that simple phenomenological models should be sufficient to explain the features of transport, if we focus on some universal aspects like the cooperativity of single molecules. Considering the recent quantitative experiments on human cytoplasmic dynein, we proposed a model where molecules with bidirectional motion will team up to produce unidirectional motion. The key concept we addressed is that the sensitivity in the assumed force-sensor mechanism critically controls the extent of cooperativity of motors, which may an important aspect of the design principle in classifying the species and super families of these linear motors.

For future developments, it is of great interest to broaden the theoretical perspectives on molecular motors, through testing how universal our modeling strategy works. For instance, the asymmetry embedded in the forward and backward stepping motion of rotary motors can be a fundamental feature that characterize the functions of rotary motors. V-ATPase, a rotary motor protein which the motion was observed recently [125], functions as an ATP catalyst in the cell, in contrast to the ATP generator F_1. It shall be intriguing to compare the asymmetric properties

in V-ATPase and F_1 , to see if the predicted asymmetry of is correlated to their thermodynamic roles in the biological context.

The qualitative correspondence of the experimental results of kinesin, myosin, and dynein with our predictions in the force-sensor model motivates us to consider perturbation experiments to see if the outcomes can also be predicted. Controlling the interaction between the molecular motors and observing the cooperativity in the sense of average velocity shall elucidate the purified feature of the motor design principles. Furthermore, our simple model sheds light on the problem of how we may artificially design such nanomachines. Towards the true understanding of molecular motors, one direction of research is to construct nanomachines, similarly to the conceptual motivation of synthetic biology [126]. Recent development in techniques such as optogenetics [127] allows us to manipulate the bio-molecular motors to function as externally controllable mini-robots, thus opening the possibility of scanning the parameter space of the simple phase diagram predicted in our model.

Although we attempted to build the simplest phenomenological models that can explain the fascinating features observed in experiment, there are, of course, many facts known in specific experiments that we did not take into account rigorously. For example, it has been reported that F_1 can catalyze ATP and even produce rotary motion in the absence of the γ shaft [67]. Although such shaft-independent motion is observed to be much slower compared with the motor with the shaft-dependent motion, the striking result provokes us to consider that there might be some general rules behind the apparent shaft dominator model, which is key in the principle of tight-coupling motors.

Some features of cytoplasmic dyneins that we cannot explain is the large heterogeneity in the velocity of unidirectional motion of the $N \geq 2$ motors case [104]. This might be caused by the constraint of the experiment, since the microtubule is attached at the bottom surface of the glass, and dynein motors can move three-dimensionally on this rail and bump into the bottom surface while walking along the rail [128]. The common problems here with the rotary and linear motors is that it is has been too appealing to model the motors in one-dimension and to forget about the other hidden degrees of freedom, including the huge possibility of protein conformation changes. It is thus left for future challenges to investigate how these hidden degrees of freedom are adding up to present the apparently simple and beautiful dynamics of molecular motors.

It shall be fair to stress that the unexplainable features of molecular motors can be questioned only by addressing what is explainable through the most simplified models. Yet, the effort of phenomenological modeling should be constantly responding to the systematic experiments providing more and more quantitative results. Our motivation throughout the thesis was that theoretical studies on biophysics have come to a different stage from the fine-tuning of large number of parameters in models, which was required in explaining the rather obscure experiments, to the era where discussions on fundamental and abstract design principles are starting to make sense.

In the quest of biological physics, it is equally important to reuse the conceptual interests and approaches in solving different classes of biological problems. Just as how the single molecule imaging of motor proteins brought novel insights into the study of thermodynamics, the combination of the three-dimensional live cell imaging techniques and the ever-growing cell state profiling methods shall cast true challenges for physicists to understand developmental and neural biology

as nonequilibrium many-body problems. Continuing the fruitful communication between experiment and theory should lead in revealing the truly non-trivial aspects of biological systems, which will inevitably bring new ideas to theoretical physics as well.

References

[1] J Howard. *Mechanics of Motor Proteins and the Cytoskeleton*. Sunderland, Sinauer, 2001.

[2] K Sekimoto. *Stochastic Energetics (Lecture Notes in Physics)*. Berlin, Springer, 2010.

[3] U Seifert. Stochastic thermodynamics, fluctuation theorems and molecular machines. *Rep. Prog. Phys.*, 75:126001, 2012.

[4] D J Evans, E G D Cohen, and G P Morriss. Probability of second law violations in shearing steady states. *Phys. Rev. Lett.*, 71:2401, 1993.

[5] C Jarzynski. Nonequilibrium equality for free energy differences. *Phys. Rev. Lett.*, 78:2690, 1997.

[6] S Toyabe, T Sagawa, M Ueda, E Muneyuki, and M Sano. Experimental demonstration of information-to-energy conversion and validation of the generalized jarzynski equality. *Nat. Phys.*, 6:988, 2010.

[7] T Sagawa and M Ueda. Generalized jarzynski equality under nonequilibrium feedback control. *Phys. Rev. Lett.*, 104:090602, 2010.

[8] N Shiraishi, S Ito, K Kawaguchi, and T Sagawa. Role of measurement-feedback separation in autonomous Maxwell's demons. *arxiv:1501.06071*, 2015.

[9] L Szilard. On the decrease in entropy in a thermodynamic system by the intervention of intelligent beings. *Z. fur Phys.*, 53:840, 1929.

[10] R D Vale and F Oosawa. Protein motors and maxwell's demons: does mechanochemical transduction involve a thermal ratchet? *Adv. Biophys.*, 26:97, 1990.

[11] F Julicher, A Ajdari, and J Prost. Modeling molecular motors. *Rev. Mod. Phys.*, 69:1269, 1999.

[12] S Toyabe, H Ueno, and E Muneyuki. Recovery of state-specific potential of molecular motor from single-molecule trajectory. *Euro. Phys. Lett.*, 97:40004, 2012.

[13] V Schaller, C Weber, C Semmrich, E Frey, and A R Bausch. Polar patterns of driven filaments. *Nature*, 467:73, 2010.

[14] Y Sumino, K H Nagai, Y Shitaka, Dan Tanaka, K Yoshikawa, H Chaté, and K Oiwa. Large-scale vortex lattice emerging from collectively moving microtubules. *Nature*, 483:448, 2012.

[15] K Kinosita Jr., R Yasuda, H Noji, and K Adachi. A rotary molecular motor that can work at near 100% efficiency. *Philos. Trans. R. Soc. Lond. B*, 355:473, 2000.

[16] S Toyabe, T Okamoto, T Watanabe-Nakayama, H Taketani, S Kudo, and E Muneyuki. Nonequilibrium energetics of a single F_1-ATPase molecule. *Phys. Rev. Lett.*, 104:198103, 2010.

[17] A Einstein. Uber einen die erzeugung und verwandlung des lichtes betreffenden heurischen gesichtpunkt. *Ann. Phys.*, 17:132, 1905.

[18] N G Van Kampen. *Stochastic processes in physics and chemistry.*, volume 1. Elsevier, 1992.

[19] N. G. Van Kampen. Elimination of fast variables. *Phys. Rep.*, 124:69, 1985.

[20] H Mori. Transport, collective motion, and brownian motion. *Prog. Theor. Phys.*, 33(3), 1965.

[21] Kyozi Kawasaki. Simple derivations of generalized linear and nonlinear langevin equations. *Journal of Physics A: Mathematical, Nuclear and General*, 6(9):1289, 1973.

[22] R Zwanzig. Nonlinear generalized langevin equations. *J. Stat. Phys.*, 9:215, 1973.

[23] Y G Sinai. Dynamical systems with elastic reflections. ergodic properties of dispersing billiards. *Uspekhi Matematicheskikh Nauk*, 25:141, 1970.

[24] T Li, S Kheifets, D Medellin, and M G Raizen. Measurement of the instantaneous velocity of a brownian particle. *Science*, 328:1673, 2010.

[25] E Leibrock, P Bayer, and H D Lüdemann. Nonenzymatic hydrolysis of adenosinetriphosphate (ATP) at high temperatures and high pressures. *Biophys. Chem.*, 54:175, 1995.

[26] K Sekimoto. Kinetic characterization of heat bath and the energetics of thermal ratchet models. *J. Phys. Soc. Jpn*, 66:1234, 1997.

[27] P Reimann. Brownian motors: noisy transport far from equilibrium. *Phys. Rep.*, 361:57, 2002.

[28] T Tlusty, A Meller, and R Bar-Ziv. Optical gradient forces of strongly localized fields. *Phys. Rev. Lett.*, 81:1738, 1998.

[29] J R Gomez-Solano, A Petrosyan, S Ciliberto, R Chetrite, and K Gawedzki. Experimental verification of a modified fluctuation-dissipation relation for a micron-sized particle in a nonequilibrium steady state. *Phys. Rev. Lett.*, 103:040601, 2009.

[30] J Kurchan. Fluctuation theorem for stochastic dynamics. *J. Phys. A*, 31:3719, 1998.

[31] J L Lebowitz and H Spohn. A Gallavotti Cohen-Type Symmetry in the Large Deviation Functional for Stochastic Dynamics. *J. Stat. Phys.*, 95:333, 1999.

[32] C Jarzynski. Hamiltonian derivation of a detailed fluctuation theorem. *J. Stat. Phys.*, 98:77, 2000.

[33] T Schmiedl, T Speck, and U Seifert. Entropy production for mechanically or chemically driven biomolecules. *J. Stat. Phys.*, 128:77, 2007.

[34] T Schmiedl and U Seifert. Stochastic thermodynamics of chemical reaction networks. *J. Chem. Phys.*, 126:044101, 2007.

[35] K Kawaguchi and Y Nakayama. Fluctuation theorem for hidden entropy production. *Phys. Rev. E*, 88:022147, 2013.

[36] T M Cover and J A Thomas. *Elements of information theory*. Wiley Interscience, New York, 1991.

[37] G E Crooks. Entropy production fluctuation theorem and the nonequilibrium work relation for free energy differences. *Phys. Rev. E*, 60:2721, 1999.

[38] C W Gardiner. *Stochastic methods, forth edition*. Berlin, Springer, 2009.

[39] U Seifert. Entropy production along a stochastic trajectory and an integral fluctuation theorem. *Phys. Rev. Lett.*, 95:040602, 2005.

[40] T Harada. Phenomenological energetics for molecular motors. *Europhys. Lett.*, 70:49, 2005.

[41] T Harada and S-i Sasa. Equality connecting energy dissipation with a violation of fluctuation-response relation. *Phys. Rev. Lett.*, 95:130602, 2005.

[42] T Harada and S-i Sasa. Energy dissipation and violation of the fluctuation-response relation in nonequilibrium Langevin systems. *Phys. Rev. E*, 73:026131, 2006.

[43] T Harada and S-i Sasa. Fluctuations, responses and energetics of molecular motors. *Math. Biosci.*, 207:365, 2007.

[44] H Wang and G Oster. The Stokes efficiency for molecular motors and its applications. *Euro. Phys. Lett.*, 134:133, 2002.

[45] H Leff and A F Rex, editors. *Maxwell's demon 2 : Entropy, classical and quantum information, computing*. CRC Press, 2003.

[46] T Speck and U Seifert. Restoring a fluctuation-dissipation theorem in a nonequilibrium steady state. *Europhy. Lett.*, 74:391, 2006.

[47] M Baiesi, C Maes, and B Wynants. Fluctuations and response of nonequilibrium states. *Phys. Rev. Lett.*, 103:010602, 2009.

[48] M Baiesi, C Maes, and Wynants. Nonequilibrium linear response for Markov dynamics , I: jump processes and overdamped diffusions. *J. Stat. Phys.*, 137:1094, 2009.

[49] M Baiesi, E Boksenbojm, C Maes, and B Wynants. Nonequilibrium linear response for markov dynamics, ii: Inertial dynamics. *J. Stat. Phys.*, 139:492, 2010.

[50] T Nemoto and S-i Sasa. Thermodynamic formula for the cumulant generating function of time-averaged current. *Phys. Rev. E*, 84:061113, 2011.

[51] C Maes, K Netočnỳ, and B Wynants. Monotonic return to steady nonequilibrium. *Phys. Rev. Lett.*, 107:010601, 2011.

[52] M D Donsker and S R S Varadhan. Asymptotic evaluation of certain markov process expectations for large time, i. *Comm. Pure Appl. Math.*, 28:1, 1975.

[53] C Maes and K Netočnỳ. Minimum entropy production principle from a dynamical fluctuation law. *J. Math. Phys.*, 48:053306, 2007.

[54] K. Sekimoto. Microscopic heat from the energetics of stochastic phenomena. *Phys. Rev. E*, 76:060103, 2007.

[55] Y Nakayama and K Kawaguchi. Invariance of steady state thermodynamics between different scales of description. *Phys. Rev. E*, 91:012115, 2014.

[56] R Phillips, J Kondev, J Theriot, N Orme, and H Garcia. *Physical biology of the cell, second edition*. New York, Garland Science, 2012.

[57] B Alberts, A Johnson, J Lewis, D Morgan, M Raff, K Roberts, and P Walter. *Molecular biology of the cell, sixth edition*. New York, Garland Science, 2014.

[58] H Noji, R Yasuda, M Yoshida, and K Kinosita Jr. Direct observation of the rotation of F_1-ATPase. *Nature*, 386:299, 1997.

[59] R Yasuda, H Noji, K Kinosita Jr, and M Yoshida. F_1-ATPase is a highly efficient molecular motor that rotates with discrete 120° steps. *Cell*, 93:1117, 1998.

[60] P D Boyer. The ATP synthase–a splendid molecular machine. *Ann. Rev. Biochem.*, 66:717, 1997.

[61] J P Abrahams, A G W Leslie, R Lutter, and J E Walker. Structure at 2.8 a resolution of f1-atpase from bovine heart mitochondria. *Nature*, 370:621, 1994.

[62] Y Rondelez, G Tresset, T Nakashima, Y Kato-Yamada, H Fujita, S Takeuchi, and H Noji. Highly coupled atp synthesis by F_1-ATPase single molecules. *Nature*, 433:773, 2005.

[63] S Toyabe, T Watanabe-Nakayama, T Okamoto, S Kudo, and E Muneyuki. Thermodynamic efficiency and mechanochemical coupling of F_1-ATPase. *Proc. Natl. Acad. Sci*, 108:17951, 2011.

[64] R Yasuda, H Noji, M Yoshida, K Kinosita, and H Itoh. Resolution of distinct rotational substeps by submillisecond kinetic analysis of F_1-ATPase. *Nature*, 410:898, 2001.

[65] K Adachi, K Oiwa, T Nishizaka, S Furuike, H Noji, H Itoh, M Yoshida, and K Kinosita. Coupling of rotation and catalysis in F_1-ATPase revealed by single-molecule imaging and manipulation. *Cell*, 130:309, 2007.

[66] K Kinosita Jr, K Adachi, and H Itoh. Rotation of F_1-ATPase: how an ATP-driven molecular machine may work. *Ann. Rev. Biophys. Biomol. Struct.*, 33:245, 2004.

[67] T Uchihashi, R Iino, T Ando, and H Noji. High-speed atomic force microscopy reveals rotary catalysis of rotorless f1-atpase. *Science*, 333:755, 2011.

[68] H Itoh, A Takahashi, K Adachi, H Noji, R Yasuda, M Yoshida, and K Kinosita. Mechanically driven ATP synthesis by F_1-ATPase. *Nature*, 427:465, 2004.

[69] H Wang and G Oster. Energy transduction in the F_1 motor of ATP synthase. *Nature*, 396:279, 1998.

[70] R D Astumian. Fluctuation driven ratchets: molecular motors. *Phys. Rev. Lett.*, 72:1766, 1994.

[71] T Elston, H Wang, and G Oster. Energy transduction in ATP synthase. *Nature*, 391:510, 1998.

[72] R Watanabe, D Okuno, S Sakakihara, K Shimabukuro, R Iino, M Yoshida, and H Noji. Mechanical modulation of catalytic power on F_1-ATPase. *Nat. Chem. Biol.*, 8:86, 2012.

[73] K Adachi, K Oiwa, M Yoshida, T Nishizaka, and K Kinosita Jr. Controlled rotation of the F_1-ATPase reveals differential and continuous binding changes for ATP synthesis. *Nat. Commun.*, 3:1022, 2012.

[74] J Monod, J Wyman, and J-P Changeux. On the nature of allosteric transitions: a plausible model. *J. Mol. Biol.*, 12:88, 1965.

[75] N J Carter and R A Cross. Mechanics of the kinesin step. *Nature*, 435:308, 2005.

[76] T Masaike, F Koyama-Horibe, K Oiwa, M Yoshida, and T Nishizaka. Cooperative three-step motions in catalytic subunits of F_1-ATPase correlate with 80 degrees and 40 degrees substep rotations. *Nat. Struct. Mol. Biol.*, 15:1326, 2008.

[77] D Okuno, R Iino, and H Noji. Stiffness of γ subunit of F_1-ATPase. *Eur. Bio. Phys. J*, 39:1589, 2010.

[78] R Watanabe, K Hayashi, H Ueno, and H Noji. Catalysis-enhancement via rotary fluctuation of $F_1 - ATPase$. *Biophys. J*, 105:2385, 2013.

[79] S Toyabe and E Muneyuki. Single molecule thermodynamics of ATP synthesis by F_1-ATPase. *New J. Phys.*, 17:015008, 2014.

[80] Y Iko, K V Tabata, S Sakakihara, T Nakashima, and H Noji. Acceleration of the ATP-binding rate of F1-ATPase by forcible forward rotation. *FEBS lett.*, 583:3187, 2009.

[81] R D Vale. The molecular motor toolbox for intracellular transport. *Cell*, 112:467, 2003.

[82] W Kühne. Untersuchungen über bewegungen und veränderungen der contractilen substanzen. *Arch. Anat. Physiol. wiss. Med.*, page 748, 1859.

[83] A F Huxley. Muscle structure and theories of contraction. *Prog. Biophys. Biophys. Chem.*, 7:255, 1957.

[84] H E Huxley. The mechanism of muscular contraction. *Science*, 164:1356, 1969.

[85] A F Huxley and R M Simmons. Proposed mechanism of force generation in striated muscle. *Nature*, 233:533, 1971.

[86] S L Reck-Peterson, D W Provance Jr., M S Mooseker, and J A Mercer. Class v myosins. *Biochim. Biophys. Acta.*, 1496:36, 2000.

[87] M Enrique, E M Ostap, and H L Sweeney. Kinetic mechanism and regulation of myosin VI. *J. Biol. Chem.*, 276:32373, 2001.

[88] A D Mehta, R S Rock, M Rief, J A Spudich, M S Mooseker, and R E Cheney. Myosin-V is a processive actin-based motor. *Nature*, 400:590, 1999.

[89] A L Wells, A W Lin, L-Q Chen, D Safer, S M Cain, T Hasson, B O Carragher, R A Milligan, and H L Sweeney. Myosin VI is an actin-based motor that moves backwards. *Nature*, 401:505, 1999.

[90] R D Vale, T S Reese, and M P Sheetz. Identification of a novel force-generating protein, kinesin, involved in microtubule-based motility. *Cell*, 42:39, 1985.

[91] S T Brady. A novel brain atpase with properties expected for the fast axonal transport motor. *Nature*, 317:73, 1985.

[92] H B McDonald, R J Stewart, and L S B Goldstein. The kinesin-like¡ i¿ ncd¡/i¿ protein of drosophila is a minus end-directed microtubule motor. *Cell*, 63:1159, 1990.

[93] Y Okada, H Higuchi, and N Hirokawa. Processivity of the single-headed kinesin kif1a through biased binding to tubulin. *Nature*, 424:574, 2003.

[94] K Svoboda, C F Schmidt, B J Schnapp, and S M Block. Direct observation of kinesin stepping by optical trapping interferometry. *Nature*, 365:721, 1993.

[95] C L Asbury, A N Fehr, and S M Block. Kinesin moves by an asymmetric hand-over-hand mechanism. *Science*, 302:2130, 2003.

[96] M Nishiyama, H Higuchi, and T Yanagida. Chemomechanical coupling of the forward and backward steps of single kinesin molecules. *Nat. Cell Biol.*, 4:790, 2002.

[97] A Yildiz, J N Forkey, S A McKinney, T Ha, Y E Goldman, and P R Selvin. Myosin V walks hand-over-hand: single fluorophore imaging with 1.5-nm localization. *Science*, 300:2061, 2003.

[98] A Yildiz, M Tomishige, R D Vale, and P R Selvin. Kinesin walks hand-over-hand. *Science*, 303:676, 2004.

[99] J R Kardon and R D Vale. Regulators of the cytoplasmic dynein motor. *Nat. Rev. Mol. Cell Biol.*, 10:854, 2009.

[100] I R Gibbons. Studies on the protein components of cilia from tetrahymena pyriformis. *Proc. Natl. Acad. Sci.*, 50:1002, 1963.

[101] A P Carter, C Cho, L Jin, and R D Vale. Crystal structure of the dynein motor domain. *Science*, 331:1159, 2011.

[102] M A DeWitt, A Y Chang, P A Combs, and A Yildiz. Cytoplasmic dynein moves through uncoordinated stepping of the AAA+ ring domains. *Science*, 335:221, 2012.

[103] W Qiu, N D. Derr, B S Goodman, E Villa, D Wu, W Shih, and S L Reck-Peterson. Dynein achieves processive motion using both stochastic and coordinated stepping. *Nat. Struct. Mol. Biol*, 19:193, 2012.

[104] T Torisawa, M Ichikawa, A Furuta, K Saito, K Oiwa, H Kojima, Y Toyoshima, and K Furuta. Autoinhibition and cooperative activation mechanisms of cytoplasmic dynein. *Nat. Cell Biol.*, 16:1118, 2014.

[105] R J McKenney, W Huynh, M E Tanenbaum, G Bhabha, and R D Vale. Activation of cytoplasmic dynein motility by dynactin-cargo adapter complexes. *Science*, 345:337, 2014.

[106] M Schlager, H T Hoang, L Urnavicius, S L Bullock, and A P Carter. In vitro reconstitution of a highly processive recombinant human dynein complex. *EMBO J.*, 33:1855, 2014.

[107] A Yildiz, M Tomishige, A Gennerich, and R D Vale. Intramolecular strain coordinates kinesin stepping behavior along microtubules. *Cell*, 134:1030, 2008.

[108] S Uemura, H Higuchi, A O Olivares, E M De La Cruz, and S Ishiwata. Mechanochemical coupling of two substeps in a single myosin V motor. *Nat. Struct. Mol. Biol.*, 11:877, 2004.

[109] Z Ökten, L S Churchman, R S Rock, and J A Spudich. Myosin VI walks hand-over-hand along actin. *Nat. Struct. Mol. Biol.*, 11:884, 2004.

[110] S Uemura and S Ishiwata. Loading direction regulates the affinity of ADP for kinesin. *Nat. Struct. Biol.*, 10:308, 2003.

[111] M Iwaki, A H Iwane, T Shimokawa, R Cooke, and T Yanagida. Brownian search-and-catch mechanism for myosin-VI steps. *Nat. Chem. Biol.*, 5:403, 2009.

[112] K Kawaguchi, T Torisawa, and K Furuta. Collective motion by force-sensor switching: unified model for cooperative molecular motors. *Manuscript under preparation*, 2015.

[113] A J Roberts, N Numata, M L Walker, Y S Kato, B Malkova, T Kon, R Ohkura, F Arisaka, P J Knight, K Sutoh, and S Burgess. AAA+ Ring and linker swing mechanism in the dynein motor. *Cell*, 136:485, 2009.

[114] J R Cooper and L Wordeman. The diffusive interaction of microtubule binding proteins. *Curr. Opin. Cell Biol.*, 21:68, 2009.

[115] M Y Ali, E B Krementsova, G G Kennedy, R Mahaffy, T D Pollard, K M Trybus, and D M Warshaw. Myosin Va maneuvers through actin intersections and diffuses along microtubules. *Proc. Natl. Acad. Sci.*, 104:4332, 2007.

[116] I Minoura, E Katayama, K Sekimoto, and E Muto. One-dimensional brownian motion of charged nanoparticles along microtubules: a model system for weak binding interactions. *Biophys. J.*, 98:1589, 2010.

[117] J A Spudich and S Sivaramakrishnan. Myosin VI: an innovative motor that challenged the swinging lever arm hypothesis. *Nat. Rev. Mol. Cell Biol.*, 11:128, 2010.

[118] K Sekimoto. Bidirectional control: a unifying view of the structure and function of proteins. *Compt. Rend. Phys.*, 8:650, 2007.

[119] K V Kumar, S Ramaswamy, and M Rao. Active elastic dimers: Self-propulsion and current reversal on a featureless track. *Phys. Rev. E*, 77:020102, 2008.

[120] A Baule, K V Kumar, and S Ramaswamy. Exact solution of a Brownian inchworm model for self-propulsion. *J. Stat. Mech.*, 2008:P11008, 2008.

[121] T D Schindler, L Chen, P Lebel, M Nakamura, and Z Bryant. Engineering myosins for long-range transport on actin filaments. *Nat. Nanotech.*, 9:33, January 2014.

[122] T Kamei, S Kakuta, and H Higuchi. Biased binding of single molecules and continuous movement of multiple molecules of truncated single-headed kinesin. *Biophys. J.*, 88:2068, 2005.

[123] N D Derr, B S Goodman, R Jungmann, A E Leschziner, W M Shih, and S L Reck-Peterson. Tug-of-war in motor protein ensembles revealed with a programmable DNA origami scaffold. *Science*, 338:662, 2012.

[124] F B Cleary, M A Dewitt, T Bilyard, Z M Htet, V Belyy, D D Chan, A Y Chang, and A Yildiz. Tension on the linker gates the ATP-dependent release of dynein from microtubules. *Nat. Commun.*, 5:4587, 2014.

[125] H Ueno, Y Minagawa, M Hara, S Rahman, I Yamato, E Muneyuki, H Noji, T Murata, and R Iino. Torque generation of Enterococcus hirae V-ATPase. *J. Biol. Chem.*, 31212:289, 2014.

[126] M Elowitz and W A Lim. Build life to understand it. *Nature*, 468:889, 2010.

[127] M Nakamura, L Chen, S C Howes, T D Schindler, E Nogales, and Z Bryant. Remote control of myosin and kinesin motors using light-activated gearshifting. *Nat. Nanotech.*, 9:693, 2014.

[128] S Can, M A Dewitt, and A Yildiz. Bidirectional helical motility of cytoplasmic dynein around microtubules. *eLife*, 3:e03205, 2014.